



SUPRAMOLECULAR NANOARCHITECTURES BASED ON CYCLODEXTRIN HOST-GUEST INTERACTIONS

Ewelina Maria Wajs

Dipòsit Legal: T 1227-2014

ADVERTIMENT. L'accés als continguts d'aquesta tesi doctoral i la seva utilització ha de respectar els drets de la persona autora. Pot ser utilitzada per a consulta o estudi personal, així com en activitats o materials d'investigació i docència en els termes establerts a l'art. 32 del Text Refós de la Llei de Propietat Intel·lectual (RDL 1/1996). Per altres utilitzacions es requereix l'autorització prèvia i expressa de la persona autora. En qualsevol cas, en la utilització dels seus continguts caldrà indicar de forma clara el nom i cognoms de la persona autora i el títol de la tesi doctoral. No s'autoritza la seva reproducció o altres formes d'explotació efectuades amb finalitats de lucre ni la seva comunicació pública des d'un lloc aliè al servei TDX. Tampoc s'autoritza la presentació del seu contingut en una finestra o marc aliè a TDX (framing). Aquesta reserva de drets afecta tant als continguts de la tesi com als seus resums i índexs.

ADVERTENCIA. El acceso a los contenidos de esta tesis doctoral y su utilización debe respetar los derechos de la persona autora. Puede ser utilizada para consulta o estudio personal, así como en actividades o materiales de investigación y docencia en los términos establecidos en el art. 32 del Texto Refundido de la Ley de Propiedad Intelectual (RDL 1/1996). Para otros usos se requiere la autorización previa y expresa de la persona autora. En cualquier caso, en la utilización de sus contenidos se deberá indicar de forma clara el nombre y apellidos de la persona autora y el título de la tesis doctoral. No se autoriza su reproducción u otras formas de explotación efectuadas con fines lucrativos ni su comunicación pública desde un sitio ajeno al servicio TDR. Tampoco se autoriza la presentación de su contenido en una ventana o marco ajeno a TDR (framing). Esta reserva de derechos afecta tanto al contenido de la tesis como a sus resúmenes e índices.

WARNING. Access to the contents of this doctoral thesis and its use must respect the rights of the author. It can be used for reference or private study, as well as research and learning activities or materials in the terms established by the 32nd article of the Spanish Consolidated Copyright Act (RDL 1/1996). Express and previous authorization of the author is required for any other uses. In any case, when using its content, full name of the author and title of the thesis must be clearly indicated. Reproduction or other forms of for profit use or public communication from outside TDX service is not allowed. Presentation of its content in a window or frame external to TDX (framing) is not authorized either. These rights affect both the content of the thesis and its abstracts and indexes.

Ewelina Maria Wajs

**SUPRAMOLECULAR NANOARCHITECTURES BASED
ON CYCLODEXTRIN HOST-GUEST INTERACTIONS**

DOCTORAL THESIS

Departament d'Enginyeria Química



UNIVERSITAT ROVIRA I VIRGILI

Tarragona

2014

Ewelina Maria Wajs

SUPRAMOLECULAR NANOARCHITECTURES BASED
ON CYCLODEXTRIN HOST-GUEST INTERACTIONS

DOCTORAL THESIS

Departament d'Enginyeria Química



UNIVERSITAT ROVIRA I VIRGILI

Ewelina Maria Wajs

SUPRAMOLECULAR NANOARCHITECTURES BASED
ON CYCLODEXTRIN HOST-GUEST INTERACTIONS

DOCTORAL THESIS

Supervised by Dr. Alex Fragoso

Departament d'Enginyeria Química



UNIVERSITAT ROVIRA I VIRGILI

Tarragona

2014



Departament d'Enginyeria Quimica
Universitat Rovira i Virgili
Campus Sescelades,
Avda. Països Catalans, 26
43007 Tarragona
Tel: 977 55 85 79
Fax: 977 55 96 67

Dr. Alex Fragoso

CERTIFIES:

That the present study, entitled "SUPRAMOLECULAR NANOARCHITECTURES BASED ON CYCLODEXTRIN HOST-GUEST INTERACTIONS" presented by Ewelina Maria Wajs for the award of the degree of Doctor, has been carried out under my supervision at the Department of Chemical Engineering of Universitat Rovira i Virgili, and that it fulfils the requirements to obtain the International Mention.

Tarragona, May 8th 2014.



Dr. Alex Fragoso

ACKNOWLEDGEMENTS

First of all I wish to thank my thesis supervisor Dr. Alex Frago; this thesis would not have been possible without his guidance and encouragement along these years. My sincere gratitude goes to the NBG group members for helping me out in difficult times sparing their knowledge.

It is also a pleasure to thank Prof. Luis Echegoyen for his supervision, hospitality and financial support during my six-month research stay in his group at the Department of Chemistry of the University of Texas at El Paso. Particular thanks go to Dr. Agustin Molina for his technical assistance and friendship.

I am also grateful to Prof. Kim Lambertsen Larsen of Aalborg University, Denmark, for hosting me for a three-month research stay in his lab at the at the Department of Biotechnology, Chemistry and Environmental Engineering. My deepest gratitude goes to Prof. Thorbjørn Terndrup Nielsen for his continuous and enthusiastic support and suggestions in the syntheses of most of the materials described in this thesis.

These research stays were possible by financial support from Generalitat de Catalunya (grant 2012-BE1-476) and Ministerio de Educación, Cultura y Deporte (grant MHE-2011-263). Financial support from Ministerio de Economía y Competitividad (grant BIO2012-30936) is also gratefully acknowledged.

ABBREVIATIONS

Ada: adamantane
AFM: atomic force microscopy
Azo: azobenzene
CD: cyclodextrin
CDNS: cyclodextrin nanosponges
CLSM: confocal laser scanning microscopy
CNO: carbon nano onion
Dex: dextran
DLS: dynamic light scattering
DPV: differential pulse voltammetry
DS: degree of substitution
EDC: 1-ethyl-3-(3-dimethyl-aminopropyl) carbodiimide
EDS: energy dispersive spectroscopy
ESEM: environmental scanning microscopy
Fc: ferrocene
FITC: fluorescein isothiocyanate
FT-IR: Fourier transform infrared spectroscopy
HRP: horseradish peroxidase
HRTEM: high-resolution transmission microscopy
LbL: layer-by-layer self-assembly
MWCNT: multi walled carbon nanotube
NHS: N-hydroxysuccinimide
PBS: Phosphate buffered saline
PDI: polydispersity index
RhB: rhodamine B
SAM: self-assembly monolayer
SEM: scanning electron microscopy
SERS: Surface-enhanced Raman spectroscopy
SWCNT: single walled carbon nanotube
TEM: transmission electron microscopy
TGA: thermogravimetric analysis
TLC: thin layer chromatography
TMB: 3,3',5,5'-tetramethylbenzidine

Table of contents

SUMMARY	1
CHAPTER 1. INTRODUCTION	5
CHAPTER 2. CYCLODEXTRIN NANOSPONGE IMMUNOCONJUGATES AS A SIGNAL ENHANCEMENT TOOL IN OPTICAL AND ELECTROCHEMICAL ASSAYS	41
CHAPTER 3. CYCLODEXTRIN AND GUEST-APPENDED DEXTRAN- BASED POLYMERS. PREPARATION AND CHARACTERIZATION	60
CHAPTER 4. NANOCAPSULE FORMATION FROM COMPLEMENTARY CYCLODEXTRIN AND ADAMANTANE-APPENDED DEXTRAN-BASED POLYMERS	82
CHAPTER 5. HOST-GUEST ENGINEERED STIMULI-RESPONSIVE NANOCAPSULES	98
CHAPTER 6. PREPARATION OF SOLUBLE CARBON NANO-ONIONS BY FUNCTIONALIZATION WITH DEXTRAN BASED SUPRAMOLECULAR POLYMERS	132
CONCLUSIONS AND FUTURE WORK	154

SUMMARY

The focus of the present thesis is to develop new supramolecular architectures based on host-guest interactions with potential applications in, for example, controlled drug release, biosensors or molecular electronics, catalysis, etc.

Chapter 1 is the introduction, which covers the general information on supramolecular interactions, different cyclodextrin based polymers and different carbon allotropes.

The core of the thesis, **Chapter 2**, is concerned with the cyclodextrin cross-linked polymer (cyclodextrin nanosponges) bearing carboxylate groups to form a nanoporous material. The surface of the particles was covalently modified with an anti-IgG antibody and then loaded with an enzyme (horseradish peroxidase). Both, the antibody and the enzyme were tagged with fluorophores in order to better visualize the nanoassemblies formation by confocal microscopy. The structures of unmodified and protein modified nanosponge particles were investigated by different characterization methods. Confocal images clearly show the modification of the surface of the particles with an antibody and an enzyme encapsulated in their inner part. The possibility to use these modified nanosponges as a signal enhancement tool in enzyme-linked colorimetric and electrochemical assays was evaluated using a sandwich format comprising immobilized gliadin as an antigen, a target anti-gliadin antibody and an anti-IgG antibody conjugated to the enzyme-loaded nanosponge immunoconjugates.

Chapter 3 described the syntheses of the different dextran based host-guest polymers used in Chapters 4, 5 and 6. The dextran-based polymers were synthesized from different combinations of molecular weights and appended host or guest molecules percentages. Cyclodextrin-dextran polymers were prepared from alkynyl dextran via click chemistry. Guest-appended polymers were prepared in two ways. To graft adamantane units the same strategy as for the cyclodextrin polymers was used. In turn, the stimuli-responsive polymers bearing ferrocene and azo groups were prepared by transesterification of native dextran with N-hydroxysuccinimide esters. Some of these polymers were also tagged with fluorophores in order to better visualize the nanoassemblies formation by confocal microscopy. For these modifications either “click” chemistry or transesterification reactions were also used. These synthesized polymers were subsequently used for the formation of different nanoarchitectures presented in the following chapters.

Chapter 4 is dedicated to the formation of a novel class of nanocapsules assembled via supramolecular interactions between specially designed complementary polymers. The proposed method yields well-ordered, stable and size-controlled architectures in short periods of time, which have been characterized by using different methods. Furthermore, we show the encapsulation properties of these nanocapsules using fluorescent molecules as a model system. Thus, in this chapter we demonstrate the proof-of-concept of the technology used in the next chapter for the formation of the supramolecularly engineered stimuli-responsive nanocapsules.

Chapter 5 represents the supramolecular self-assembly of materials through host-guest interactions to form biodegradable nanocapsules with stimuli responsive properties. Redox-responsive nanocapsules were fabricated employing non-covalent interactions between β CD and ferrocene (Fc) units and light-responsive nanocapsules were formed by using α CD and azobenzene (Azo) host-guest interactions. Different biocompatible polymers, dextran- β CD (β CD-Dex) and dextran-ferrocene (Fc-Dex), dextran- α CD (α CD-Dex) and dextran-azobenzene (Azo-Dex) were assembled in alternating way on gold nanoparticles of different sizes, ranging from 40 nm, 100 nm and 400 nm. The gold particles were removed by chemical degradation and dye molecules (rhodamine B) were encapsulated inside the carriers as a model drug. The encapsulation process of was additionally accelerated by oxidation step or by UV-light of the nanocapsules wall, thus enabling easier and faster diffusion through the polymer layers. Different techniques were employed for the characterization and visualization of the nano capsules as well as for their encapsulation and release properties.

Finally, in **Chapter 6**, the construction of the supramolecular self-assembled nanostructures able to solubilize highly hydrophobic multilayered fullerenes (carbon nano-onions) is described. Small carbon nano-onions (6–12 shells) were prepared in high yields, functionalized with carboxylic groups by chemical oxidation and reacted with aminated β CDs. A biocompatible dextran polymer was employed for the layer-by-layer supramolecular self-assembly on the β CD-CNOs surfaces. β CD acts as a host molecule and ferrocene as a guest grafted into dextran backbone (Fc-Dex) allowing the formation of an inclusion complex. After their functionalization these

nanostructures showed excellent water solubility. Moreover, the deposition of the subsequent layers on the surface of the particles was studied using different methods. Through-space interactions between the Fc moieties and the CNOs core and the influence of an additional dextran- β CD outer layer were measured electrochemically.

Overall, the presented thesis has contributed to the development of a new class of polymeric nanomaterials based on supramolecular host-guest interactions. These well-organized nanomaterials were prepared in a controlled manner by simple layer-by-layer deposition technique in aqueous solutions. They were successfully implemented in enzyme-encapsulating particle-based signal enhancement tools in biosensors and also could be used for different biomedical applications. Moreover, the prepared highly soluble carbon based polymeric nanostructures opens up new possibilities for many other applications such as photovoltaics or molecular electronics where the dispersion of acceptor molecules plays an important role in device fabrication and performance.

CHAPTER 1

INTRODUCTION

1.1 SUPRAMOLECULAR CHEMISTRY

Supramolecular chemistry is defined by Lehn as the "... chemistry of molecular assemblies and of the intermolecular bond." In other words, supramolecular chemistry can be explained as "chemistry beyond the molecule", "the chemistry of the non-covalent bond", "non-molecular chemistry" or "Lego chemistry."¹

Supramolecular chemistry as we understand it today covers all the aspects of self-assembly. It covers the design and function of molecular devices and molecular assemblies, non-covalent polymers, and soft materials such as liquid crystals, informed nanoscale chemistry, and "bottom-up" nanotechnology. The current research on this topic is centered on increasing complexity and hence increasingly sophisticated functionality and on the information stored in molecular components that allow this complexity to be achieved. Therefore, supramolecular chemistry is focused on the interactions between molecules, based on a very wide variety of chemistry and materials science including molecular host-guest chemistry, solid-state host-guest chemistry, crystal engineering and the understanding and control of the molecular solid state (including crystal structure calculation), supramolecular devices, self-assembly and self-organization, soft materials, nanochemistry and nanotechnology, complex matter, and biological chemistry.²

Accordingly, the evolution of supramolecular chemistry can be traced from the original solid-state “clathrate” paradigm (Figure 1.1a), through the molecular host–guest paradigm (Figure 1.1b) to the self-assembly paradigm (Figure 1.1c).

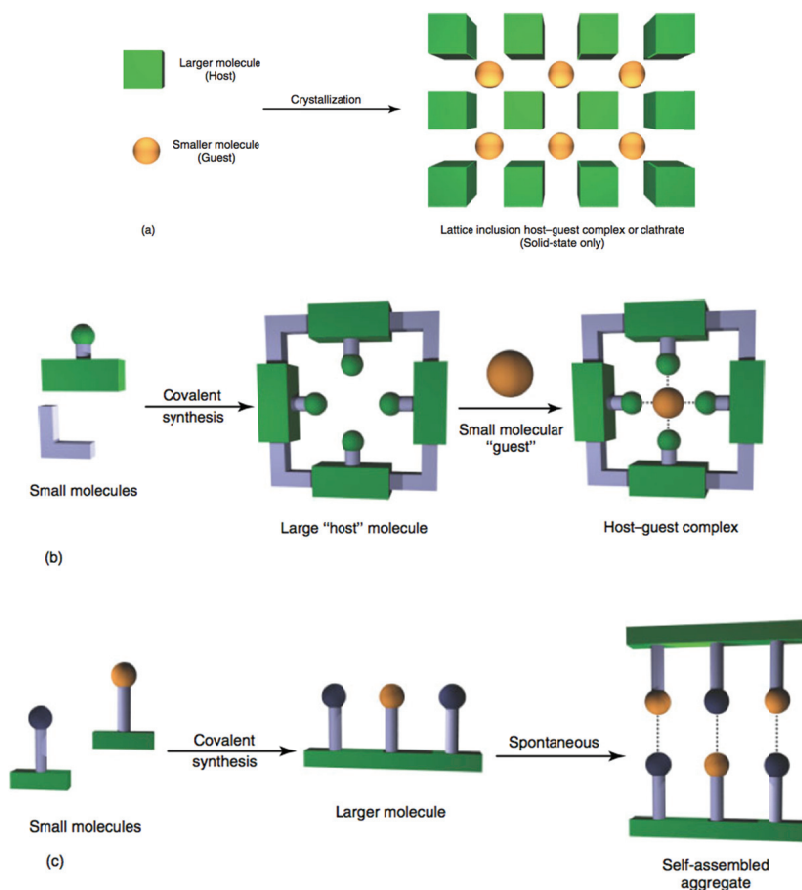


Figure 1.1. Key paradigms in supramolecular chemistry. (a) Solid-state clathrate paradigm, (b) molecular host–guest paradigm, and (c) self-assembly paradigm.²

In other words, a sense of modularity is the key for better understanding the whole meaning of supramolecular chemistry as it involves the mutual non-covalent type of interactions between molecules or molecular entities with

discrete properties. These type of interactions form “supermolecules” or aggregates in which a number of components (of one or more type) come together, either spontaneously or by design, to form larger materials with properties derived from those of its components. These aggregates can be of the host-guest type in which one molecule encapsulates the other. They can also involve mutually complementary or self-complementary components of similar size in which there is no host or guest.²

The host molecule possesses convergent binding sites, typically Lewis basic donor atoms, hydrogen bond donors, natural or synthetic cyclic compounds with a cavity or central hole of specific size, etc. On the other hand, the guest molecule possesses divergent binding sites such as Lewis acidic metal cations, hydrogen-bond-accepting halide anion, an ion pair, or more complex molecules with a shape and size compatible with a cavity. The binding side is defined as a region of the host or guest capable of taking part in a non-covalent interaction.^{2,6}

All this information was concisely summarized by one of the founders of the field of supramolecular chemistry, Donald James Cram and in his definition he states the following:³

“Complexes are composed of two or more molecules or ions held together in unique structural relationships by electrostatic forces other than those of full covalent bonds ... molecular complexes are usually held together by hydrogen bonding, by ion pairing, by π -acid to π -base interactions, by metal-to-ligand binding, by van der Waals attractive forces, by solvent reorganizing, and by partially made and broken covalent bonds (transition states) ... High structural organization is usually produced only through multiple binding sites ... A highly structured molecular complex is composed of at least one host and one guest

component ... A host-guest relationship involves a complementary stereo-electronic arrangement of binding sites in host and guest ... The host component is defined as an organic molecule or ion whose binding sites converge in the complex ... The guest component as any molecule or ion whose binding sites diverge in the complex ..."

Nevertheless, as he refers to the host molecule as to an organic molecule or ion, recent work in the area of supramolecular complexes shows as well the existence of inorganic hosts, such as zeolites⁴ and polyoxometallates,⁵ or mixed metal-organic coordination compounds, such as metal-organic frameworks (MOFs).²

A good example of forming supramolecular, strong inclusion complexes based on host-guest interactions is cyclodextrin (CD) molecule and its guests. These unique complexes will be explained in more detail in the next chapters.

1.2 STRUCTURE AND APPLICATIONS OF CYCLODEXTRINS

CHEMICAL STRUCTURE OF CYCLODEXTRINS.

Cyclodextrins are a family of cyclic oligosaccharides composed of α -(1,4)-linked D-glucopyranose units in the 4C_1 chair conformation possessing a conical and hydrophobic cavity (Figure 1.2).⁷

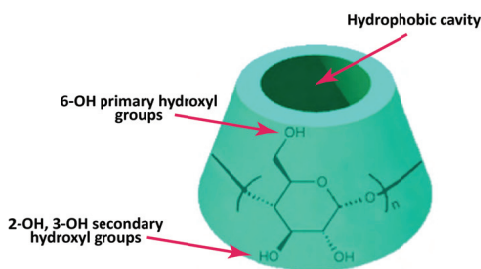


Figure 1.2. Chemical structure of CD, where $n = 6, 7,$ and 8 represents α -, β -, and γ -CD, respectively.⁸

The better-known members of the family are α -, β - and γ -CDs, which have six, seven and eight D-glucopyranose units, respectively. CDs are produced industrially by the action of a family of enzymes called cyclodextrin glucosyltransferases (CGTases) on starch. CGTases are produced by several microorganisms such as *Bacillus macerans* and *Bacillus circulans* and catalyze the cleavage and subsequent cyclization of linear α -(1-4)-linked gluco-polysaccharides. Although a number of larger CDs exist it is very difficult to isolate them on a commercial scale. Therefore, the production of CDs is limited to the three smaller members α -, β - and γ -CD. Additionally, no CDs less than five glucose units have been reported so far due to the ring strain.⁷⁻⁹ All of the three types of CDs are truncated cone-shaped molecules with a hollow, tapered cavity, which is limited by hydroxyl groups of a different chemical character. The primary alcohol groups C₆-OH are located at the narrower side of the cone and come from position 6 of the glucopyranose unit, whereas the secondary hydroxyl groups C₂-OH and C₃-OH are located at the wider entrance and are less prone to chemical reactions. The reactivity of the hydroxyl groups strongly depends on the reaction conditions, which should be selected carefully in order to avoid the substitution of more groups than those needed for a particular purpose. The interior of the CD is primarily constituted of hydrogen atoms and the oxygen bonds linking the glucopyranose units. This leads to a relative hydrophobic cavity, while the exterior is hydrophilic due to the presence of the alcohol groups (Figure 1.2).^{10,11} The inner diameter of the cavity in unmodified cyclodextrins varies from 5 to 10 Å, and it is about 8 Å in depth. These dimensions allow the inclusion of several types of guest molecules of appropriate size to form

inclusion complexes with relatively high stability constants ($10^4 - 10^5 \text{ M}^{-1}$).^{7,9-12}

In cyclodextrin chemistry, the intramolecular interaction between CD and guest can lead to the partial or complete penetration of the guest molecule into the cavity of the CD. Moreover, an encapsulation interaction can occur if some guest molecules only reside in the packing interstice of CD. Undeniably, host-guest complexation is the main driving force of inclusion phenomena between CD and guest. It has been established in the past that the process of inclusion complexation between CD and guest is driven by electrostatic forces, van der Waals forces, hydrophobic interactions, hydrogen bonding and release of conformational strain. It is interesting that these driving forces always coexist or have a synergistic effect. The relative strength of each force is usually related with the guest type. More specifically, the size of the CD cavity and the nature of modified groups of CD; the shape, volume, polarity, number and character of substituting groups of guest, as well as reaction medium, temperature, ionic strength and other factors will affect the form and relative strength of these forces. CD molecule exists in the form of a hydrate in aqueous solution and always accommodates several water molecules in a disordered network using its cavity as binding site. When guests are added into the system, water molecules included in the CD cavity may be partially or completely excluded from the cavity by these guests. Hence, in a few CD inclusion systems some of the guests can be incorporated in the sandwich structure formed by intermolecular hydrogen bonds between two CD molecules or stay completely out of the cavity. The guest molecules lying outside the CD cavity may be able to change the spectroscopic properties of CD or in some cases the physical properties of

the guests may also be altered. Sometimes there is no actual inclusion of the guest in the cavity; this kind of interaction can be defined as an encapsulation interaction and takes place mainly in the solid state. Figures 1.3 and 1.4 show the differences between inclusion complexation and encapsulation interaction, depending whether the guest is included in the cavity of CD or not.¹³

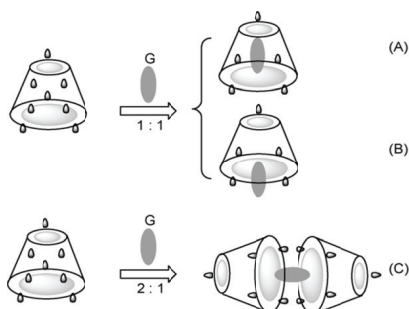


Figure 1.3. The three kinds of the most common inclusion complexes between CD and guests.¹³

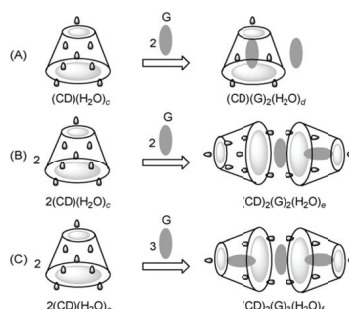


Figure 1.4. The three kinds of encapsulation interaction accompanying inclusion complexation between β CD and guests.¹³

APPLICATIONS OF CYCLODEXTRINS.

Cyclodextrins, due to their very low toxicity, excellent biocompatibility and good complexation capacity with a variety of lipophilic molecules, are among the most widely employed host units to construct assemblies for agrochemical, food, cosmetic, research and biomedical applications.¹¹ Nowadays, the pharmaceutical industries have several advantages from using CDs for the drugs formulation. One of them is an increase of the solubility and what comes with it the bioavailability of the drug formulated with CDs. Moreover, CDs may also constitute as a unique stabilizers for the drug against enzymatic or chemical degradation. There are about 35 drug

formulations containing CDs or their derivatives on the market today.¹⁴ CDs can also act as chaperones for enzymes, hence preventing their premature folding and aggregation, what plays crucial role for their activity and functionality.⁷⁻⁹

1.3 CYCLODEXTRIN CONTAINING POLYMERS.

Even though, β CD is the cheapest type of all CDs, it has low water solubility and it can be toxic when injected intravenously. Furthermore, the native CDs cannot form inclusion complexes with hydrophilic or high-molecular-weight molecules. Thus, many chemical modifications of cyclodextrins have been studied to overcome these limitations.

CDs can be incorporated into larger covalently linked structures, such as dimers, trimers or even cyclodextrin polymers.¹⁶ They can be prepared by cross-linking the cyclodextrin rings, by polymerizing bifunctional substituents containing cyclodextrin derivatives, or linking cyclodextrins to a polymer backbone.¹⁷ These modifications may alter their solubility or other chemical properties and provides new opportunities for their future applications.

In fact, CD-polymers have attracted the interest of many scientific branches and industries. Improvement in the polymerization of CDs allowed researchers to synthesize CD-polymers with tailored architectures adjusted for various biomedical needs. Depending on the future function for the CD-polymers, different types can be designed and synthesized. The main types of CD-polymers are described below.

CROSS-LINKED AND BRANCHED CD-POLYMERS.

This type of CD-polymers can be synthesized by using appropriate cross-linking agents, such as aldehydes, ketones, allyl halides, isocyanates, epoxides (e.g. epichlorohydrin, ethyleneglycol, diepoxypropyl ether), etc.¹⁷ Although, they are fairly easy to synthesize, the main drawback of this method is that the structure of cross-linked or branched CD-polymer cannot be well defined. The distinction between cross-linked and branched CD-polymer relay in their differences in aqueous solubility. Generally speaking, branched CD-polymers are soluble and cross-linked CD-polymers become insoluble in water.¹⁸ However, some of these randomly cross-linked polymers are water-soluble; for example, low molecular weight epichlorohydrin cross-linked β CD has higher aqueous solubility than β CD itself. Therefore, the aqueous solubility of the CD-polymers highly depends on their degree of cross-linking. By controlling the reaction conditions, e.g. concentration of reactants, stoichiometry, reaction time, etc. we can obtain either water soluble or insoluble CD-polymers.¹¹

The most thoroughly studied cross-linking agent for synthesizing CD-polymers is epichlorohydrin. The synthesis reaction of CDs with epichlorohydrin in alkaline solution is also very well described in the literature. The commercially available CD-polymers with epichlorohydrin have molecular weights in the range 3000-6000 Da. The main advantage of the synthesis of this soluble polymer is that the starting materials are inexpensive and production on a large scale is also possible.¹⁸

The other type of cross-linked CD-polymers is called cyclodextrin nanosponges. It is a novel nanostructured material consisting of hyper cross-linked CDs. This new intriguing material shows many important

characteristics, e.g. capacity to encapsulate a great variety of substances that can be transported through aqueous media or, from the opposite perspective, removed from contaminated water. As a result, they could act as very efficient tool for either removing pollutants from water or carrying substances for biomedical applications. Thanks to their capacity to complex various molecules, nanosponges have been proposed as very efficient drug delivery systems.^{19,20}

Although, the reaction conditions allow the organic chemists to control to some extent the degree of cross-linking between the CDs, the main drawbacks remain that the outcome can be both unpredictable and difficult to reproduce.¹⁸ However, this type of β CD hyper-cross-linked polymer (CD nanosponge) with “free” carboxylic groups was prepared by Trotta and coworkers. They cross-linked β CD with pyromellitic anhydride and described it as the microscopic and almost spherical shape particles (Figure 1.5).¹⁹

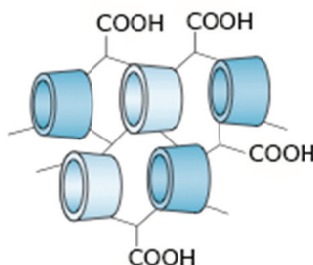


Figure 1.5. Schematic structure of CD nanosponges.¹¹

This particular type of CD polymer will be described in much more details in Section 3.

LINEAR POLYMERS WITH PENDANT CDs.

Other classes of CD-containing polymers are those that contain CDs as pendent moieties of the polymer backbone (Figure 1.6). These types of polymers have been prepared by using various polymer backbones and functionalized CDs.¹¹ The polymer of interest can be attached to the CD-derivatives by either radical polymerization of vinyl- or acrylic CD-monomers or simply by grafting mono functionalized CDs. Recent methods for the synthesis of linear polymers with pendant CDs include: atom transfer radical polymerization (ATRP), ring opening polymerization and nitroxide-mediated living radical polymerization.^{18,21}

Nevertheless, the main disadvantage from synthesizing this type of CD-polymers is the need of pure mono functionalized CDs. In order to obtain linear and water soluble polymer with pendant CDs, the purification process of mono functionalized CDs very often involves preparative chromatography techniques. This is not only a challenging task but also time consuming and preparation on a larger scale could be very difficult.¹⁸

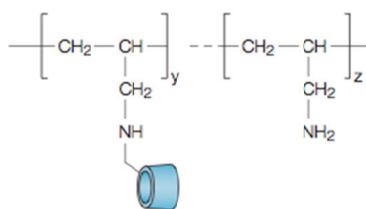


Figure 1.6. Schematic representation of poly-allylamine with pendant CDs.¹¹

TUBULAR CD-POLYMERS.

The third example of the CD-containing polymers have a tubular structure (Figure 1.7) that is formed using molecules or other linear polymers that

organize the CDs into a tubular configuration to form a cylinder-like structure. Threading CDs onto polyethylene glycol polymer chain is one example of this approach. The polymers are then formed from the tubular configurations by crosslinking between the CDs. The tubular structures need not be isolated as shown in Figure 1.7, but can form bundles because the crosslinking can occur not only in the axial direction of the tube, but perpendicular to that direction as well. This class of tubular polymers is actually an ordered sub-class of cross-linked polymers, and the two types of polymers might therefore show similar behavior when used as drug delivery vehicles, although, there are no reports in use of them in biomedical science so far.^{11,18} On the other hand, there are existing reports on employing this types of polymers as molecular sensors and catalysts.^{18,22}

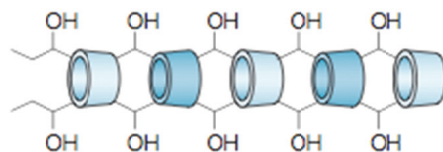


Figure 1.7. Schematic representation of tubular CD-polymer.¹¹

LINEAR CD-POLYMERS.

The last class of CD-containing polymers is composed of linear CD-polymers and has CD as part of the backbone (Figure 1.8). For the successful preparation of this type of CD-containing polymer the synthesis of a di-functionalized CD-containing co-monomer is needed.¹¹ However, their production is extremely difficult due to need of multi step synthesis of di-functionalized CDs involving extensive purification in between each step.¹⁸

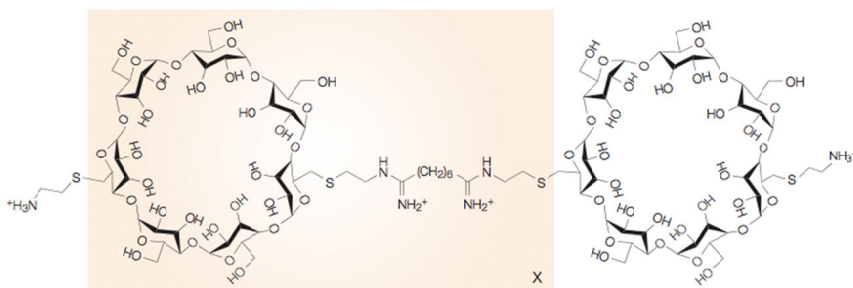


Figure 1.8. Schematic representation of a linear cyclodextrin polymer.¹¹

Other existing types of CD-polymers are known as star polymers, CD based artificial ion channels and “click” clusters. In this class of CD-polymers, CDs are not part of the polymers but they only act as synthetic scaffolds.¹⁸

1.4 CYCLODEXTRIN BASED NANOSPONGES.

As briefly mentioned in a previous section cyclodextrin nanospoenges are fairly new innovations in cross-linked cyclodextrin polymers. These are nanostructured porous insoluble particles with a crystalline or amorphous structure and spherical shape showing swelling properties. They can be obtained from α -, β - and γ -cyclodextrins, either alone or as mixtures containing relevant amounts of linear dextrin, cross-linked with a suitable cross-linking agent. Their name “cyclodextrin nanospoenges” appeared in the literature for the first time in 1998 and was reported by DeQuan Li and Min Ma.¹⁵ Preparation of those insoluble multifunctional cyclodextrin derivatives involves cross-linking of the native cyclodextrin with organic diisocyanates

leading to an insoluble network that shows a very high inclusion constant with several organic molecules.¹⁶

However, the main properties of this type of cyclodextrin nanosponges were centered on the water treatment and they succeeded in being more effective than active carbon. For the first time Troтта and co-workers reported a new type of cyclodextrin nanosponges, which showed new functions mainly as drug carriers. They can be synthesized by using an active carbonyl compound, e.g., carbonyldiimidazole, triphosgene, diphenyl carbonate, or organic dianhydrides producing cyclodextrin carbonate- and cyclodextrin carboxylate nanosponges (Figure 1.9).¹⁶

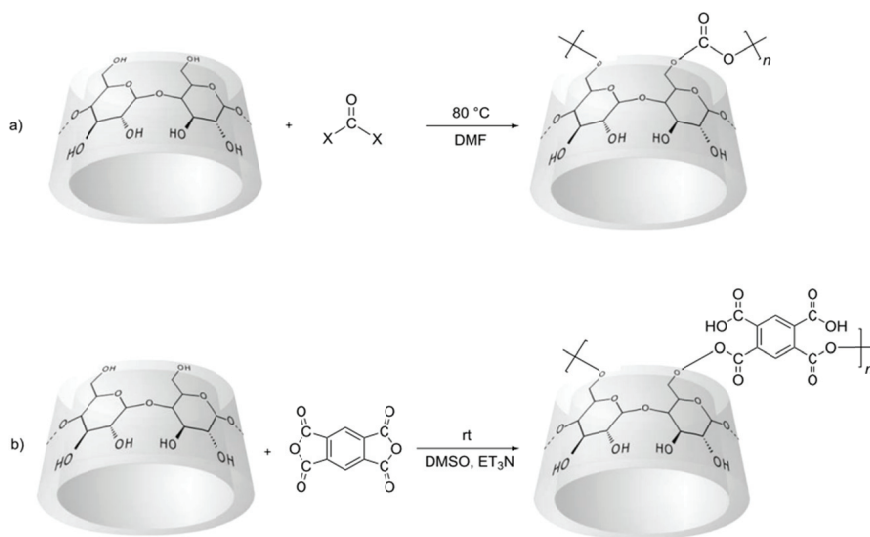


Figure 1.9. Synthetic routes to cyclodextrin nanosponges. (a) Cyclodextrin carbonate nanosponges. (b) Cyclodextrin carboxylate nanosponges.¹⁶

In these reactions the primary hydroxyl groups are mainly involved in the formation of the cross-linking network. The final product is a fine powder consisting of cyclodextrin connected by nanochannels to form a cage-like structure (Figure 1.10.)¹⁶

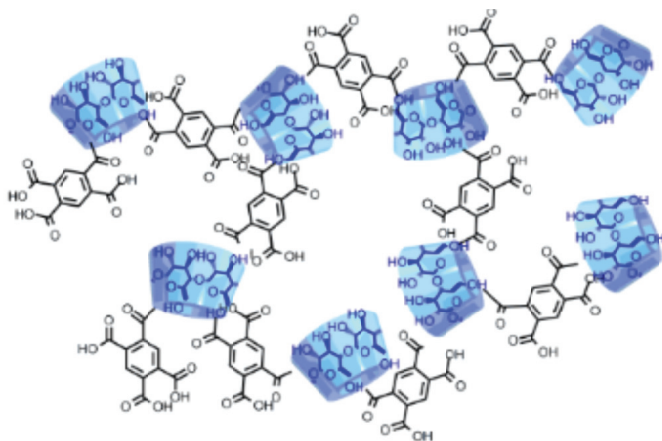


Figure 1.10. Proposed structure of cyclodextrin carboxylate nanosponges.¹⁶

The channels between the cyclodextrin molecules can be tuned by changing the reaction conditions, for instance: the type of cyclodextrin or the amount of the cross-linking agent being used. This also influences the formation of the porous network what has further impact on their solubility as well as the inclusion complexation capacity. The big advantage of this multichannel network in nanosponges over the native cyclodextrin molecules is that they show different mesh polarities (hydrophobic cyclodextrin cavities surrounded by hydrophilic nanochannels of the polymeric network) thereby enabling significant interactions between molecules with different lipophilicities and structures.¹⁶

By cross-linking pyromellitic anhydride or other dianhydrides with a chosen type of cyclodextrin Trota *et al.* have been able to produce acidic nanosponges with free carboxylic groups, thus forming cation exchange sites. The fact that these structures possess additional hydroxyl groups in their network allows for their even further surface modification. Therefore, carboxylated nanosponges could be also synthesized by reacting carbonate nanosponges with succinic anhydride.¹⁶

The two main classes of cyclodextrin nanosponges, cyclodextrin carbonate nanosponges and cyclodextrin carboxylate nanosponges show different physicochemical properties. Cyclodextrin carboxylated nanosponges are less chemically and thermally stable, but can swell more than 30-fold in water. They also have more negative zeta potential when compared to the cyclodextrin carbonate nanosponges and can simultaneously host cations, organic molecules and even macromolecules.¹⁶

Nanosponges have colloidal sizes with a mean diameter of less than 1 μm and narrow size distribution and form opalescent suspensions on dispersion in water. However, it is also possible to synthesize nanosponges with a mean diameter in the range of 200–300 nm.¹⁶

The manufacturing process of cyclodextrin nanosponges is very flexible, cheap and effective. They have been proved to be great enhancers in solubility of different molecules; they possess very good encapsulation properties and are non-toxic. Therefore, cyclodextrin nanosponges are a new window for many applications in pharmacy, medicine, agriculture, cosmetics and environment. They are also being great potential drug carriers of active molecules in nanomedicine.¹⁶

1.5 POLYMER BASED MICRO- AND NANO-CAPSULES.

Polymeric micro- and nano- capsules are vesicle-like architectures made of a polymeric wall encapsulating a liquid core. The walls can be made of natural or synthetic polymers. The most common used natural polymers are chitosan, gelatin or sodium alginate, while examples of synthetic polymers include poly (acrylic acid), polyesters or polylactones. In contrast to liposomes, polymeric capsules are permeable to polar molecules and are much more chemically and physically resistant. Organic and inorganic particles, oil droplets and even biological cells can be used as templates for capsule fabrication. The size of the resulting capsules strongly depends on the template employed and on the number of polymeric layers deposited on its surface.²³

LAYER-BY-LAYER (LBL) SELF-ASSEMBLY

Self-assembly is a process that occurs due to the spontaneous and uninstructed structural reorganization that forms from a disordered system. Such processes are reversible and held together by non-covalent intermolecular forces. As explained previously in first section, this area of study belonging to non-covalent molecular interactions is referred to as supramolecular chemistry, and it has important implications with regards to the formation of well-organized structures. Self-assembled surface monolayers have very unique properties that are useful for the fabrication of various devices. For instance, if the monolayer is conductive, it results in a two dimensional conductive sheet. This concept can be extended to three-dimensional structures if a stack or a collection of monolayers can be achieved. This is where layer-by-layer (LbL) self-assembly plays a role.²⁴

The LbL method allows the construction of a thin film atop a substrate of almost any composition or topology by alternating its exposure to solutions containing species of complementary affinities. LbL assembly is mostly achieved by exploiting attractive forces and by alternating immersions, so that the multilayer films are attained. This method, initially developed to prepare multilayer assemblies electrostatically, has been successfully extended to various other driving forces, such as hydrogen bonding, charge transfer, acid-base pairs, metal-ion coordination, intermolecular interactions in the dried state, covalent bonds, bio specific interactions (e.g. sugar-lectin interactions) and finally host-guest interactions. LbL assembly has been achieved with a large number of materials including polymers, inorganic particles, clay, organic components, carbon nanotubes, dendrimers, and biological macromolecules such as proteins and DNA.^{25,26} In this technique we can employ either polyelectrolytes or neutral polymers for the fabrication of multilayered hollow capsules. Some of the advantages and disadvantages from electrostatically or supramolecularly engineered capsules are described below.

POLYELECTROLYTE MICROCAPSULES.

Polyelectrolytes are polymers with ionizable groups. In polar solvents such as water, these groups can dissociate, leaving charges on polymer chains and releasing counter ions in solution. Examples of polyelectrolytes include polystyrene sulfonate, polyacrylic and polymethacrylic acids and their salts, DNA and other polyacids and polybases.²⁷

Polyelectrolyte chains at surfaces and interfaces represent an example of both two- and three dimensional polyelectrolyte solutions in which the local

polymer concentration is controlled by interactions between adsorbing substrate and polyelectrolyte chains. As the surface charge density increases, the dilute solution of adsorbed chains transforms into a two-dimensional semi dilute solution. If the surface charge density increases even further, the chains in the adsorbed layer form a concentrated polyelectrolyte solution with thickness increasing with surface charge density. The new and unusual phenomenon observed in the adsorbed layers is the surface overcharging (overcompensation of surface charge) by adsorbed polyelectrolyte chains. The amount of surface overcharging can be tuned by varying the solution ionic strength. The charge inversion plays a central role in the layer-by-layer deposition technique. This self-assembly method has been introduced for fabrication of the molecularly layered multicomposite films with a high degree of complexity. The film growth is achieved by alternating the deposition of polyanions and polycations from their aqueous solutions. The simplicity of the electrostatic assembly technique with practically no limitations on the shape of charge bearing species allows fabrication of multilayer films from synthetic polyelectrolytes, DNA, proteins, inorganic platelets, nanoparticles, and viruses.²⁷

Polyelectrolyte capsules fabricated by layer-by-layer adsorption technique are based on the consecutive assembly of oppositely charged synthetic polymer layers around a preformed charged spherical core. Fundamentally, the two main components for capsule fabrication are the core templates and the polyelectrolyte pairs. At the end of the LbL adsorption process, the cores can be successfully removed to obtain hollow and stable capsules whose inner cavity and polymer wall can be loaded and functionalized, respectively, with a variety of substances such as molecular dyes, drugs, nanoparticles and

biomolecules, which retain their distinctive properties after the embedding procedure (Figure 1.11).²⁸

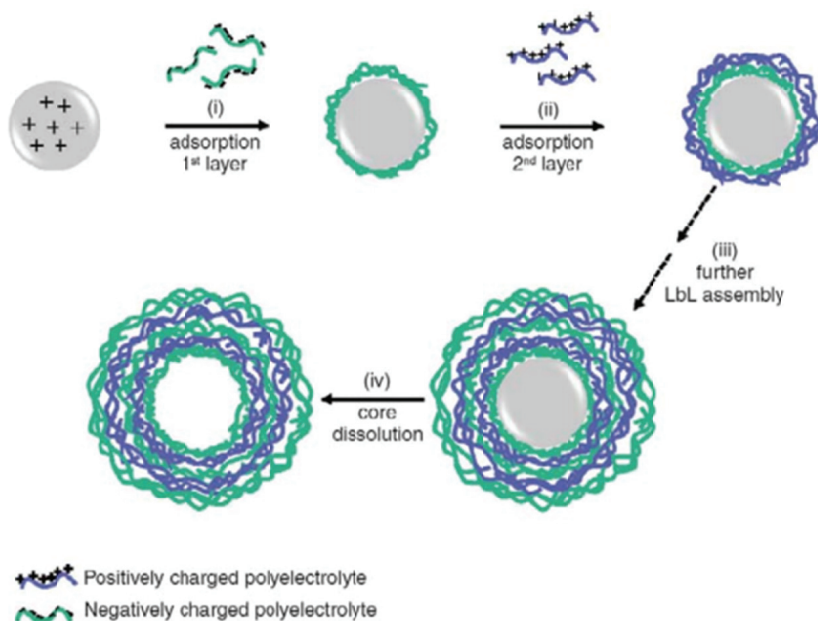


Figure 1.11. Polyelectrolyte capsule fabrication by layer-by-layer (LbL) assembly. (i) Initial electrostatic adsorption of a negatively charged polymer onto a positively charged template core. (ii) Second adsorption of positively charged polymer onto the now negatively charged template. (iii) Multilayer growth via alternating adsorption of oppositely charged polymers. (iv) Removal of the template by dissolution to obtain a capsule with an empty cavity. Capsules are not drawn to scale.²⁸

The resulting hollow capsules usually have a wall thickness between a few tens and several hundreds of nanometers and a diameter ranging from tens of nanometers to several micrometers depending, on the size of the original core.²⁸

An ideal template has to be stable under the LbL process, soluble in mild conditions, and completely removable from the inside of the capsules,

without affecting the morphology and stability of the multilayer assembled on top of it. The capsule wall composition also plays a crucial role for the fabrication of functional capsules, as their permeability/porosity strongly depends on the chemical structure and the molecular weight of the employed polyelectrolyte pairs. The majority of polyelectrolyte capsules described in the literature are composed of pairs of synthetic anionic poly (sodium) styrene sulfonate and cationic poly (allylamine) hydrochloride. These multilayers are known to have numerous advantages, but for therapeutic purposes there is a special interest in using more biocompatible materials, which are potentially biodegradable under physiological conditions.²⁸ Additionally, polyelectrolyte microcapsules are limited to the building blocks with a narrow range of charged species. As it is already proven, electrostatic interactions are generally strong enough to hold the integrity of LbL microcapsules, but they are still susceptible to high ionic strength, extreme pH and strong polar organic solvents, and the properties of microcapsules may thus become adverse, consequently influencing their applications.²⁹ Therefore, other materials that can be potentially more stable in such environments and synthesized using milder reaction conditions are still desirable.

SUPRAMOLECULARLY ENGINEERED NANO-CAPSULES.

Recently, the multilayer hollow microcapsules based on different driving forces such as covalent bonding, base pair interactions, van de Waals interactions and guest–host interactions have been fabricated, which show unique properties.

swelling and shrinking behavior. With these smart features, the microcapsules can serve as reservoirs for drugs, DNAs, enzymes, etc.²⁹

Using cyclodextrin-containing polymers became very attractive approach to construct host-guest nano-assemblies because of their excellent biocompatibility, complexation capacity, and chemical-sensitivity. Such nanocarriers may be advantageous also because of the broad availability of cyclodextrins, their flexibility for structure/property modulation and their chemical-responsive characteristics. There is wide variety of polymers that can be modified with either host or guest molecules and thus used as building blocks for the formation of core-shell structures.⁸

Importantly, the ease of chemical modification of this wide range of available polymers makes it possible to synthesize structures with desired properties to form stimulus-responsive assemblies. They have emerged as promising carriers that may enhance the therapeutic efficacy and minimize many side effects. Compared with other systems, chemical-sensitive assemblies can more conveniently achieve their responsive function by utilizing the biological or chemical signals that are specific to cells, tissues, organs, or disease sites. Alternatively, the administration of another compound can trigger the release of payload to achieve its therapeutic effect. Due to the reversibility of the host-guest interactions between the β CD and hydrophobic guests, the supramolecular systems based on such non-covalent interactions frequently display chemical-sensitivity.⁸

Supramolecular delivery systems are considered the most promising carriers for drug and gene delivery as well as other biomedical applications. This can be attributed to their high biocompatibility, prolonged circulation in bloodstream, broad payload spectrum from small molecules to

biomacromolecules, unique size characteristics for tissue permeability and passive targeting as well as cellular endocytosis and organelle translocation, excellent formulation capability, easy tailoring/decoration for active targeting, and facile control of cargo release by the delicate molecular design. Introducing the host CDs into nanocarriers can further enhance the biocompatibility and lower the in vitro/in vivo toxicity, and increase the convenience for additional surface functionalization.⁸

1.6 CARBON NANO MATERIALS – (A VERY) BRIEF DESCRIPTION.

The term *nanotechnology* was originated in 1974 by Japanese professor of Tokyo University of Science Norio Taniguchi. Since then nanotechnology has become the fastest growing discipline and the shooting star in materials science and engineering. Its impact can be seen in everyday products with improved or novel properties and is widely present in the news and popular media. The field of nanotechnology is massive and is ranging from high-performance computer chips and UV-blocking sun care cosmetics to nature's very own nanotechnology including the adhesion of gecko feet even to smooth surfaces or the incredible strength of spider webs. Thanks to high-resolution characterization techniques and advanced computer modeling scientists started to understand the bottom line of the "nano world" so that they can exploit its unique phenomena and use material properties for making nanoscale devices.³⁰

Since the discovery of carbon nanomaterials, such as fullerenes, carbon nanotubes or graphene, carbon nanotechnology has gained significant attention. Undoubtedly, carbon is the most versatile element in the periodic table with a large variety of allotropes and structures of various

dimensionalities. Certain carbon allotropes as being advanced materials possess unique properties, in nanoscale, leading to unprecedented functions with numerous applications. The broad range of applications of carbon include energy or gas storage, catalysis, water treatment, medical implants, drug delivery, biofiltration, electronics, etc.³⁰

Examples of these carbon allotropes include, but are not limited to: nanodiamond, fullerene, carbon onion, carbon nanotubes, and graphene (Figure 1.13).³¹

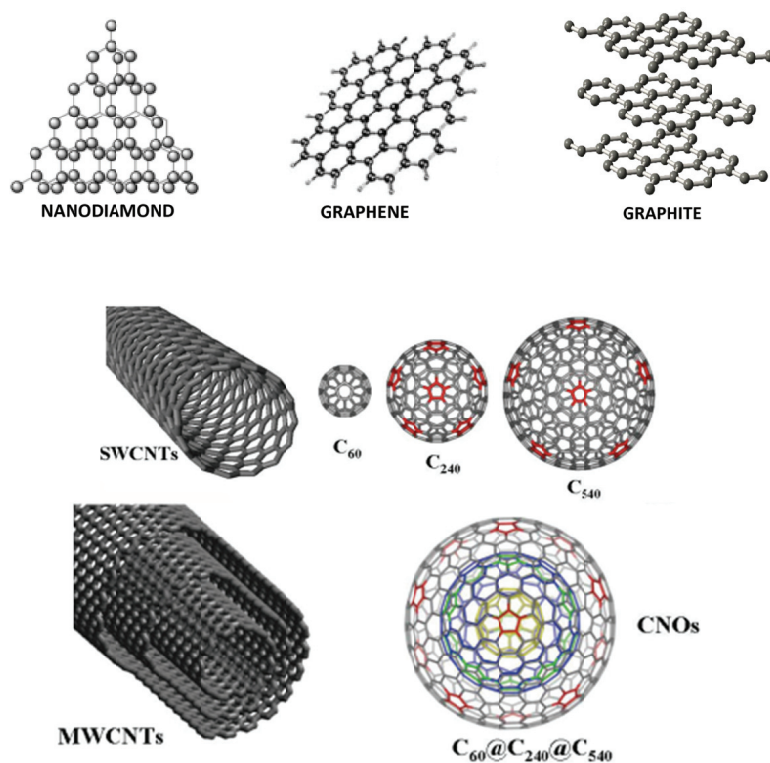


Figure 1.13. Examples of carbon-based nanomaterials, nanodiamonds,³² graphene,³¹ graphite,³⁴ single-walled carbon nanotubes (SWCNTs), multi-walled carbon nanotubes (MWCNTs), fullerenes (C₆₀, C₂₄₀ and C₅₄₀) and a carbon nano-onion (CNO).³³

Carbon is the closest chemical element to the human being. It was essential for the appearance of life in our planet and it is present in a large extent in our body. In the current nanoscience and nanotechnology revolution that we are watching, carbon has undoubtedly a prominent role and plays an important role in our lives.³³

As stated above carbon has many allotropes and some of them can be described as follow:

- Nanodiamond is a diamond that originates from detonation. In other words, nanodiamonds are 5 nm particles formed from oxygen-deficient explosive mixture of TNT/RDX, detonated in a closed chamber. It can be used for the production of carbon nano onions by annealing nanodiamonds with extremely high temperatures. Carbon nano onions will be explained in more details in the next chapter.³⁶
 - Graphene is a flat monolayer of carbon atoms tightly packed into a two-dimensional (2D) honeycomb structure made out of hexagons, and is a basic building block for graphitic materials of all other dimensionalities. It can be wrapped up into fullerenes, rolled into nanotubes or stacked into graphite.³⁴
 - Thanks to the very fast growing interest in research in carbon chemistry fullerenes and carbon nanotubes are already very well known in comparison with other carbon allotropes. It is clear that the incorporation of these systems in practical applications requires the development of larger-scale production methods, already implemented for carbon nanotubes.³³ Fullerenes are molecules where carbon atoms are arranged spherically and from the physical point of view, are zero-dimensional objects (0D) with discrete energy states. Fullerenes can be
-

obtained from graphene with the introduction of pentagons (that create positive curvature defects), so that fullerenes can be thought as wrapped up graphene.³⁴ Among already known species of fullerenes, C₆₀ with distinctive symmetrical carbon cage structure have been the object of intense research. Fullerene reactivity has been widely described in the literature but it is still possible to discover new reactions on the fullerene surface. Fortunately, this will lead scientists to the better understanding of the chemical reactivity of other new carbon allotropes present and will help in predicting the properties expected for these new carbonaceous structures in different disciplines.³³

- Carbon nanotubes are one-dimensional objects (1D) build from hexagons. They can be obtained by rolling graphene along a given direction and reconnecting the carbon bonds. Graphite is a three-dimensional (3D) allotrope of carbon is made out of stacks of graphene layers that are weakly coupled by van der Waals forces.³⁴

1.7 OVERVIEW OF CARBON NANO ONIONS.

Carbon nano-onions (CNOs) (Figure 1.13) can be described as quasi-spherical multi-shelled fullerenes often compared to the Russian dolls. The number of onion shells can be presented by the series: C₆₀@C₂₄₀@C₅₄₀@C₉₆₀@C₁₅₀₀@C_{60n²}..., where n is the shell number.^{33,35} Depending on the preparation method, CNOs are typically 3 – 50 nm in diameter with successive layers of graphene around a hollow or filled core 0.7 – 5 nm in diameter. They have high conductivity and relatively large specific surface area, with unique physical properties, and have been widely investigated.⁴⁸

The main production methods of CNOs are carbon arc discharge in deionized water,⁴⁹ thermal annealing of nano-diamond at 1100–1500 °C,⁵⁰ and recently reported catalytic cracking of methane.^{48,51} CNOs obtained by annealing carbon nanodiamond particles at high temperatures or by arcing between two graphite electrodes under water are different in terms of physical properties and chemical reactivity.

Only a few reports have been made so far, regarding the reactivity of CNOs. According to them, CNOs made by thermal annealing of nanodiamonds (N-CNOs) are more reactive than CNOs made by underwater arcing graphite (A-CNOs).^{33,35} The annealing of the ultradispersed nanodiamond particles (5 nm average) under vacuum produces mainly small CNOs with 6–12 shells (5 nm). The arcing of graphite under water, however, leads to the formation of large CNOs with diameters in the range of 15–25 nm (20–30 shells).³³ Other preparation methods described in the literature include: carbon-ion implantation at high temperature into copper substrates, thermal treatment of laser pyrolysis carbon blacks and co-sputtering, etc. However, most of these are rather low yield processes and have not been pursued further.³⁶ Nevertheless, many research groups have worked on the production of the CNOs for studies of the growth mechanism, yield, structural adjusting, and reduction of production cost over the past years.⁵⁷ Therefore, the annealing of nanodiamonds has been employed, for instance, by Echegoyen's group with relatively high yields and thus, led to the further study of carbon nano onions and their physical properties. In this method upon heating nanodiamonds above 900°C their outer surface undergoes graphitization. However, this temperature is not sufficient to remove all the remaining nanodiamond crystals from the core of the particle. Therefore, further

heating up to 1500°C transforms all nanodiamonds completely into graphitic structures. However, at temperatures of 1500–1800°C the existence of the separate onions becomes energetically less favorable than the formation of joint graphitic layers of neighboring onions. This results in the appearance of extended multi-shell graphitic cages with hollow centers as well as graphite-like ribbons with parallel graphitic planes. At the highest annealing temperatures (2100°C) nanodiamonds transform into a faceted multi-shelled structure.³⁶

However, many efforts have been made in the development of the techniques to synthesize CNOs, the as-prepared carbon nanomaterials have a lot of impurities, such as amorphous carbon, metal catalyst, and carbon nanotubes, which greatly affect the systematic studies on their properties. Therefore, purification of CNOs would cast a basis for the study of properties and applications of CNOs. Most studies have been focused on purification of CNTs and fullerene (C₆₀). In contrast, few reports can be found about purification and modification of CNOs. Although nondestructive physical and effective chemical separation and purification have their own advantages, the optimal purification method for CNOs seems to be an integration of both. Physical purification is carried out by different ways, such as centrifugal separation, ultrasonic concussion, and sublimation by virtue of difference in sizes, solubility in organic solvents and sublimation temperatures between CNOs and impurities. Chemical purification is achieved by the different oxidation resistances between CNOs and impurities.⁵⁷ Xu et al. reported the purification of raw CNOs by different ways, such as a two-step method including CS₂ separation and air oxidization,⁵⁸ HNO₃ refluxing,⁵⁹ and another two-step method including air oxidization and HCl refluxing.⁵⁷ Results

indicated that carbon nanotubes and CNOs were effectively separated, amorphous carbon and metal catalyst particles were removed by nitric acid treatment, and the purity of CNOs were improved, whereas, the structures of CNOs were not influenced.⁵⁷

Furthermore, the pristine CNOs are not readily dispersed in water and organic solvents in general, and they tend to aggregate like carbon nanotubes (CNTs) which have been solubilized using a variety of surfactants, for example polypropionylethylenimine co-ethylenimine (PPEI-EI),⁵² polyvinyl acetate-co-vinyl alcohol (PVA-VA),⁵³ polyvinyl pyrrolidone (PVP),⁵⁴ and phosphonated and sulfonated calixarenes.^{48,55,56} Thus, it is also very important to improve their dissolvability through surface modification, as their applications in many fields, such as photoelectricity, bio-medicine, and the chemical industry, have been influenced due to their inert chemical property and strong hydrophobicity.⁵⁷ In the recent years various functionalization reactions have been employed on CNOs, for instance: 1,3-dipolar cycloaddition reaction³⁷, amidation reactions³⁸⁻³⁹, [2+1] cycloaddition reactions, free-radical addition reactions³⁵, fluorination⁴⁰, polymerization^{38,41-42} or oxidation of defects³⁹ mainly in order to increase their extremely poor solubility in common organic solvents and in water but also to ease their physicochemical characterization.³⁶

Up to date, there are numbers of reports stating their increased solubility after surface modifications but it still remains the main issue for using them in a broad range of potential applications. Hence, CNOs are very promising materials for electronics,⁴³⁻⁴⁵ optics,⁴⁶ hyperlubricants,⁴⁰ energy conversion and storage.^{37,40,41,47}

More information about CNOs and their functionalizations will be included in the chapter 6.

1.8 THESIS OBJECTIVES

Supramolecular chemistry has emerged as a very powerful tool in the construction of novel nanometer-sized architectures with remarkable properties. The combination of covalent modification with a wide range of non-covalent interactions allows the fine tuning of nanomaterial properties and the creation of innovative and advanced materials with distinct applications.

The main objective of this thesis it to explore the possibility to combine the unique guest-complexing properties of cyclodextrins with polymeric materials to create novel nanoarchitectures.

To achieve this goal, we have focused on the following aspects:

- The preparation of novel cyclodextrin nanosponge immunoconjugates able to encapsulate the enzyme peroxidase with the aim to apply them as signal enhancement tool in optical and electrochemical bioassays.
- The proof-of-concept of the preparation of novel self-assembled nanoarchitectures based on the layer-by-layer deposition of complementary cyclodextrin and adamantane appended polymers on a gold nanoparticle template which upon redissolution would render nanocapsules with sufficient permeability to encapsulate low molecular weight compounds.
- The application of the above-mentioned concept in the construction of stimuli-responsive nanocapsules by selecting polymers modified with

guest units able to react to an external stimulus such as oxidation or light and a study of their encapsulation properties.

- The use of supramolecular interactions to achieve stable, water soluble preparations of carbon nano-onions, a highly hydrophobic carbon allotrope with unique properties, by modification of these materials by self-assembly of complementary cyclodextrin and ferrocene appended polymers.

This thesis is thus a contribution to the development of new classes of polymeric nanomaterials based on supramolecular host-guest interactions.

1.9 REFERENCES

1. J. M. Lehn, *Angew. Chem. Int. Ed. Engl.*, 1988, **27**, 89.
2. J. W. Steed, J. L. Atwood, P. A. Gale, *Supramol. Chem.: From Molecules to Nanomaterials*, John Wiley & Sons, Ltd., 2012
3. D. J. Cram, *Angew. Chem. Int. Ed. Engl.*, 1986, **25**, 1039.
4. R. Szostak, *Molecular Sieves*, Van Nostrand Reinhold, New York, 1989.
5. A. Muller, E. Krickemeyer, J. Meyer, *Angew. Chem. Int. Ed. Engl.*, 1995, **34**, 2122.
6. J. M. Lehn, *Supramol. Chem.*, 1st edn., Wiley-VCH Verlag GmbH, Weinheim, 1995.
7. R. Villalonga, R. Cao, A. Frago, *Chem. Rev.*, 2007, **107**, 3088.
8. J. Zhang, P. X. Ma, *Nano Today*, 2010, **5**, 337.
9. J. Szejtli, *Chem. Rev.*, 1998, **98**, 1743.
10. R. Holm, J. Ch. Madsen, W. Shi, K. L. Larsen, L. W. Ståde, P. Westh, *J. Incl. Phenom. Macrocycl. Chem.* 2011, **69**, 201.

11. M. E. Davis, M. E. Brewster, *Nat. Rev. Drug Disc.* 2004, **3**, 1023.
12. A. Frago, B. Sanromà, M. Ortiz, C.K. O'Sullivan, *Soft Matt.* 2009, **5**, 400.
13. L. X. Song, B. Lei, M. X. Xiao, H. Jian, Z. P. Shu, *Coord. Chem. Rev.*, 2009, **253**, 1276..
14. T. Loftsson, M. E. Brewster, *J. Pharm. Pharm. Sci.* 2010, **62**, 1607..
15. Li, D.; Ma, M. *Cyclodextrin polymer separation materials*. WO 9822197, May 28, 1998.
16. F. Trotta, M. Zanetti, R. Cavalli, *Beilstein J. Org. Chem.* 2012, **8**, 2091.
17. J. Szejtli, *Cyclodextrin technology*, Kluwer Academic Publishers, Netherlands, 1988.
18. T. T. Nielsen, *Ph.D. Dissertation, Aalborg University, Denmark*, 2010, p 12-15.
19. F. Trotta, R. Cavalli, *Composite Interfaces*, 2009, **16**, 39.
20. R. Cavalli, F. Trotta and V. Tumiatti, *J. Incl. Phenom. Macrocycl. Chem.* 2006 **56**, 209.
21. G. Wenz, *Angew. Chem. Int. Ed. Engl.* 1994, **33**, 803.
22. A. Harada, Y. Takashima, H. Yamaguchi, *Chem. Soc. Rev.*, 2009, **38**, 875.
23. E. Donath, G. B. Sukhorukov, F. Caruso, S. A. Davis, H. Möhwald, *Angew. Chem. Int. Ed.* 1998, **37**, 2201.
24. A. P.R. Johnston, C. Cortez, A. S. Angelatos, F. Caruso, *Curr. Op. Coll. Interf. Sci.* 2006, **11**, 203.
25. O. Crespo-Biel, B. Dordi, D. N. Reinhoudt, J. Huskens, *J. Am. Chem. Soc.* 2005, **127**, 7594.
26. A. Frago, B. Sanromà, M. Ortiz, C. K. O'Sullivan, *Soft Matt.* 2009, **5**, 400.
27. A. V. Dobrynin, M. Rubinstein, *Prog. Polym. Sci.*, 2005, **30**, 1049.

28. P. R. Gil, L. L. del Mercato, P. del_Pino, A. Muñoz_Javier, W. J. Parak, *NanoToday*, 2008, **3**, 12.
 29. W. Tong, Ch. Gao, *J. Mater. Chem.*, 2008, **18**, 3799.
 30. Y. Gogotsi, V. Presser, *Carbon nanomaterials*, 2nd edn., CRC Press, Taylor and Francis Group, 2014.
 31. Ch. Zhuo, Y. A. Levendis, *J. Appl. Polym. Sci. Rev.*, 2014, 39931.
 32. Z. Liu, X. J. Liang, *Theranostics* 2012, **2**, 235.
 33. J. L. Delgado, M. Á. Herranz, N. Martín, *J. Mater. Chem.*, 2008, **18**, 1417.
 34. A. H. Castro Neto, F. Guinea, N. M. R. Peres, K. S. Novoselov, A. K. Geim, *Rev. Mod. Phys.* 2009, **81**, 109.
 35. A. Palkar, F. Melin, C. M. Cardona, B. Elliott, A. K. Naskar, D. D. Edie, A. Kumbhar, L. Echegoyen, *Chem. Asian J.* 2007, **2**, 625.
 36. L. Echegoyen, A. Ortiz, M. N. Chaur, A. J. Palkar, *Chemistry of Nanocarbons*, 2010, John Wiley & Sons, Ltd.
 37. C. T. Cioffi, A. Palkar, F. Melin, A. Kumbhar, L. Echegoyen, M. Melle-Franco, F. Zerbetto, G. M. A. Rahman, Ch. Ehli, V. Sgobba, D. M. Guldi, M. Prato, *Chem. Eur. J.*, 2009, **15**, 4419.
 38. A. S. Rettenbacher, B. Elliott, J. S. Hudson, A. Amirkhania, L. Echegoyen, *Chem. Eur. J.*, 2006, **12**, 376.
 39. A. Palkar, A. Kumbhar, A. J. Athans, L. Echegoyen, *Chem. Mater.*, 2008, **20**, 1685.
 40. Y. Liu, R. L. Vander Wal, V. N. Khabashesku, *Chem. Mater.* 2007, **19**, 778.
 41. L. Zhou, Ch. Gao, D. Zhu, W. Xu, F. F. Chen, A. Palkar, L. Echegoyen, E. S.-W. Kong, *Chem. Eur. J.* 2009, **15**, 1389.
 42. K. Flavin, M. N. Chaur, L. Echegoyen, S. Giordani, *Org. Lett.* 2010, **12**, 840.
 43. M. E. Plonska-Brzezinska, L. Echegoyen, *J. Mat. Chem.*, 2013, **44**, 13703.
-

44. S. Sek, J. Breczko, M. E. Plonska-Brzezinska, L. Echegoyen, *Chem. Phys. Chem.*, 2013, **14**, 96.
45. M. S. Wang, D. Goldberg, Y. Bondo, *ACS Nano*, 2010, **4**, 4396.
46. V. L. Kuznetsov, S. I. Moseenkov, K. V. Elumeeva, T. V. Larina, V. F. Anufrienko, A. I. Romanenko, O. B. Anikeeva and E. N. Tkachev, *Phys. Status Solidi B*, 2011, **248**, 2572.
47. J. Luszczyn, M. E. Plonska-Brzezinska, A. Palkar, A. T. Dubis, A. Simionescu, D. T. Simionescu, B. Kalska-Szostko, K. Winkler, L. Echegoyen, *Chem. Eur. J.*, 2010, **16**, 4870.
48. F. M. Yasin, R. A. Boulos, B. Y. Hong, A. Cornejo, K. S. Iyer, L. Gao, H. T. Chua, C. L. Raston, *Chem. Comm.*, 2012, **48**, 10102.
49. N. Sano, H. Wang, M. Chhowalla, I. Alexandrou, G. A. J. Amaratunga, *Nature*, 2001, **414**, 506.
50. V. L. Kuznetsov, A. L. Chuvilin, Y. V. Butenko, I. Y. Malcov, V. M. Titov, *Chem. Phys. Lett.*, 1994, **222**, 43.
51. A. Cornejo, W. Zhang, L. Gao, R. R. Varsani, M. Saunders, K. S. Iyer, C. L. Raston and H. T. Chua, *Chem. Eur. J.*, 2011, **17**, 9188.
52. J. E. Riggs, Z. Guo, D. L. Carroll and Y. P. Sun, *J. Am. Chem. Soc.*, 2000, **122**, 5879.
53. S. S. Wong, E. Joselevich, A. T. Wooley, C. L. Cheung, C. M. Lieber, *Nature*, 1998, **394**, 52.
54. M. J. O'Connell, P. Boul, L. M. Ericson, C. Huffman, Y. Wang, E. Haroz, C. Kuper, J. Tour, K. D. Ausman, R. E. Smalley, *Chem. Phys. Lett.*, 2001, **342**, 265.
55. L. J. Hubble, T. E. Clark, M. Makha, C. L. Raston, *J. Mater. Chem.*, 2008, **18**, 5961.
-

56. I. Ling, Y. Alias, M. Makha, C. L. Raston, *New J. Chem.*, 2009, **33**, 1583.
57. X. Bing-she, *New Carbon Mat.*, 2008, **23**, 289.
58. B. Hui-qiang, H. Pei-de, L. Tian-bao, L. Tian-Bao, J. Hu-Sheng, L. Xu-Guang, X. Bing-She, *Acta Phys. Chim. Sin.*, 2005, **21**, 296.
59. S. Rui-ping, L. Guang-huan, L. Tian-bao, H. Pei-de, L. Xu-Guang, X. Bing-She, *Mat. Rev.*, 2006, **20**, 206.

CHAPTER 2

CYCLODEXTRIN NANOSPONGE IMMUNOCONJUGATES AS A SIGNAL ENHANCEMENT TOOL IN OPTICAL AND ELECTROCHEMICAL ASSAYS¹

2.1 ABSTRACT

Cyclodextrin nanospheres bearing carboxylate groups have been prepared by crosslinking β -cyclodextrin with pyromellitic dianhydride to form a carboxylic acid terminated nanoporous material. The surface of the particles was covalently modified with an anti-IgG antibody and then loaded with horseradish peroxidase. The structures of unmodified and protein modified nanosphere particles were investigated by Raman spectroscopy and imaging methods. Confocal microscopy indicates that the antibody is located in the outside of the particle while HRP is encapsulated in the inner part. The possibility to use these modified nanospheres as a signal enhancement tool in enzyme-linked colorimetric and electrochemical assays was evaluated using a sandwich format comprising immobilized gliadin as an antigen, a target anti-gliadin antibody and an anti-IgG antibody conjugated to the enzyme-loaded nanosphere immunoconjugates.

2.2 INTRODUCTION

Cyclodextrins (CDs) belong to a family of cyclic oligosaccharides, composed of α (1,4)-linked D-glucopyranose units in the 4C_1 chair conformation.

¹ This chapter has been published in E. Wajs, F. Caldera, F. Trotta, A. Fragoso, *Analyst*, **2014**, 139, 375.

Commercially available CDs are α , β and γ -CD, with six, seven and eight glucopyranose units, respectively.^{1,2} They play an important role in supramolecular chemistry due to their ability for molecular encapsulation with a wide range of guest molecules and are of high interest in the pharmaceutical field, biomedical science and biotechnology due to their low price, good availability and a large number of applications such as formation of nanoparticles,³ gels,⁴ drug carrier systems,⁵ and biosensors⁶ have been reported.

In recent years, different types of CD polymers have been synthesized ranging from branched polymers by reacting CDs with epichlorohydrin,⁷ linear polymers with pending CDs,⁸ or linear polymers with CDs incorporated into its backbone.⁹ A relatively new type of CD-containing structures called "nanosponges" has recently emerged and take their name by their ability to form a sponge-like structures when lyophilized and possess interesting properties like swelling or absorption/release of active compounds.¹⁰

These hyper-cross-linked cyclodextrins can be obtained by reaction of CD hydroxyl groups with an appropriate polyfunctional cross-linker to form solid particles with rather spherical morphology and a very high solubilizing power over poorly soluble substances. They can host a large number of different molecules inside their hydrophobic pockets, while the external surface is solvated. Furthermore, their interaction with various drugs or enzymes by forming inclusion/non-inclusion complexes may result in enzyme stabilization and also they can act as hydrophobic supports for enzyme immobilisation, which generally triggers enzymes interfacial activation.^{11,12} Nanosponges usually form suspensions as soon as they are dispersed in water, thereby forming a matrix-like structure in aqueous

media and allowing a free transfer of entrapped molecules.¹³ The different cross-linking agents may dramatically modify important parameters such as swelling capability and hydrophilicity/hydrophobicity balance of the final structure.

Here we present the preparation and characterisation of novel cyclodextrin nanosponge bioconjugates and their possible use in biosensor applications. Carboxylate-modified CDNS, prepared by crosslinking β -cyclodextrin with pyromellitic acid, were modified with an anti-IgG antibody and then loaded with horseradish peroxidase, an enzyme commonly used as a label in biosensor assays. The possibility to use these modified nanosponge as signal enhancement tool in enzyme-linked colorimetric and electrochemical assays was evaluated using a sandwich format comprising immobilized gliadin as antigen, a target anti-gliadin antibody and anti-IgG antibody (labelled with peroxidase or conjugated to the enzyme-loaded nanosponge immunoconjugates). This type of assay has been recognized as a diagnostic and therapeutic tool in celiac disease since levels of anti-gliadin antibodies in serum are used for monitoring celiac patients' compliance with a gluten-free diet.^{6b}

2.3 EXPERIMENTAL SECTION

Materials.

All chemicals used were of analytical grade and used as received without any further purification. CDNS were prepared by crosslinking β CD and pyromellitic dianhydride in 1:8 molar ratio.¹⁴ Phosphate-buffered saline (PBS), 1-ethyl-3-(3-dimethyl-aminopropyl) carbodiimide hydrochloride (EDC), N-hydroxysuccinimide (NHS), gliadin, rabbit anti-gliadin polyclonal-

IgG-antibody, anti-rabbit IgG (whole molecule)-peroxidase antibody produced in goat (Ab-HRP) and horseradish peroxidase were purchased from Sigma Aldrich. Biotin hydrazide was purchased from Pierce and dithiol SPT-0014A6 was obtained from Sensopath Technologies Inc. (Bozeman, Montana, USA).

Conjugation of CDNS with anti-IgG antibody (CDNS-Ab).

40 mg of CDNS were dissolved in 1 mL of sodium acetate buffer pH 5. Next, 50 mg of EDC and 75 mg of NHS were added to the carboxylated surface of CDNS and allowed them to react for 15 minutes at 4°C. After this time, a freshly prepared 0.2 mL of aqueous solution of the antibody (1 mg mL⁻¹) was added to the reaction and the mixture was stirred for another 2 hours at 4°C. The unreacted carboxylate groups were deactivated by reaction with 1.5 M ethanolamine (0.2 mL) at pH 8.5 for 1 hour.

The obtained product was then purified by gel filtration using Sephadex G-200 column and the amount of protein was determined by the Bradford method with ovalbumin as standard.¹⁵

Preparation of HRP-loaded nanosponges (CDNS-Ab-HRP)¹⁶

The preparation of HRP-loaded nanosponges was done by mixing 5 mg HRP (310 units/mg) with 10 mg lyophilized antibody-modified CDNS in 1 mL of 50 mM phosphate buffer at pH 6.5 and then incubated for 62 hours at 4°C under stirring.

The resulting solution was subsequently purified using Microcon® centrifugal filters (MW 100 kDa) and HRP-loaded nanosponges were collected by inverting the filter and centrifuging at 10000 rpm for 2 minutes. The amount of enzyme was estimated by absorption at 402 nm using a molar

extinction coefficient $93500 \text{ M}^{-1}\text{cm}^{-1}$ and the immobilisation yield was calculated as the difference between the quantity of HRP incubated and the quantity of protein not bonded to the carrier.

Labeling of antibody and HRP with red and green amine-reactive fluorophores for confocal imaging.

The amine-reactive fluorophores (Rhodamine Red-X for antibody and 6-carboxyfluorescein NHS ester for HRP, respectively) were dissolved in DMSO at 10 mg mL^{-1} immediately before starting the reaction. While the protein solution (5 mg mL^{-1}) was under stirring, $100 \mu\text{L}$ of the reactive dye solution was slowly added to the reaction and the mixture was stirred for 1-2 hours at room temperature.

The resulting conjugates were purified by gel filtration using Sephadex G-25 column and PBS pH 7 as eluent. The fractions corresponding to the first fluorescent band of the eluate corresponding to the conjugates were collected and used immediately for further conjugation to or encapsulation into CDNS.

Confocal images were obtained using a NIKON Eclipse, model TE2000-E (Hamamatsu digital camera C8484) confocal microscope, using oil objective $100\times$ with $\text{NA} = 1.4$. Photographs were made using zeta stack (the step size of $0.05 \mu\text{m}$) and lambda mode with two channels at 488 nm (Ar laser, blue) and at 543 nm (He-Ne laser, green).

Transmission electron microscopy (TEM) imaging.

Transmission Electron Microscopy (TEM) analyses were performed using a JEOL 1011 transmission electron microscope operated at 80 keV . Micrographs ($1024 \text{ pixels} \times 1024 \text{ pixels}$) were acquired using a Megaview III

multiscan-CCD camera. Images were analyzed with an iTEM image analysis platform and the mean diameter was calculated measuring at least 100 particles in triplicate.

A drop of a nanosponge aqueous solution was placed on a 200 mesh copper grid with a thin film of Formvar polymer and the excess of the liquid was carefully removed, using a filter paper. Next, the sample was left at room temperature until a dry film was obtained. For negative staining of the sample, a drop of phosphotungstic acid was spotted on the prepared grid containing the sample and incubated for 3-5 minutes, removed with filter paper and air dried.

Raman characterization of modified CDNS.

Raman spectra of CDNS were recorded at 20°C by means of a microprobe setup (Raman Spectroscopy, FT-IR. Renishaw). Exciting radiation at 785 nm was focused onto the sample surface with a spot size of about 1 μm^2 through a 100 \times objective with NA = 0.9. To avoid unwanted laser-induced transformations, neutral filters of different optical densities were used, whenever necessary.

Spectra were collected in the wavenumber ranges 100–3700 cm^{-1} with an integration time of 300 s. The resolution was about 0.35 cm^{-1} per pixel with a typical laser power set at 10 mW. For each sample, 3 series of independent measurements were carried out and for each set, the Raman experiment was repeated 6 times to check the reproducibility of the measurement and to minimize the noise ratio of the signals.

HRP activity measurements for the free enzyme in solution and immobilized on CDNSs.

The peroxidase activity of the free HRP and CDNS-Ab-HRP were determined colorimetrically using 3,3',5,5'-tetramethylbenzidine (TMB) as substrate following the formation of 3,3',5,5'-tetramethylbenzidine diimine. The resulting diimine causes the solution to develop a blue color and this color change can be read at 650 nm. An aliquot (5 mL) of the substrate was added to a reaction mixture containing $0.0125 \mu\text{M L}^{-1}$ of enzyme in both free and encapsulated forms in phosphate-citrate buffer (pH 3-6) or phosphate buffer (pH 7-9) at 25°C and the absorbance was measured with time.

The values obtained in the blank reactions, performed in the presence of TMB without enzyme were subtracted from all readings.

Colorimetric detection of anti-gliadin antibody on streptavidin-coated plates.

Digested gliadin^{6b} (10 mg) was biotinylated by reaction with 5 mg biotin hydrazide in PBS buffer pH 7 for 1 hour at 4°C. The protein was purified using Sephadex G-25 column and PBS pH 7 as eluent.

Streptavidin plates were first incubated with 50 μL of biotinylated gliadin at different concentrations ranging from $0 \mu\text{g mL}^{-1}$ to $6 \mu\text{g mL}^{-1}$ for 1 h at room temperature. Next, the plate was washed 3 times with PBS buffer at pH 7.4 and incubated with 50 μL of a target (anti-gliadin antibody produced in rabbit) at different concentrations (from $0 \mu\text{g mL}^{-1}$ to $10 \mu\text{g mL}^{-1}$) for 45 minutes at room temperature. After that time the plate was washed again with PBS buffer at pH 7.4 and 50 μL of $1 \mu\text{g mL}^{-1}$ of HRP labelled anti-rabbit

antibody or CDNS-Ab-HRP conjugate was added and incubated for 30 minutes.

After the last washing step was accomplished, the plate was incubated for 15 minutes with 25 μL of TMB and the reaction stopped using 50 μL of 0.5 M H_2SO_4 . The absorbance was measured at 450 nm.

Electrochemical measurements.

Electrochemical measurements were performed on a PC controlled PGSTAT12 Autolab potentiostat (EcoChemie, The Netherlands) with a built-in frequency response analyzer FRA2 module using a standard three-electrode configuration: Ag/AgCl (sat) reference electrode, counter electrode Pt wire and a gold disc $\phi = 2$ mm as working electrode. The electrodes were first mechanically polished using polycrystalline diamond suspensions (3 μm , 1 μm and 0.1 μm) and then electrochemically cleaned applying a series of 25 potential cycles in 1 M H_2SO_4 in the range 0-1.6 V vs. Ag/AgCl. The quality of the cleaning step was checked using cyclic voltammetry with 1 mM $\text{K}_3\text{Fe}(\text{CN})_6$ in 0.1 M KCl.

Modification of gold electrodes and anti-gliadin antibody detection.

The working electrodes were modified with a 1 mM solution of COOH-terminated dithiol¹⁷ for 3 hours and rinsed with ethanol. The carboxyl groups of the SAM were sequentially modified with an aqueous mixture of EDC (0.2 M) and NHS (50 mM) for 30 min. Gliadin was covalently immobilized on the NHS-activated SAM by incubating a 1 mg/mL⁻¹ solution in 10 mM acetate buffer pH 5.0 for one hour. The remaining NHS active ester sites were blocked with 1.0 M ethanolamine pH 8.5 for 30 minutes.

The electrodes were rinsed with PBS and the target anti-gliadin antibody was incubated for 15 minutes at room temperature. After rinsing with PBS the electrodes were incubated with $2 \mu\text{g mL}^{-1}$ of HRP labelled anti-IgG antibody or CDNS-Ab-HRP conjugate for 15 minutes. The amperometric measurements were carried out by first recording the background response at 0.2 V in 10 mM PBS + 0.15 M NaCl pH 6, followed by the addition of 20 μL of TMB substrate.

2.4 RESULTS AND DISCUSSION

Figure 2.1 shows the general procedure for the preparation of nanosponge immunoconjugates. CDNS bearing free carboxylic acid groups were obtained by cross-linking βCD with pyromellitic dianhydride in the presence of ammonia. The COOH groups of the nanoparticles were then activated and reacted with an excess of anti-IgG antibody to give CDNS-Ab. The amount of antibody covalently linked to the CDNS was $0.27 \mu\text{g}/\text{mg}$. CDNS-Ab was further loaded with free HRP by stirring the nanoparticles with the enzyme for three days to give CDNS-Ab-HRP having $0.53 \mu\text{g}$ HRP per mg of nanosponge.

TEM analysis of the formed nanoparticles showed an almost spherical morphology with size ranging from 50-100 nm with an average of $(81 \pm 9 \text{ nm})$ (Figure 2.2). Zeta potential analysis of both CDNS ($-35 \pm 2 \text{ mV}$) and CDNS-Ab before ethanolamine backfilling ($-15 \pm 2 \text{ mV}$) indicated a decrease of negative surface charge consistent with the partial transformation of COO⁻ groups to neutral -CONH-.

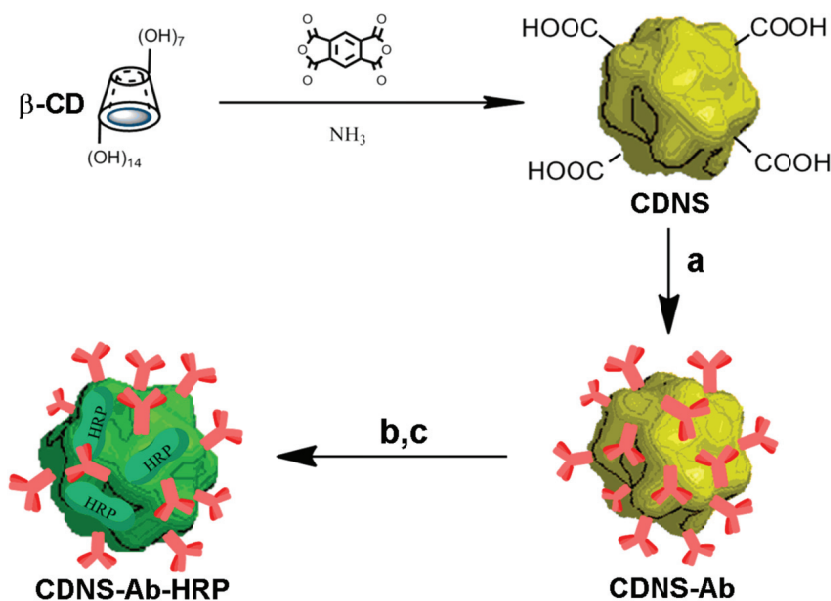


Figure 2.1. Preparation of CDNS-Ab-HRP: a) EDC/NHS (15 min, 4°C), anti-IgG antibody (2 h, 4°C), b) ethanolamine (1 h, 4°C), c) HRP (62 h, 4°C, ph 6.5).

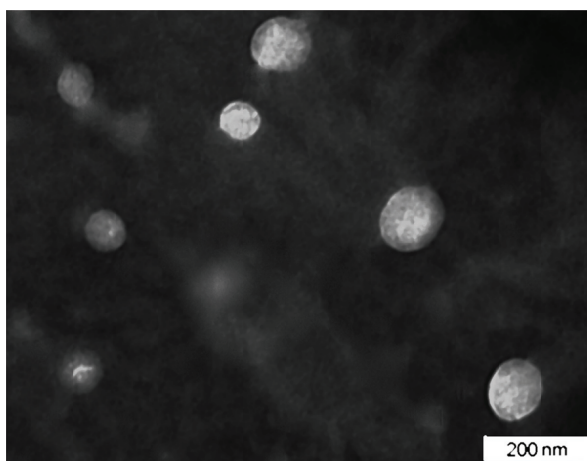


Figure 2.2. TEM micrograph of CDNS-Ab-HRP particles in aqueous suspension after the negative staining with phosphotungstic acid.

Figure 2.3 shows a comparison of CDNS and CDNS-Ab Raman spectra. As can be seen, new bands appear in the spectrum of CDNS-Ab at 620, 700, 830 and 920 cm^{-1} which have also observed in the spectra of the IgG proteins and have been assigned to $\nu_{\text{C-C}}$ and ρ_{CH_2} vibrations.¹⁸ Another strong band is also observed at 1416 cm^{-1} ($\nu_{\text{C=C}}$ tryptophan) as well as $\nu_{\text{C-H}}$ bands of aliphatic side-chains between 2850 cm^{-1} and 3000 cm^{-1} . The spectrum of CDNS-Ab also shows a decrease in intensity in the band at 1691 cm^{-1} ($\nu_{\text{C=O}}$ carboxylate group) with respect to CDNS consistent with the covalent linking of antibody molecules through these groups with the formation of amide bonds.

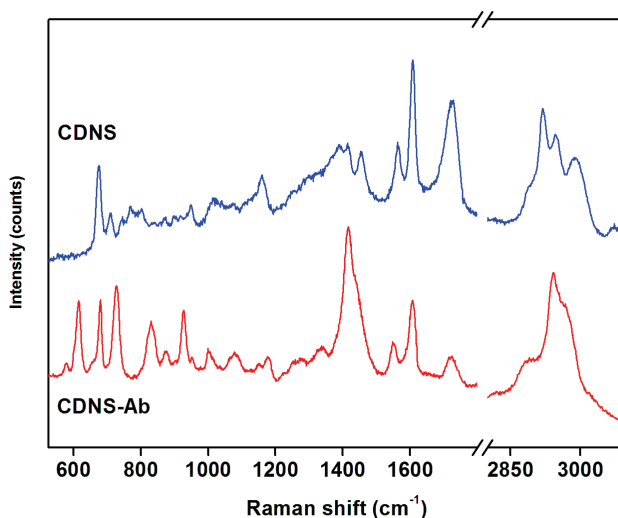


Figure 2.3. Raman spectra of CDNS and CDNS-Ab conjugate in dry state. Conditions: time acquisition, 300s, wavelength, 785 nm, nominal power laser 10 mW, optical microscope objective 100 \times .

Confocal microscopy allows the building of three-dimensional reconstructions of a volume by assembling a series of thin slices taken along

the vertical axis. We have used this technique to visualize CDNS-Ab-HRP nanoassemblies. In this experiment, the anti-gliadin antibody and HRP were tagged with rhodamine red ($\lambda_{em} = 570$ nm) and 6-carboxyfluorescein ($\lambda_{em} = 494$ nm), respectively, prior to their incorporation to unmodified CDNS using the same route as depicted in Figure 2.1. As shown in Figure 2.4, the red emission corresponding to the antibody appears only in the outside of the particle, while the green fluorescence is distributed in the inner part. This indicates that HRP is actually encapsulated inside the particles.

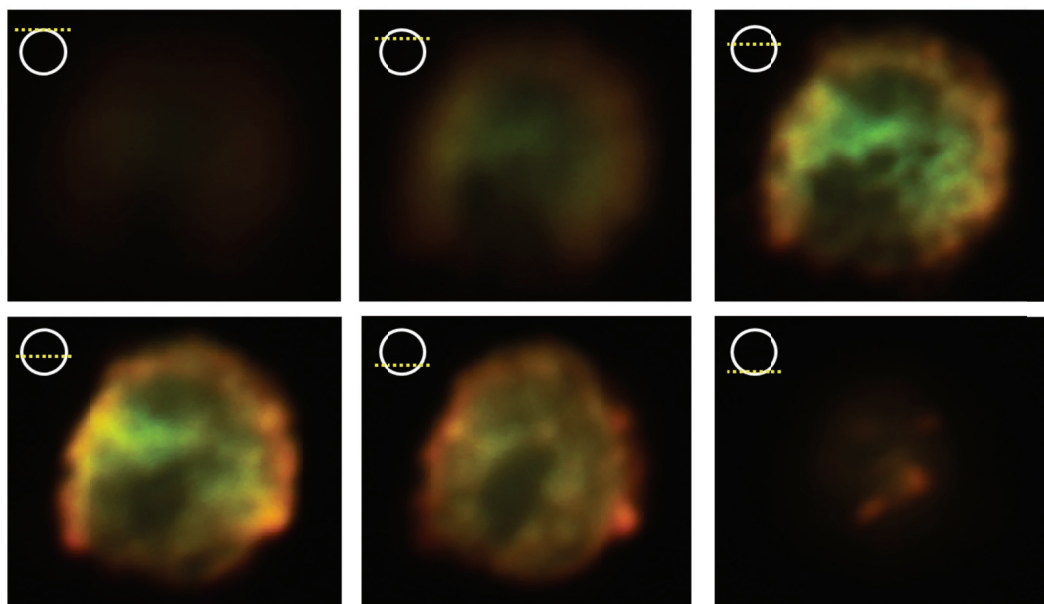


Figure 2.4. Confocal images of a 200 nm CDNS-Ab-HRP particle.

The effect of pH on the enzymatic activity of CDNS-Ab-HRP was compared with that of free HRP (Figure 2.5). The maximum activity of encapsulated enzyme was observed at pH 7. Interestingly, above pH 7, the activity of free

HRP drops rapidly while in the nanosponge structure a plateau of high activity is seen between pH 6-8. Therefore, the microenvironment provided by CDNS favours the activity of the enzyme,¹² presumably by promoting an increase of local concentration of the hydrophobic TMB substrate around the enzyme by complexation in the β CD cavities.

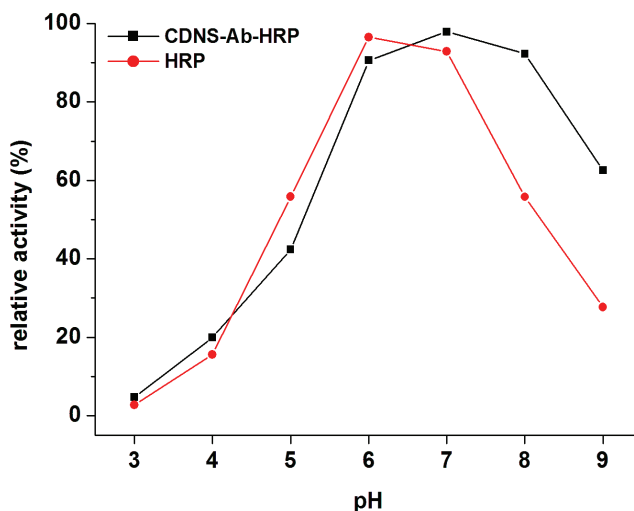


Figure 2.5. Dependence of enzymatic activity with pH for CDNS-Ab-HRP and free HRP at 25°C using TMB as a substrate.

The possibility to use CDNS-Ab-HRP as signal enhancement tool in enzyme-linked colorimetric and electrochemical assays was evaluated using a sandwich format (Figure 2.6). In the colorimetric assay, biotinylated gliadin was immobilized on the surface of streptavidin-coated plates at different concentrations, followed by incubation with the target anti-gliadin antibody. The sandwich structure was constructed using either CDNS-Ab-HRP or an anti-IgG-HRP conjugate.

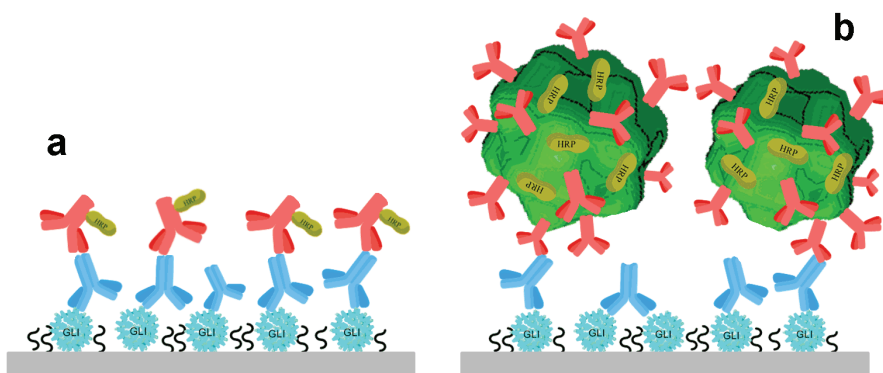


Figure 2.6. Sandwich constructions used in the enzyme-linked colorimetric detection of anti-gliadin antibodies with Ab-HRP (a) and CDNS-Ab-HRP (b) as detecting conjugates. The plates were coated with digested gliadin via biotin-streptavidin interactions.

Figure 2.7 shows a comparison of the calibration curves obtained at different coating concentrations (0, 1.5, 3 and 6 $\mu\text{g/mL}$). As can be seen, the optical response increased with both coating and target concentrations and the response is markedly higher in the presence of the nanosponge bioconjugate. Assuming a linear behaviour at low target concentrations (0–2.5 $\mu\text{g/mL}$), the highest sensitivities (taken as the slope of the A vs. c curve) were observed at 6 $\mu\text{g/mL}$ coating concentration with values of 0.78 and 0.24 $\text{AU } \mu\text{L } \mu\text{g}^{-1}$ for CDNS-Ab-HRP and Ab-HRP systems, respectively, representing a 3.2-fold signal enhancement with a decrease in limit of detection from 0.22 ng mL^{-1} to 0.08 ng mL^{-1} .

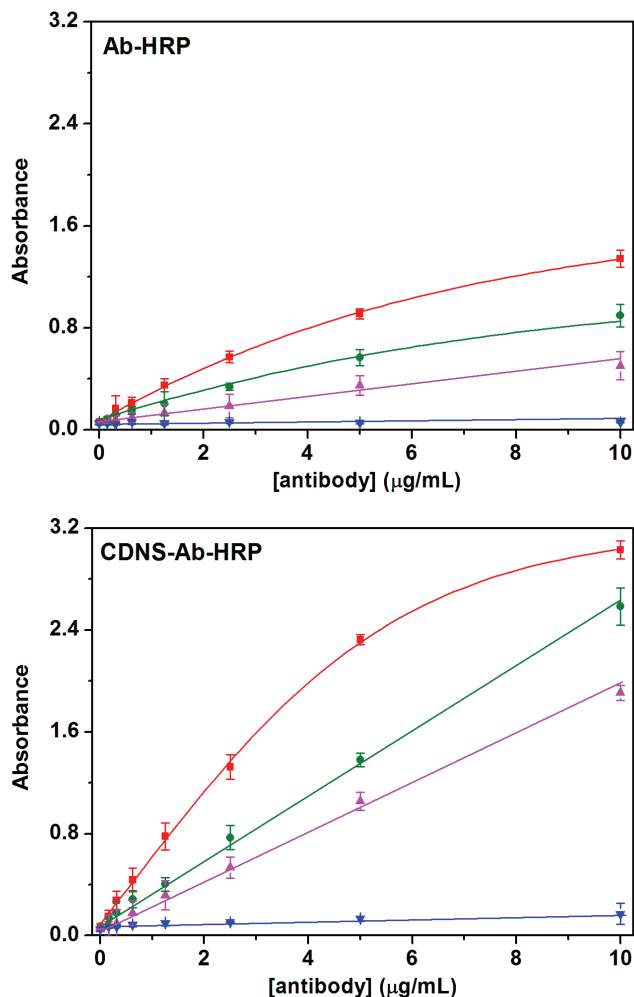


Figure 2.7. Calibration curves obtained in the colorimetric detection of anti-gliadin antibody using Ab-HRP and CDNS-Ab-HRP at different concentrations of biotinylated gliadin coating. ▼ (0 µg/mL), ▲ (1.5 µg/mL), ● (3 µg/mL), ■ (6 µg/mL).

In the case of the electrochemical assay, gliadin was covalently immobilized on the surface of a gold electrode using a COOH-terminated bipodal ditiol using standard EDC/NHS chemistry (Figure 2.8). The other components of the sandwich assay were similar to those used in the colorimetric assay and

after substrate addition, the electrochemical response was measured corresponding to the reduction of the oxidized substrate was measured. The current values showed a sigmoidal relationship with the concentration of anti-gliadin antibody with saturation above 2.5 $\mu\text{g/mL}$. As in the case of the colorimetric assay, the sensitivity in the presence of CDNS-Ab-HRP was significantly higher ($165 \text{ nA mL } \mu\text{g}^{-1}$) than in the presence of the covalent Ab-HRP conjugate ($43 \text{ nA mL } \mu\text{g}^{-1}$). In this case, the signal enhancement factor was 3.8 and limit of detection decreased from 0.11 to 0.03 $\mu\text{g/mL}$ (Figure 2.9).

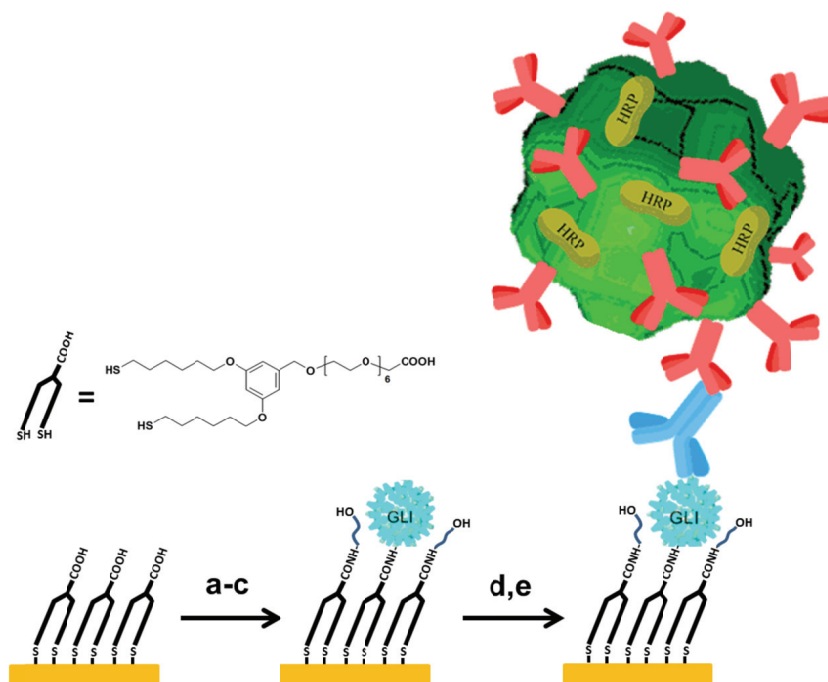


Figure 2.8. Modification of the gold electrode surface for the electrochemical detection of anti-gliadin antibody with CDNS-Ab-HRP. a) EDC/NHS, 30 min, 4°C, b) gliadin, 1 h, 4°C, c) ethanolamine, 30 min, 4°C, d) anti-gliadin antibody, 15 min, 25°C e) CDNS-Ab-HRP, 15 min., 25°C.

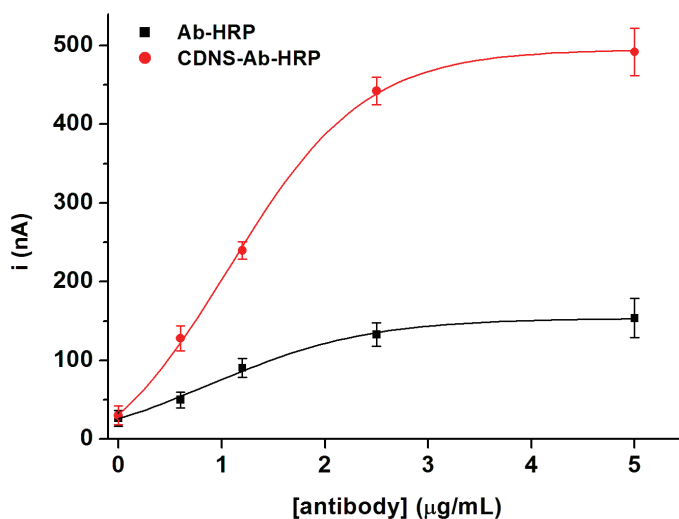


Figure 2.9. Dependence of the amperometric responses with anti-gliadin antibody concentration using CDNS-Ab-HRP and Ab-HRP conjugates.

2.5 CONCLUSIONS

In this paper we have described the preparation and characterisation of cyclodextrin nanosponge bioconjugates containing a model antibody and peroxidase. Confocal microscopy indicates that the antibody is located in the outside of the particle while HRP is actually encapsulated in the inner part. CDNS offer the advantage of one step multi-gram preparation and ease of bioconjugation in mild conditions and the signal amplification obtained in the presence of CDNS-Ab-HRP indicates that this type of nanobioconjugates are promising candidates in the development of ultrasensitive biosensors. This signal enhancement is lower compared to similar results recently reported by our group using peroxidase-encapsulated liposomes,¹⁹ where a factor of ~ 10 was obtained, although in our case, the assay has not been optimized in terms of incubation times or concentration of detecting conjugate. On the

other hand, the long encapsulation time required for HRP loading compared with the time required for anti-IgG linking seems to lead to a certain spacing between HRP and IgG which leads to a compartmentalization of the two proteins into the nanosponge, hindering in part the access of the enzyme substrate and thus partially decreasing the analytical performance of the assay. This could be solved by using smaller CDNS particles or decreasing the amount of loaded HRP. Work is ongoing in order to further optimise the assay performance and apply these novel type of cyclodextrin bioconjugates in the detection of other targets such as DNA sequences.

REFERENCES

1. J. Szejtli, *Chem. Rev.*, 1998, **98**, 1743.
2. R. Villalonga, R. Cao, and A. Frago, *Chem. Rev.*, 2007, **107**, 3088.
3. R. Gref, C. Amiel, K. Molinard, S. Daoud-Mahammed, B. Seville, B. Gillet, J. C. Beloeil, C. Ringard, V. Rosilio, J. Poupaert, and P. J. Couvreur, *J. Contr. Rel.*, 2006, **111**, 316.
4. V. Wintgens, S. Daoud-Mahammed, R. Gref, L. Bouteiller, and C. Amiel, *Biomacromolecules*, 2008, **5**, 1434.
5. H. Gonzales, S. J. Hwang, and M. E. Davis, *Bioconjugate Chem.* 1999, **10**, 1068.
6. a) M. Ortiz, E. M. Wajs, A. Frago, and C. K. O'Sullivan, *Chem. Comm.*, 2012, **48**, 1045. b) M. Ortiz, A. Frago, and C. K. O'Sullivan, *Anal. Chem.*, 2011, **83**, 2931.
7. E. Renard, A. Deratani, G. Volet, and B. Seville, *Eur. Polym. J.*, 1997, **33**, 49.
8. E. Renard, G. Volet, and C. Amiel, *Polym. Int.*, 2005, **54**, 594.

9. H. Gonzales, S. J. Hwang, and M. E. Davis, *Bioconjugate Chem.*, 1999, **10**, 1068.
 10. a) A. Mele, F. Castiglione, L. Malpezzi F. Ganazzoli, G. Raffaini, F. Trotta, B. Rossi, A. Fontana, and G. J. Giunchi, *J. Incl. Phenom. Macrocycl. Chem.*, 2010, **69**, 403. b) F. Trotta, and W. Tumiatti, *WO Patent 03/085002*, 2003, c) E. Y. Ozmen, M. Sezgin, and M. Yilmaz, *J. Mol. Catal. B: Enzym.* 2009, **57**, 109. d) B. Boscolo, F. Trotta, and E. Ghibaudi, *J. Mol. Catal. B: Enzym.*, 2010, **62**, 155.
 11. a) S. Swaminathan, L. Pastero, L. Serpe, F. Trotta, P. Vavia, D. Aquilano, M. Trotta, G. Zara, and R. Cavalli, *Eur. J. Pharm. Biopharm.*, 2010, **74**, 193. b) R. Cavalli, F. Trotta, and W. Tumiatti, *J. Incl. Phenom. Macrocycl. Chem.*, 2006, **56**, 209.
 12. G. Di Nardo, C. Roggero, S. Campolongo, F. Valetti, F. Trotta and G. Gilardi, *Dalton Trans*, 2009, 6507.
 13. S. J. Torne, K. A. Ansari, P. R. Vavia, F. Trotta, and R. Cavalli, *Drug Deliv.*, 2010, **17**, 419.
 14. a) F. Trotta, W. Tumiatti, and R. Vallero, *Italian Patent No. A000614, MI*, 2004. b) F. Castiglione, V. Crupi, D. Majolino, A. Mele, B. Rossi, F. Trotta and V. Venuti, *J. Phys. Chem. B*, 2012, **116**, 13133.
 15. M. M. Bradford, *Anal. Biochem.*, 1976, **72**, 248.
 16. G. Gilardi, F. Trotta, R. Cavalli, P. Ferruti, E. Ranucci, G. Di Nardo,, C. M. Roggero, and V. Tumiatti, *WO Patent 149883A.*, 2009.
 17. A. Fragoso, N. Laboria, D. Latta, and C. K. O'Sullivan., *Anal. Chem.*, 2008, **80**, 2556.
 18. R. Tuma, *J. Raman Spectr.*, 2005, **36**, 307.
 19. R. Genç, D. Murphy, A. Fragoso, M. Ortiz, and C. K. O'Sullivan, *Anal. Chem.*, 2011, **83**, 563.
-

CHAPTER 3

CYCLODEXTRIN AND GUEST-APPENDED DEXTRAN-BASED POLYMERS. PREPARATION AND CHARACTERIZATION

3.1 ABSTRACT

In this section, results of syntheses of different dextran based host-guest polymers are described. The dextran based polymers were synthesized from different combinations of molecular weights and appended host or guest molecules percentages. Cyclodextrin-dextran polymers were prepared from alkylnyl dextran via click chemistry. Guest-appended polymers were prepared in two ways. To graft adamantane units the same strategy as for the cyclodextrin polymers was followed. In turn, the stimuli-responsive polymers bearing ferrocene and azo groups were prepared by transesterification of native dextran with N-hydroxysuccinimide esters. Some of these polymers were also tagged with fluorophores in order to better visualize the nanoassemblies formation by confocal microscopy. For these modifications also used either click chemistry or transesterification reactions.

3.2 INTRODUCTION

Dextran is a linear natural glucose polymer with a broad range of molecular weights ranging from 1 to 2000 kDa. The glucose units are linked by α -1,6 – glycosidic bonds and few short α -1,4 – linked branches. Dextran has a very

high solubility in water, it has great biocompatibility and it is biodegradable and non-toxic polymer.¹

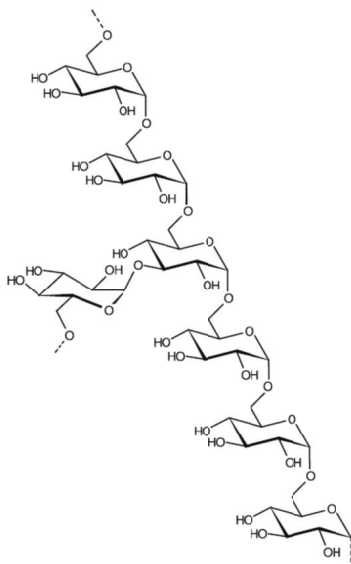


Figure 3.1 Structure of dextran showing the main chain composed of α -(1 \rightarrow 6) glycosidic bonds with an α -(1 \rightarrow 4) branch.

Dextran can be used in a broad range of applications, for instance:

- biomedical science as a reducer of blood viscosity, a volume expander in anemia, in some eye drops as a lubricant.
- laboratory uses as size-exclusion chromatography matrices (Sephadex), in immobilization in biosensors, stabilising coating to protect metal nanoparticles from oxidation and improve biocompatibility.⁴

Dextran can be chemically or chemoenzymatically esterified or etherified to generate a wide range of derivatives ranging from ionic inorganic esters to neutral alkylated products.² Dextran oxidation with sodium periodate is also an important reaction giving dextran aldehydes that can be further oxidized to carboxylic acids or reductively alkylated in the presence of amines. These modifications allow the design of new functional polymers with very promising and interesting properties.

Organic esters of dextran with short chain aliphatic acids can be prepared in heterogeneous reactions of the polymer suspended in pyridine using the carboxylic acid anhydride. For longer chain substituents, the carboxylic acid or their anhydrides are converted in situ in reactive mixtures of mixed chloroacetyl or trifluoroacetyl anhydrides. On the other hand, homogeneous acylation reactions between dextran and an acyl halide or anhydride in DMF/LiCl has also been accomplished due to the solubility of the polysaccharide in this mixture. This latter reaction is preferred for less reactive or bulky electrophiles.

Alkylation of dextran is one of the most studied and versatile reactions. It has been carried out in the past by treatment of dextran with alkyl halides or epoxides in the presence of a base. When the side chain of the alkyl halide is a linear hydrocarbon (methyl, ethyl, octyl, benzoyl, etc.) the result is an amphiphilic product with decreased water solubility. In a similar way, 2-hydroxyalkyl and carboxymethyl ethers can be prepared but in this case the solubility in water is maintained due to the hydrophilic character of the side chains.

In this chapter we describe the synthetic strategies used for the preparation of the polymers used in chapters 4, 5 and 6. Since our interest is to prepare complementary cyclodextrin and guest-appended polymers, the synthesis routes have been adapted to produce the target polymers in bulk amounts and simplify the preparation as much as possible (Figure 3.2). In order to connect the substituents to the dextran backbone in controlled manner different functional groups needed first to be introduced on both dextran and the pendant group. The dextran based polymers were synthesized from different combinations of molecular weights and appended host or guest

molecules percentages. The molecular weights of dextran polymers used for the syntheses were 10 and 40 kDa. Cyclodextrin-dextran polymers were prepared from alkynyl dextran via click chemistry.³ Guest-appended polymers were prepared in two ways. To graft adamantane units the same strategy as for the cyclodextrin polymers was followed. In turn, the stimuli-responsive polymers bearing ferrocene and azo groups were prepared by transesterification of native dextran with N-hydroxysuccinimide esters. Some of these polymers were also tagged with fluorophores in order to better visualize the nanoassemblies formation by confocal microscopy. For these modifications also used either click chemistry or transesterification reactions.

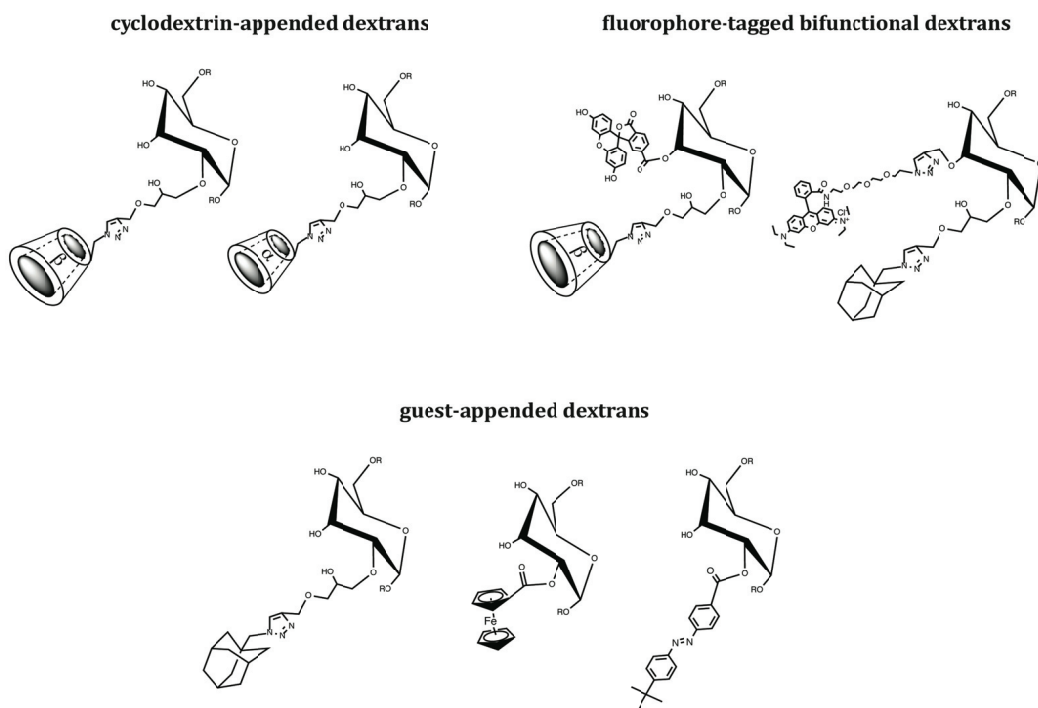


Figure 3.2 Structures of the prepared polymers.

3.3 EXPERIMENTAL SECTION

Materials

All chemicals used were of analytical grade and used as received without any further purification. 1-ethyl-3-(3-dimethyl-aminopropyl) carbodiimide hydrochloride (EDC), N-hydroxysuccinimide (NHS), ferrocene carboxylic acid, (*E*)-4-((dimethylamino)phenyl)diazenyl) benzoic acid, 2-propanol, dioxane, DMF, *N,N*-isopropylethylamine 99%, amberlite GT73 resin, epichlorohydrin, DMAP, LiCl, Methyl 4-aminobenzoate, 4-(tert-butyl)aniline, 1-amino-11-azido-3,6,9-trioxaundecane, Rhodamine B and 5(6)-Carboxyfluorescein N-hydroxysuccinimide ester were purchased from Sigma Aldrich. L (+)-ascorbic acid sodium salt 99% (NaAsc), copper (II) sulphate 99%, dichloromethane and glycidyl propargyl ether 90% were from Fluka. α , β -cyclodextrins were purchased from Wacker-Chemie. Dextran (D10, M_w 1×10^4 Da, D40 M_w 4×10^4 Da) were obtained from Pharmacosmos A/S. Tris-(benzyltriazolylmethyl)amine (TBTA)⁴ and *p*-toluenesulfonyl imidazole⁵ were prepared according to the literature.

Instrumentation

¹NMR analysis of the polymers were conducted in D₂O (30 g/L) and DMSO-d₆ with a Bruker DRX 600 spectrometer (5 mm TXI (H/C/N) xyz gradient probe) with a delay time (d1) set for 30 s.

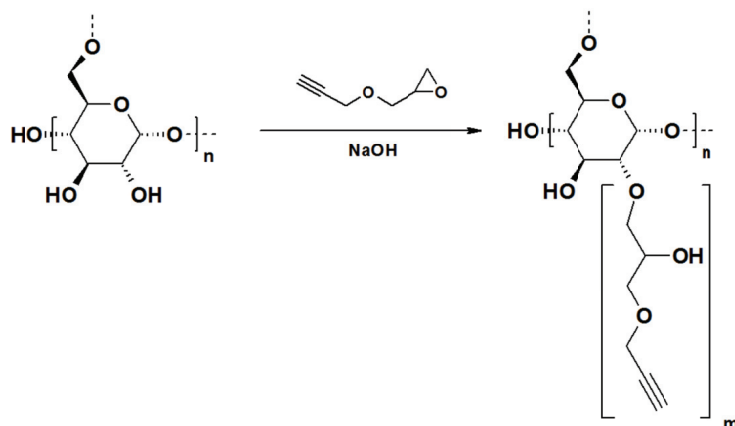
TLC analyses were made with ALUGRAM SIL G/UV₂₅₄ TLC plates with 0.2 mm silica gel, visualized with 5% H₂SO₄ in ethanol.

Flash chromatography was made using columns TSK-gel type SW 4000-3000 and detected by a Wyatt miniDawn light scattering (LS) detector and a Wyatt Optilab Rex. refractive index detector.

Fourier transform infrared spectroscopy (FT-IR) was made on Bruker Tensor 27 FT-IR spectrometer. Dialysis was made with Spectrum Spectra/Por, MWCO 8000-50000 25.5 mm diameter, 5 mL/cm and freeze-drying on a Heto CT 60e.

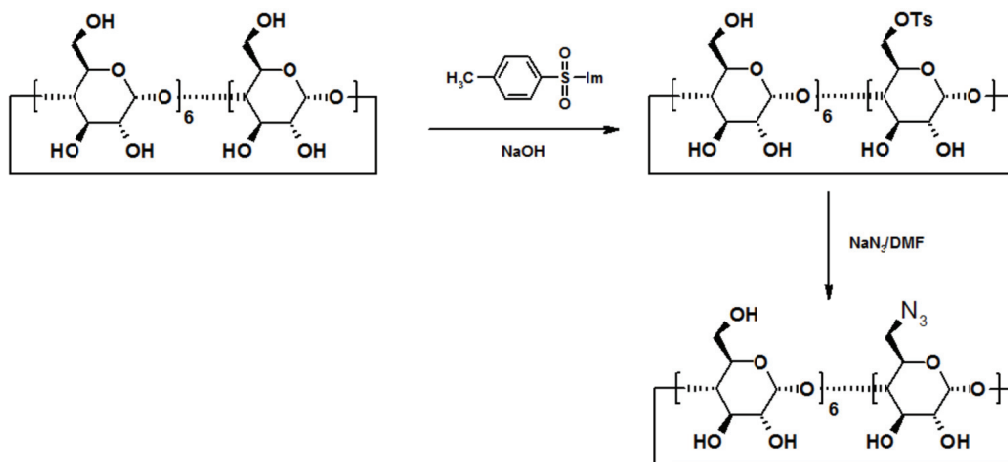
Preparation of intermediate compounds

*Dextran Propargyl Glycerol (Dextran GP)*³



One gram of dextran (10 or 40 kDa, 6.2 mmol of glucose units) was dissolved in 30 mL of 0.5 M NaOH and glycidyl propargyl ether was added in different amounts (0.31, 0.62, 0.93, 1.23, 1.54, 2.16, 2.78, 3.40 mmol). The solution was stirred for 16 h at 35 °C, the product was precipitated in 2-PrOH, filtered, washed with 2-PrOH and dried under nitrogen. The crude product was then redissolved in water, dialyzed and freeze-dried, yielding a white solid. The average yield was 1 g. ¹H-NMR (D₂O): δ (ppm) 3.05 (s, C≡CH), 3.6-4.1 (m, H_{2,3,4,5}, glycerol protons), 4.35 (s, CH₂C≡C), 5.1 (d, H₁).

6-O-deoxy-monoazido- β CD (β CD- N_3).³

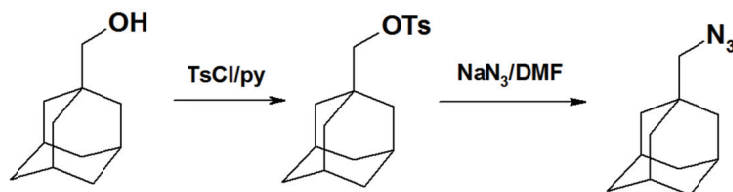


6-O-deoxy-monoazido- β CD (β CDN₃) was prepared in two steps. Initially, 6-O-mono-tosyl- β CD was synthesized by adding tosyl imidazole (3.1 g, 14 mmol) to a warm (45°C) aqueous solution of β CD (4 g, 3.5 mmol).⁵ The suspension was stirred for 2 h and cooled to room temperature. Next, NaOH (1.8 g, 4.5 mmol) was added slowly and the mixture was stirred for another 10 min. The mixture was quickly filtered into a flask containing ammonium chloride and concentrated by blowing air over the surface overnight. The precipitate was filtered off and washed with ice-cold water and acetone. The product was dried in vacuo and recrystallized twice (DMSO/water) until pure TsO β CD was obtained (Yield: 1.1 g).

In the second step, TsO β CD (1 g) and sodium azide (0.5 g) were dissolved in 10 mL DMF and the mixture was stirred at 75 °C for 24 h, then precipitated in acetone and filtered. The purification step involved multiple recrystallizations (water/acetone) until IR showed no peak from residual sodium azide (2138 cm⁻¹). Next, the product was dialyzed and freeze-dried.¹

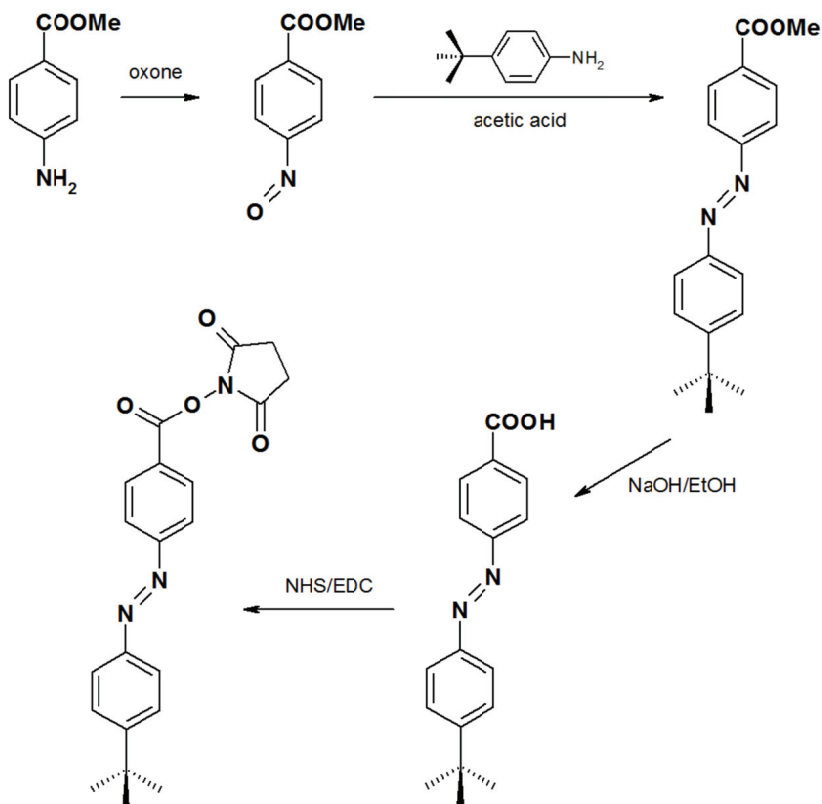
Yield: 0.8 g. $^1\text{H-NMR}$ (D_2O): δ (ppm) 3.2-3.8 (m, H_{2,3,4,5,6}), 5.1 (m, H₁).
MALDI-TOF m/z 1181 ($\text{M}+\text{Na}^+$).

1-(Azidomethyl)-adamantane (ADA-N₃).



ADA-N₃ was prepared by treating 1-adamantanemethanol (1.6 g, 10 mmol) with tosyl chloride (1.9 g, 10 mmol) in pyridine (20 mL). The reaction mixture was stirred at room temperature overnight. Next, the solvent was removed in vacuo and the crude product (ADA-Ts) dissolved in ethyl acetate. ADA-Ts was purified by washing with saturated NaHCO₃ and brine several times. After that, crude ADA-Ts and sodium azide (1 g) were dissolved in DMSO and stirred at 80 °C for 48 h. Water was added to cool down the reaction mixture and the product was subsequently extracted with ethyl acetate and washed with water and brine several times. The organic layer was dried over sodium sulfate, filtered and concentrated in vacuo and further purified by flash chromatography (dichloromethane:methanol = 99:1). Yield: 1.2 g. $^1\text{H-NMR}$ (DMSO-d_6): δ (ppm): 1.5 (s, 6H, CH₂), 1.65 (dd, 6H, CH₂), 1.95 (s, 3H, CH), 3.04 (s, 2H, CH₂-N₃).

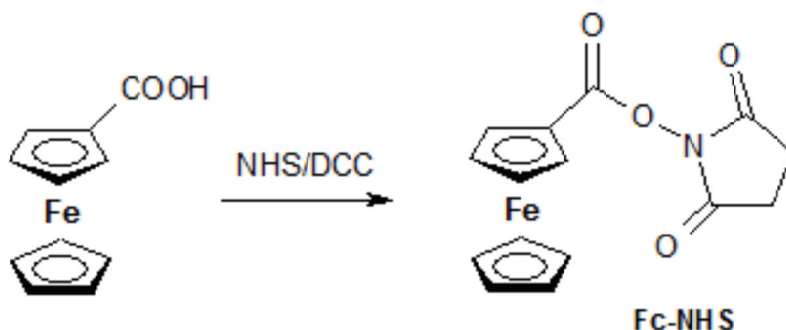
***(E)*-4-((*tert*-butyl)phenyl)diazenyl) benzoic acid NHS ester (Azo-NHS)**



The precursor acid was prepared according to reference 6 using 4-(*tert*-butyl) aniline instead of 4-bromoaniline. Methyl 4-nitrosobenzoate was first synthesized by treating methyl 4-aminobenzoate with oxone (potassium peroxomonosulfate) in dichloromethane under nitrogen atmosphere. Next, the resulting methyl 4-nitrosobenzoate was reacted with 4-(*tert*-butyl) aniline to give (*E*)-methyl 4-((4-(*tert*-butyl)phenyl)diazenyl) benzoate, which was subsequently hydrolyzed in the presence of NaOH to give the final product (*E*)-4-((*tert*-butyl)phenyl)diazenyl) benzoic acid. All intermediate products were identified by ¹H-NMR.

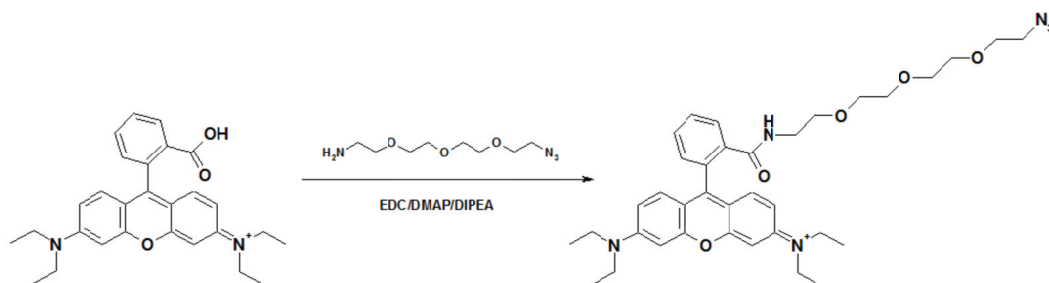
To prepare the ester, N-hydroxysuccinimide (0.783 g, 6.8 mmol) and EDC·HCl (1.3 g, 6.8 mmol) were added to a solution of 4-(E-4'-tert-butylphenylazo)-benzoic acid (1.0 g, 3.4 mmol) in 20 mL DMF. The reaction mixture was stirred at room temperature overnight and the product was purified by column chromatography using pentane:EtOAc 6:4. Yield: 640 mg. $^1\text{H-NMR}$ (D_2O): δ (ppm) 0.97 (s, 9H, CH_3), 2.7 (s, 4H, $\text{O}=\text{C}-\text{CH}_2$), 7.6, 7.9, 8.0, 8.2, (d, 2H, aromatic protons),

Ferrocene carboxylic acid NHS ester (Fc-NHS)⁷



A solution of ferrocenecarboxylic acid (1 g, 2.2 mmol) and N-hydroxysuccinimide (0.58 g, 2.5 mmol) in 40 ml of dioxane was added with stirring to a solution of dicyclohexylcarbodiimide (0.5 g, 2.5 mmol) in 10 ml of dioxane. The mixture was left stirring for 24 hours at room temperature and then checked by TLC. The remaining precipitate was removed by filtration, the filtrate was concentrated under reduced pressure and the obtained crude product was purified by flash column chromatography using dichloromethane:methanol (99:1) as eluent. Yield: 1.3 g (92%) $^1\text{H-NMR}$ (CDCl_3): δ (ppm): 2.9 (s, 4H, $\text{O}=\text{C}-\text{CH}_2$), 4.4 (s, 5H, Fc CH protons), 4.6 (m, 2H, Fc CH protons), 5.0 (m, 2H, Fc CH protons).

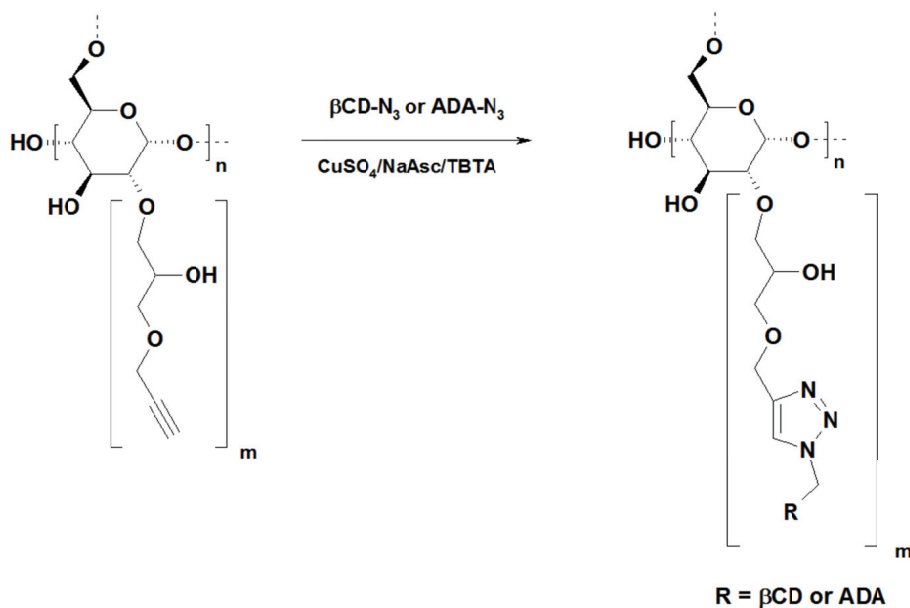
1-azido-11-rhodamidyl-3,6,9-trioxaundecane (Rh-N₃)



Rhodamine B (409 mg, 0.85 mmol) and 1-amino-11-azido-3,6,9-trioxaundecane (100 mg, 0.57 mmol) were dissolved in 10 mL dichloromethane and mixed with under stirring with DIPEA (0.3 mL), EDCI (26 mg, 1.17 mmol) and a catalytic amount of DMAP. The reaction mixture was stirred at room temperature. The solvent was evaporated and the residue was purified by flash chromatography (dichloromethane:methanol 4:1) to afford the product as bright pink oil. Yield: 310 mg (84%). ¹H-NMR (CDCl₃): 1.15 (t, 12H), 3.2-3.5 (m, 24H), 6.23 (d, 1H), 6.25 (d, 1H), 6.35 (d, 2H), 6.4 (d, 2H), 7.03 (m, 1H), 7.4 (m, 2H), 7.9 (m, 1H).

Synthesis of dextran polymers.

General procedure for the preparation of dextran-βCD and dextran-ADA by alkyne-azide cycloaddition

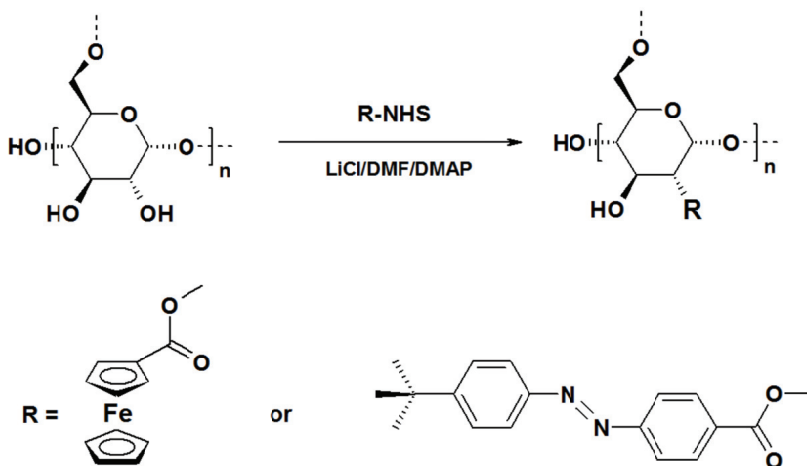


0.25 g of alkyne-grafted dextran (0.072-0.305 mmol alkyne), $\beta\text{CD-N}_3$ or ADA-N_3 (0.134-0.610 mmol), and TBTA (0.011-0.456 mmol) were dissolved in 25 mL of degassed DMSO/water 1:1 under nitrogen atmosphere. Sodium ascorbate (0.0144-0.061 mmol) was added and the solution was degassed by ultrasound and subsequent bubbling with nitrogen for 10 min while reaching 50°C. CuSO_4 (0.0072-0.0305 mmol) was added and the solution was stirred for 24 h and subsequently dialyzed against water for 72 h. The polymers were obtained as white solids by freeze-drying.

$\beta\text{CD-Dex}$: $^1\text{H-NMR}$ (D_2O): δ (ppm) 3.05, 3.25 (d, 2H, $\text{H}_{6'a,b}$), 3.6-4.2 (m, $\text{H}_{2,3,4,5}$, glycerol protons), 4.8 (s, 1H, triazol- CH_2O -), 5.0-5.3 (m, $\text{H}_{1\text{dextran}}$ and $\text{H}_{1\beta\text{CD}}$), 8.2 (s, 1H, $\text{H}_{\text{triazol}}$).

ADA-Dex : $^1\text{H-NMR}$ (DMSO-d_6): δ (ppm) 1.45 (s, 6H, CH_2), 1.6 (dd, 6H, CH_2), 1.95 (s, 3H, CH), 3.0-3.8 (m, $\text{H}_{2,3,4,5}$, glycerol protons), 4.0 (s, 2H, ADA-CH_2 -), 4.4-5.0 (m, $\text{H}_{1\text{dextran}}$ and OH), 7.9 (s, 1H, $\text{H}_{\text{triazol}}$).

General procedure for the preparation of Fc-dextran and Azo-dextran by transesterification.



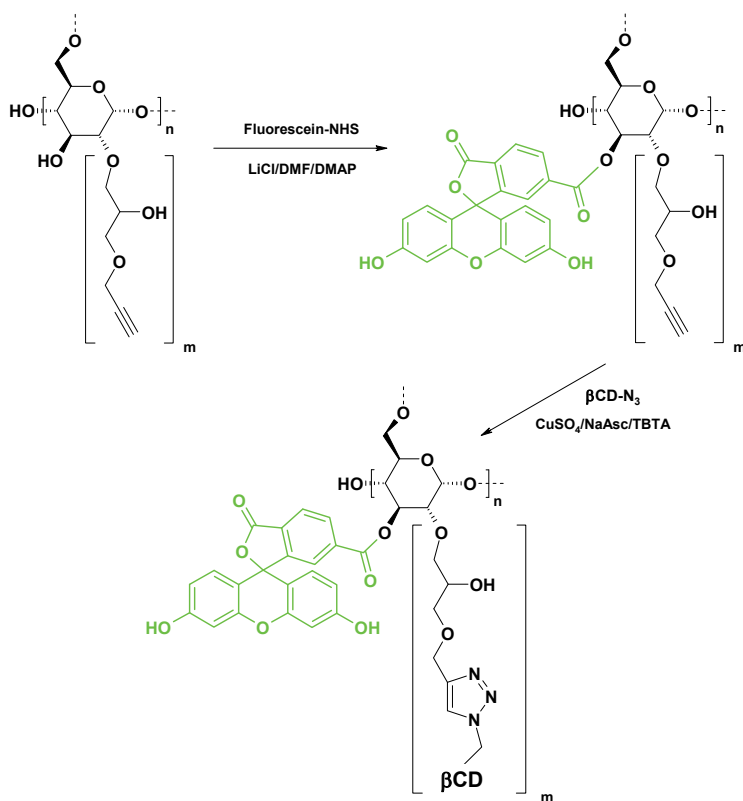
Lithium chloride (0.125 g) was dissolved in 10 mL of anhydrous DMF, under nitrogen atmosphere at 70°C with magnetic stirring. Previously dried dextran (0.5 g, M_w 40 kDa, dried at 115 °C in vacuum overnight) was added to the and stirred until complete dissolution. Subsequently, DMAP (0.8 mmol) and Fc-NHS or Azo-NHS ester (0.2 mmol) were added, the temperature was increased to 90°C and the reaction continued for the next 2 hours with continuous stirring. After two hours, the temperature was switched off and the reaction was left stirring overnight at room temperature. Then, the product was precipitated with EtOH, dialyzed against water and freeze dried. The ferrocene content in the polymers was estimated by UV-Visible spectrophotometry using ferrocenecarboxylic acid as standard.

Fc-Dex: $^1\text{H-NMR}$ (DMSO- d_6): δ (ppm) 3.0-4.4 (m, $\text{H}_{2,3,4,5}$, Fc protons), 4.5-5.0 (m, $\text{H}_{1\text{dextran}}$ and OH).

Azo-Dex: $^1\text{H-NMR}$ (DMSO-d_6): δ (ppm) 1.3 (s, 9H, $-\text{C}(\text{CH}_3)_3$), 3.0-4.0 (m, $\text{H}_{2,3,4,5}$), 4.5-5.0 (m, $\text{H}_{1\text{dextran}}$ and OH), 7.6, 7.9, 8.0, 8.2 (s, 8H, aromatic azo protons).

Synthesis of fluorescent dextran polymers for confocal microscopy

β CD-dextran-fluorescein

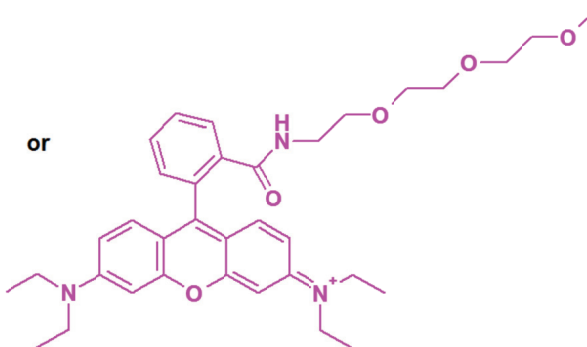
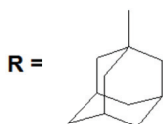
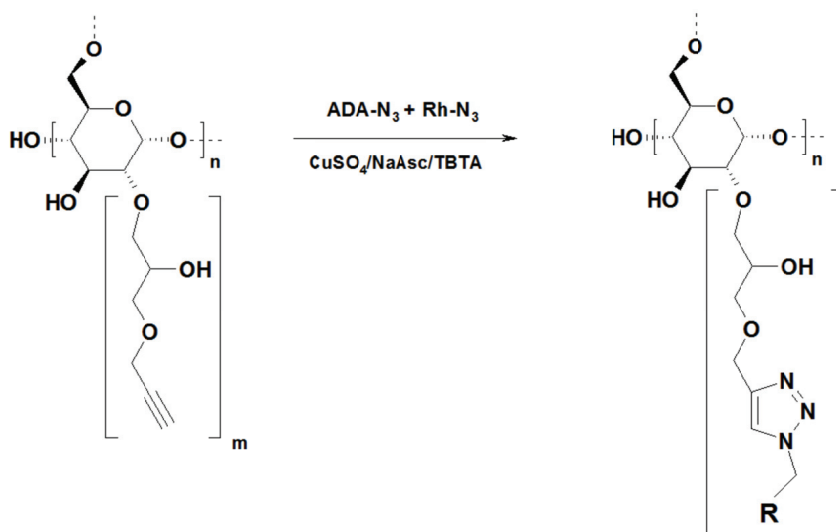


Lithium chloride (0.125 g) was dissolved in 10 mL of anhydrous DMF, under nitrogen atmosphere at 70°C with magnetic stirring. Dextran GP (0.5 g, dried at 115°C in vacuum overnight) was added and stirred until complete dissolution. Subsequently, DMAP (0.8 mmol) and carboxyfluorescein-NHS ester (0.2 mmol) were added, the temperature was increased to 90°C and the reaction continued for the next 2 hours with continuous stirring. After two

hours, the temperature was switched off and the reaction was left stirring overnight at room temperature. Then, the product was precipitated with EtOH, dialyzed against water and freeze dried.

The resulting carboxyfluorescein grafted dextran (FITC-Dex) was then treated with β CD- N_3 under “click chemistry” conditions as described above and purified by precipitation and dialysis.

ADA-dextran-rhodamine



This polymer was prepared by essentially the same procedure used for the preparation of ADA-dextran, except that Rh-N₃ (0.005 mmol) was also added to the reaction mixture. The polymer was purified by precipitation and dialysis.

3.3 RESULTS AND DISCUSSION

In this work, dextran was selected as backbone for the attachment of complementary host-guest units due to its hydrophilicity and biocompatibility, availability of a wide range of molecular weights and facility of modification.

Two synthetic routes were used for the preparation of the polymers. The first route involved etherification of dextran with propargyl glycerol followed by a “click” reaction with an azide.³ This route was used to prepare cyclodextrin and adamantane appended polymers. The ferrocene and azo polymers were prepared in one step by transesterification of the corresponding NHS esters with dextran in aprotic conditions.

Tables 1 and 2 show the degrees of substitution of the prepared polymers as determined by ¹H-NMR (for dextran GP, cyclodextrins, adamantane and azo polymers) or spectrophotometry (for ferrocene).

Table 1. Degrees of substitution of the different batches of 10 kDa and 40 kDa dextrans modified with propargyl glycerol (dextran-GP).

Mw	10 kDa		40 kDa	
DS [mol] %	8	19	5	16
	11	25	8	20
	15	29	13	25

Table 2. Degrees of substitution (DS) of the different batches of 10 kDa and 40 kDa dextrans modified with guest (Ada, Azo and Fc) and host groups (α - and β CDs).

Dextran	Guest molecule [mol]%			Host molecule [mol]%	
	Ada	Azo	Fc	β CD	α CD
10 kDa	4	2	3	23	19
	6	3	9	29	24
	10	6	15	-	-
40 kDa	7	1	6	19	18
	9	2	9	23	25
	11	10	10	-	-

Figure 3.3 shows the ^1H -NMR spectra of dextran-GP (DS 0.20) and the corresponding dextran- β CD in D_2O . The main distinct feature of the proton spectrum of dextran-GP is the presence of two signals at 3.0 and 4.4 ppm, corresponding to the methine and methylene protons of the propargyl group. The integration ratio of any of these protons with respect to the anomeric signal of the dextran glucose units (at 5.1 ppm) gave the degree of substitution of the polymer (0.20 in the example of Figure 3.3a). After reaction of this polymer with β CD mono-azide the signals disappear and a new signal appears at 8.2 ppm, corresponding to the proton of the newly formed 1,4 disubstituted 1,2,3-triazol group. New signals in the region of the anomeric protons (5.0-5.4 ppm) are also visible accounting for the presence of the cyclodextrin ring. In addition, the diastereotopic protons of position 6 of the substituted glucose ring in β CD can be observed at 3.0 and 3.3 ppm. The degree of substitution was calculated by the relationship $1.1/5.7 = 0.19$ where 1.1 is the integral of the triazol proton and 5.7 comes from the difference $12.7-7$ (subtracting the contribution of the seven anomeric protons of β CD to the overall anomeric integral). As can be seen, the DS values of both dextran-GP and dextran- β CD match very well indicating a quantitative alkyne-azide reaction.

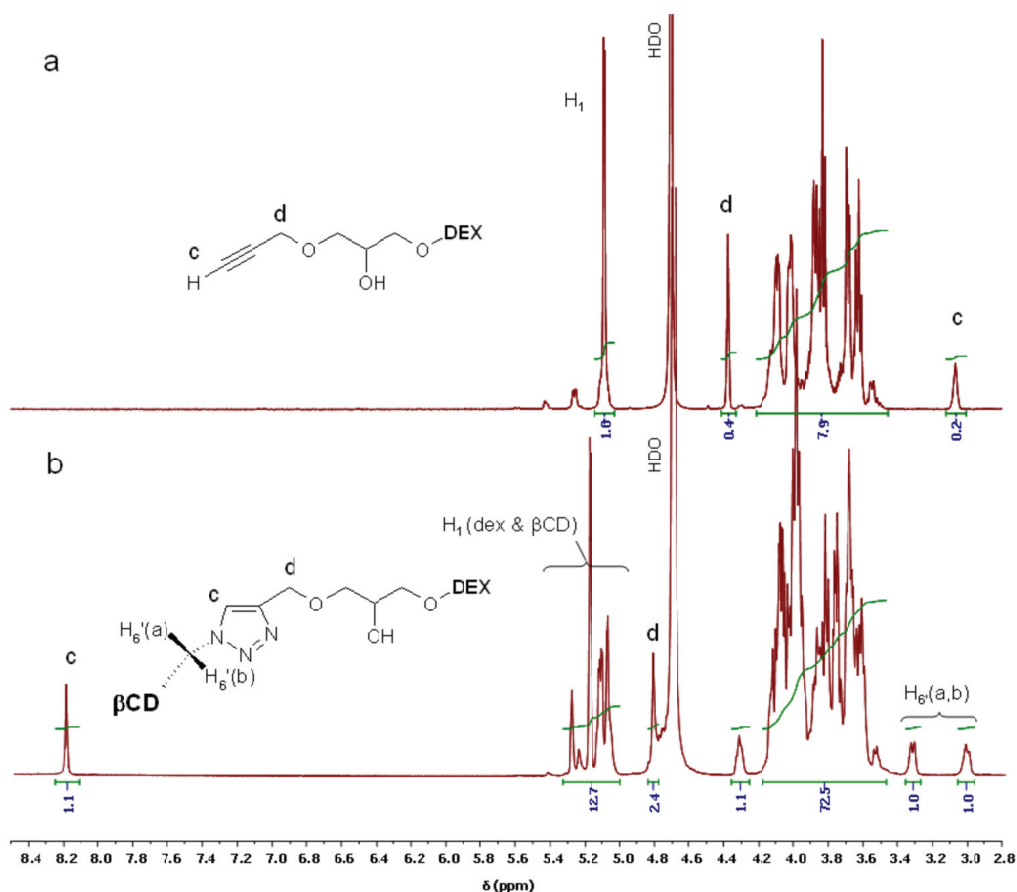


Figure 3.3 600 MHz ^1H -NMR spectra of dextran-GP (a) and dextran-cyclodextrin (b) in D_2O .

Figure 3.4 shows the ^1H -NMR spectra of ADA- N_3 and dextran-ADA in DMSO-d_6 . In the spectrum of the polymer the signals of the ADA unit are present below 2 ppm while the triazol signal appears at 8 ppm. The assignment of the signals between 4.3 and 5 ppm was made by comparison with literature reports on the NMR spectra of dextran in DMSO .⁸ This facilitated the assignation of the anomeric protons at 4.7 ppm which allowed the calculation of the degree of substitution by the integral ratio triazole/anomeric ($0.9/7.8 = 0.11$).

Doctoral Thesis

In the case of the dextran-azo polymer, the aromatic signals of the 4,4'-disubstituted azobenzene group appear as broad singlets between 7.5-8.5 ppm while the ^tBu group is shown at 1.3 ppm (Figure 3.5). The calculation of the DS of the dextran-azo polymer was done by assigning to the ^tBu group an integral value of 9, resulting in a value of 9.7 for the anomeric protons and thus a degree of substitution of $1/9.7 = 0.103$.

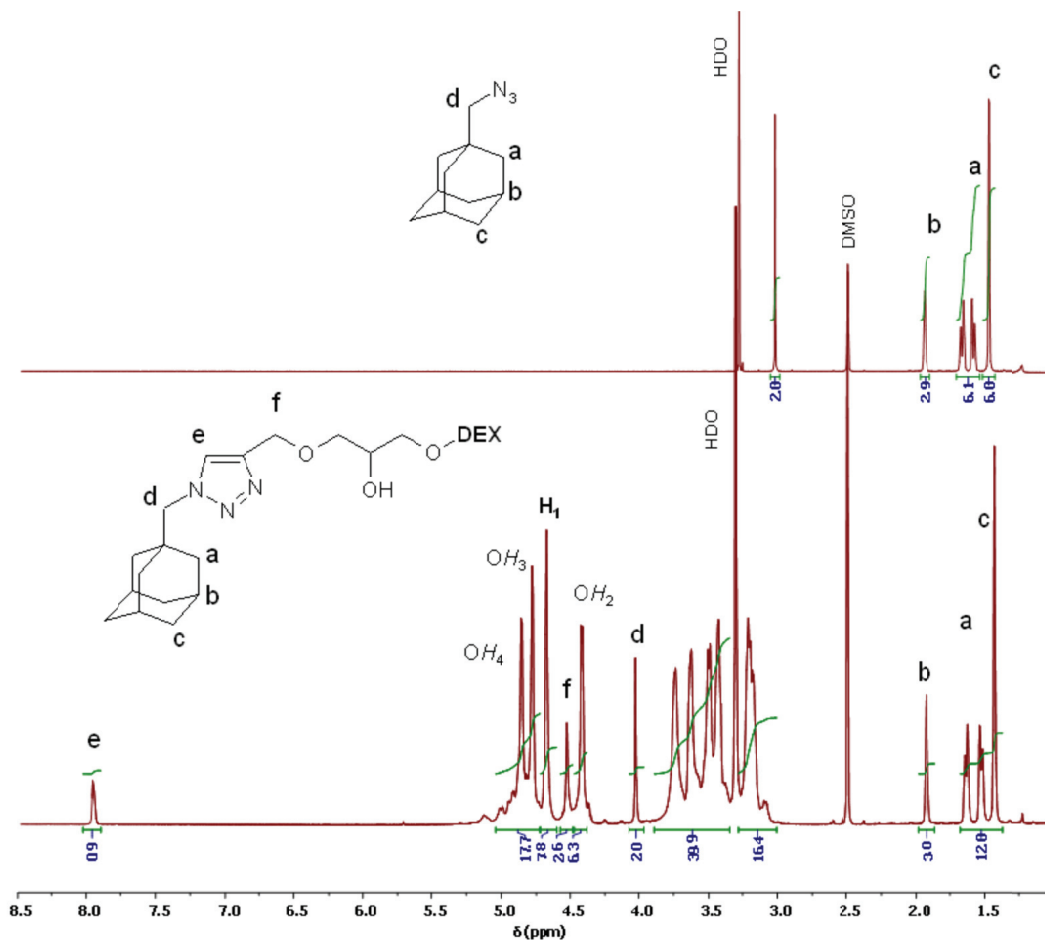


Figure 3.4 600 MHz ¹H-NMR spectra of ADA-N₃ (a) and dextran-ADA (b) in DMSO-d₆.

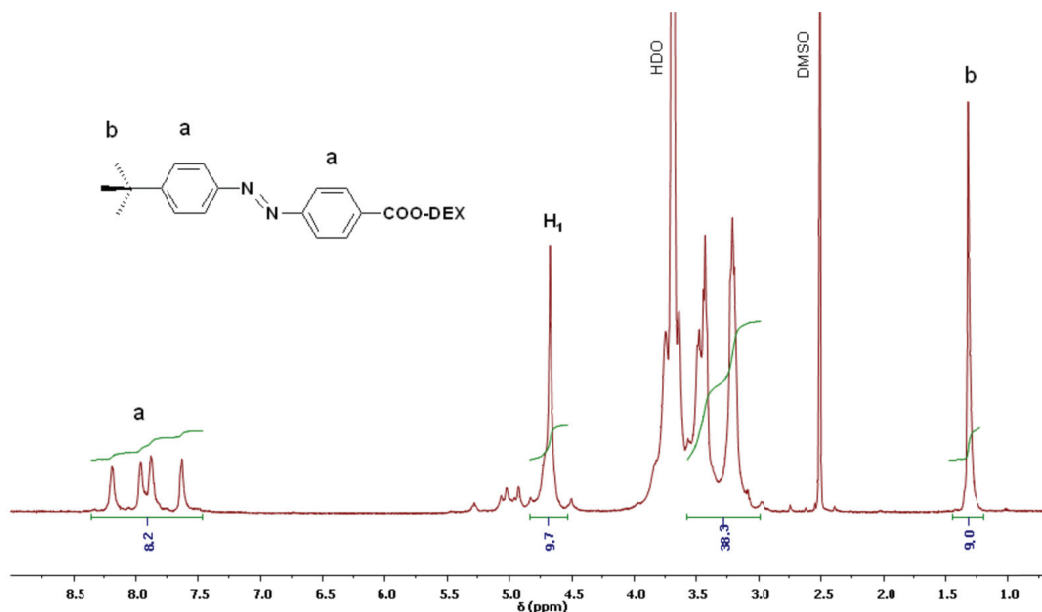


Figure 3.5 600 MHz ¹H-NMR spectra of dextran-azo in DMSO-d₆.

3.5 CONCLUSIONS

Copper(I) catalyzed azide-alkyne cycloaddition reactions has proven to be a convenient method to attach different substituents to a dextran polymer backbone, from hydrophilic cyclodextrins to hydrophobic adamantane units. The requirement to modify the precursor materials to attach azide and alkynyl groups is compensated by versatility of this reaction, giving the possibility to obtain a wide range of polymer with different molecular weights and substitution degrees. On the other hand, transesterification reactions allowed the preparation of ferrocene and azo containing polymers in one step, although the degrees of substitution in this case are in general lower than those obtained using the “click” reaction. These materials will be used in the next chapters to prepare a series of self-assembled nanocontainers with interesting properties.

REFERENCES

1. S. R. Van Tomme, W. E. Hennink, *Exp. Rev. Med. Dev.* 2007, **4**, 147.
2. T. Heinze, T. Liebert, B. Heublein, S. Hornig, *Adv. Polym. Sci.* 2006, **205**, 199.
3. T. T. Nielsen, V. Wintgens, C. Amiel, R. Wimmer, K. L. Larsen, *Biomacromolecules*, 2010, **11**, 1710.
4. T. R. Chan, R. Hilgraf, K. B. Sharpless, V. V. Fokin, *Org. Lett.*, 2004, **6**, 2853.
5. H.-S. Byun, N. Zhong, R. Bittman, *Org. Synth.* 2004, **10**, 690.
6. B. Priewisch, K. Rück-Braun, *J. Org. Chem.* 2005, **70**, 2350
7. S. Takenaka, Y. Uto, H. Kondo, T. Ihara, M. Takagi, *Anal. Biochem.* 1993, **218**, 436
8. K. Fiege, H. Lünsdorf, S. Atarijabarzadeh, P. Mischnick, *Beilstein. J. Org. Chem.*, 2012, **8**, 66.

CHAPTER 4

NANOCAPSULE FORMATION FROM COMPLEMENTARY CYCLODEXTRIN AND ADAMANTANE-APPENDED DEXTRAN-BASED POLYMERS

4.1 ABSTRACT

In this chapter we report the formation of a novel class of nanocapsules assembled via supramolecular interactions between specially designed complementary polymers. The proposed method yields well-ordered, stable and size-controlled architectures in short periods of time, which have been characterized by SEM, confocal microscopy, dynamic light scattering and absorption spectroscopy. These capsules are able to encapsulate fluorescent molecules used as a model system and are stable for several weeks.

4.2 INTRODUCTION

The layer-by-layer method relies on a sequential deposition of one material onto another while utilizing different forces. This technique has been used to create capsules or deposit some materials on the surface of a solid substrate. Very often polyelectrolytes are used for the deposition on oppositely charged nanoparticles to create nano- or micro- capsules with well-controlled shell composition and thickness. The main drawback of using polyelectrolytes for the capsules formation or surface deposition is their high dependence on the pH and ionic strength of the surroundings which usually leads to polymer detachment from the surface or capsule walls or induce particle aggregation. One alternative to polyelectrolyte deposition is the use of complementary polymers bearing host and guest moieties able to form supramolecular

aggregates. One of the most popular host/guest pairs is formed by β -cyclodextrin (β CD) and adamantane (ADA), which form a very strong inclusion complex with $K \sim 10^6$ - 10^7 M⁻¹. In recent years, many Ada/ β CD based self-assembling polymeric systems have been developed. For instance, Li at al. synthesized two complementary polymers by grafting either mono-6-amino- β CD or an aminated adamantane derivative to poly (acrylic acid) (pAA).¹ Mixing of both polymers in aqueous solution led to the formation of a reversible polymer network that could be broken by addition of competitive non-bound β CD or by increasing temperatures. The strongest networks were obtained at equimolar ratios of grafted β CD and ADA groups, indicating that binary 1:1 interactions between these functional groups were responsible for network formation.² Natural polysaccharides such as hyaluronic acid³⁻⁵ and chitosan⁶⁻⁸ as well as thermoresponsive dendrimer-like star copolymers⁹ with pendant ADA and β CD units have also been reported to yield self-assembling structures.^{4,9,10}

Nanocapsules are considered one of the most important polymeric self-assembled systems for drug delivery, diagnostics, and sensing.¹¹⁻¹³ The most common approach for nanocapsule preparation based on ADA- β CD interactions is the mixing of solutions containing complementary polymers.¹⁴⁻¹⁶ Jiang and co-workers have prepared stable polymeric micelles and submicrometer size hollow spheres by adding a large volume of water to a mixed solution of ADA-derivatized poly- (*tert*-butyl acrylate-*co*-hydroxyethyl acrylate) as hydrophobic polymer and β CD-modified poly-(glycidylmethacrylate) in DMF.¹⁴ Using a similar approach, the same researchers described the formation of multicore or core-shell architectures from ADA-end-capped poly (ϵ -caprolactone) and polyvinylpyrrolidone-

β CD.¹⁵ Cho and Allcock showed that formation of polymeric micelles could also be achieved by addition of β CD to a hydrophobic polymer composed of ADA-pending polyphosphazene-polystyrene block copolymer.¹⁷ This resulted in a pseudo-amphiphilic polymer tending to form micellar structures (~ 200 nm) in water. More recently, Zhang et al. reported pH-responsive degradable microcapsules (diameter ~ 4 μ m) composed of two biocompatible polymers, dextran-grafted- β CD and poly- (aspartic-grafted-ADA) assembled around a CaCO_3 core containing rhodamine B (RhB). After removing the core with EDTA, hollow microcapsules loaded with RhB were obtained. As β CD was grafted to polyaldehyde dextran (PAD) through pH-sensitive C=N bonds, the capsules could degrade and release RhB in an acidic environment, showing a pH-sensitive release behavior.¹⁸

Here we present a versatile method for the preparation of stable nanometer-scale self-assembled capsules based on supramolecular forces with sufficient permeability to encapsulate small molecules such as fluorophores (Figure 4.1). Gold nanoparticles were chosen to serve as templates for the alternating deposition of ADA and β CD containing polymer layers (Figure 4.2). Commercially available gold colloids (100 and 400 nm) were first wrapped with a thiolated β -cyclodextrin polymer (CDPSH)¹⁹ that acts as a first support layer for the nanocapsule formation. This type of Au/CDPSH modified particles has already been proven to support ADA-modified enzymes.²⁰ Next, complementary layers of polymers **2a** and **1a** were deposited in an alternating way using the strong host-guest interaction between ADA and β CD as a driving force. The capsules were then formed by core dissolution using iodine.

Doctoral Thesis

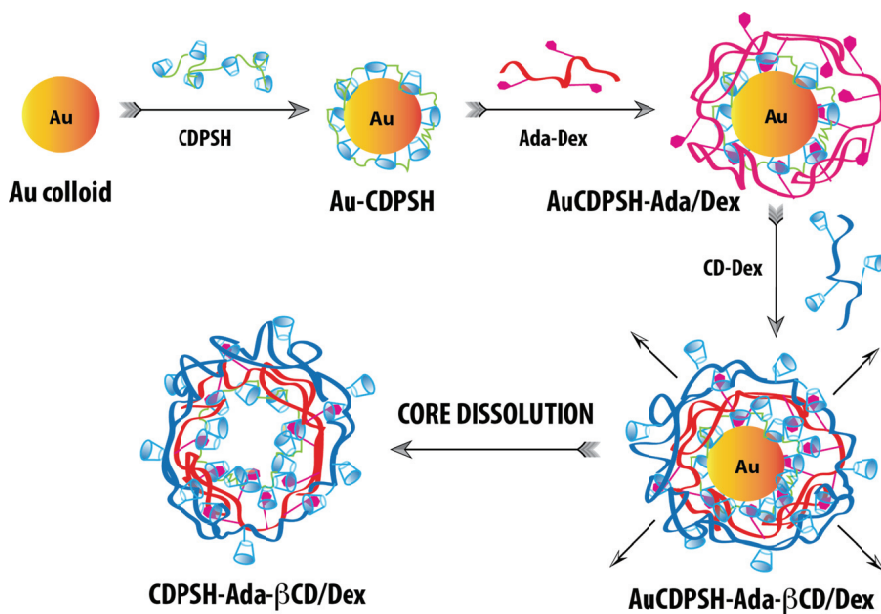


Figure 4.1. Formation of self-assembled nanocapsules via host-guest interactions between complementary β CD and adamantane appended dextran polymers.

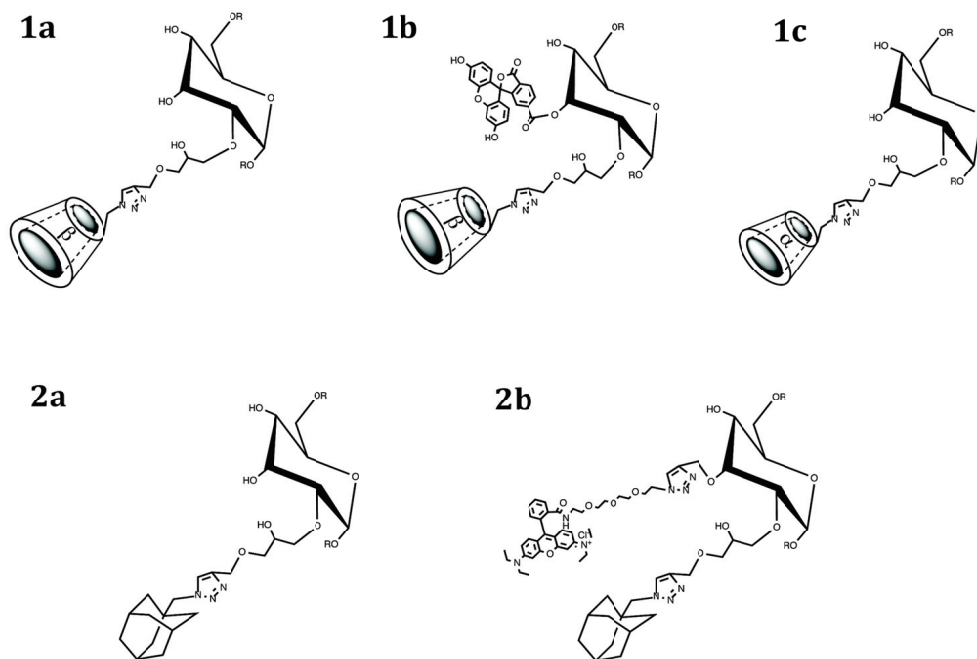


Figure 4.2 Structures of polymers used in this work.

4.3 EXPERIMENTAL SECTION

Materials

The polymers used in this work were prepared as described in Chapter 3. Gold nanoparticles (stabilized suspension in citrate buffer) were purchased from Aldrich and used as received. Solutions were prepared in water purified by a Milli-Q purification system (Millipore) to a resistivity of 18.2 M Ω cm.

Instrumentation

Zeta-sizer

The mean hydrodynamic diameter and the polydispersity index (PDI) of the nanocapsules were determined by dynamic light scattering (DLS) using a Zetasizer Nano ZS (Model ZEN3500) from Malvern Instrument equipped with a He-Ne laser ($\lambda=633$ nm, scattering angle 173 $^\circ$). Each sample was measured ten times for ten seconds at 25 $^\circ$ C and the measurements were made in duplicate; the standard deviation is around 2%. The reported mean value (or Z average size) and the PDI are obtained by cumulant analysis (fit of the logarithm of the correlation function by a third order polynomial) and they are the average of at least three different experiments.

Confocal microscopy

Confocal images were obtained using a NIKON Eclipse, model TE2000-E (Hamamatsu digital camera C8484) confocal microscope, having an oil objective 100x with NA = 1.4. Photographs were taken using zeta stack (the step size of 0.05 μ m) and lambda mode with two channels at 488 nm (Ar laser, blue) and at 543 nm (He-Ne laser, green).

EDS analysis and SEM

The elemental analysis by X-Ray fluorescence and SEM images were performed in a scanning electron microscope JEOL model JSM-6400.

Preparation of self-assembled nanocapsules

In the initial step, an aqueous suspension of gold nanoparticles (1 mL, at different sizes 100 nm and 400 nm) was added to the aqueous solution of the β CDPSH polymer (1 mg/mL). The reaction mixture was then vortexed immediately and incubated at 4°C overnight, followed by centrifugation at 14000 rpm for 5 min. Next, the supernatant was discarded and sample purified two more times in water, then re-suspended in water. The resulting solution of gold nanoparticles with β CDPSH was added dropwise to the Ada-Dex polymer solution (10 kDa, at concentration 1 mmol) and incubated for another 8 hours. The reaction mixture was then purified by centrifugation and the process was repeated with complementary β CD-Dex polymer (10 kDa, at concentration 1 mmol). The whole process was repeated depending on how many of the complementary polymer layers (n-layers) were going to be deposited on the Au templates.

4.4 RESULTS AND DISCUSSION

Figure 4.3 shows the variations in average hydrodynamic particle size upon deposition of the polymer layers onto 100 and 400 nm gold nanoparticles. For the 100 nm Au nanoparticles deposition of CDPSH initially increased the particle sizes in about 50 nm. Next, up to four **2a/1a** layers were deposited on this template in aqueous medium. Interestingly, after each step of attachment of **2a**, the particles either contracted or only slightly increased in

size. This effect can be explained considering the occurrence of a surface reordering of the polymer structures with a partial fusion or interlocking of the layers induced by the very strong and stable interaction between ADA and β CD. In addition, after each deposition of **2a** the outer layer becomes less hydrophilic and can thus repel water, which also influences the value of the hydrodynamic particle size. In a control experiment, the deposition of α CD modified polymer **1c** caused a negligible increase in particle size (Figure 4.3), which is expected considering that the adamantane moiety does not fit in the α CD cavity. This indicates that specific host-guest interactions between the β CD cavities and adamantane are the main driving force for the observed particle growth. A similar size increase trend was observed for the 400 nm particles indicating that the method can also be applied to larger particles.

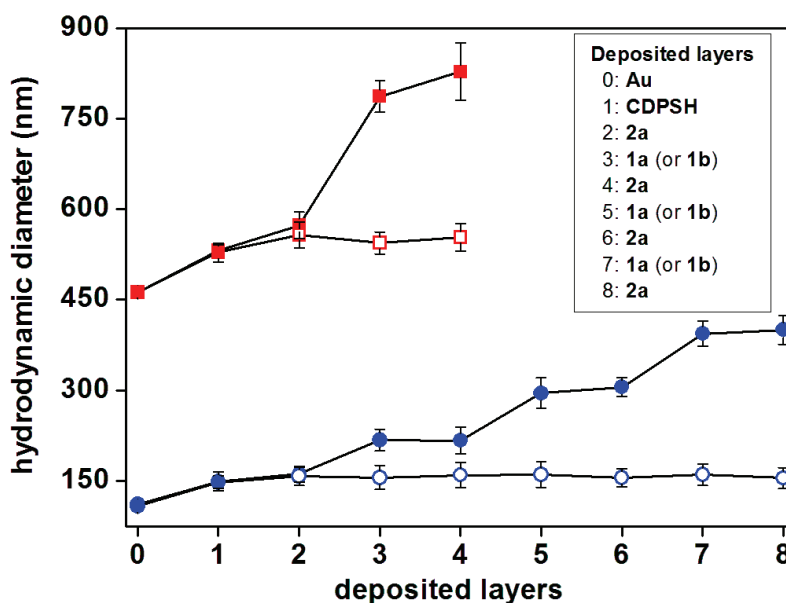


Figure 4.3. Average hydrodynamic particle size as a function of the number of deposited polymer layers onto 100 nm (●) and 400 nm (■) gold nanoparticles. The open symbols correspond to the deposition of α CD polymer **1c**.

A visual proof obtained by confocal microscopy of the formation of well-ordered, self-assembled nanostructures can be seen in Figure 4.4 after the sequential deposition of fluorophore labeled polymers **2b** (red) and **1b** (green) on a 400 nm gold template modified with CDPSH.

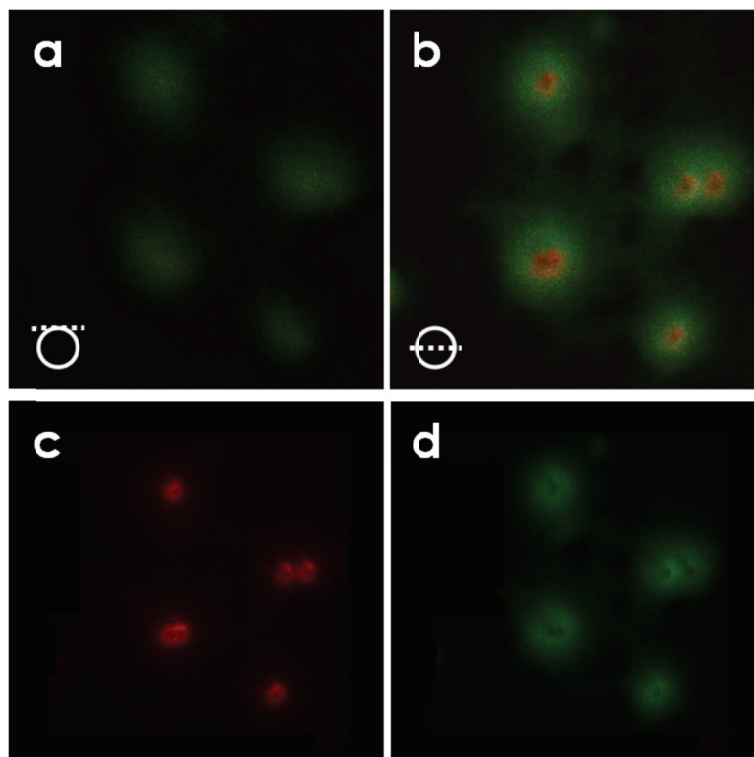


Figure 4.4. a) and b) Z-stack volume reconstruction of precursor nanocapsules made of Au (400 nm)/CDPSH/**2b/1b**. c) and d) filtered images showing the red and green fluorescent layers, respectively from **2b** and **1b**.

The gold core was then removed using excess I₂ in aqueous KI,¹⁹ yielding nanoarchitectures that retained the shape of the central template. The absence of gold was confirmed by EDS analysis (Figures 4.5) and the corresponding SEM images of nanocapsules prepared from 400 nm

nanoparticles reveal an increase of surface roughness after core removal while the average size remains unaltered (Figure 4.6).

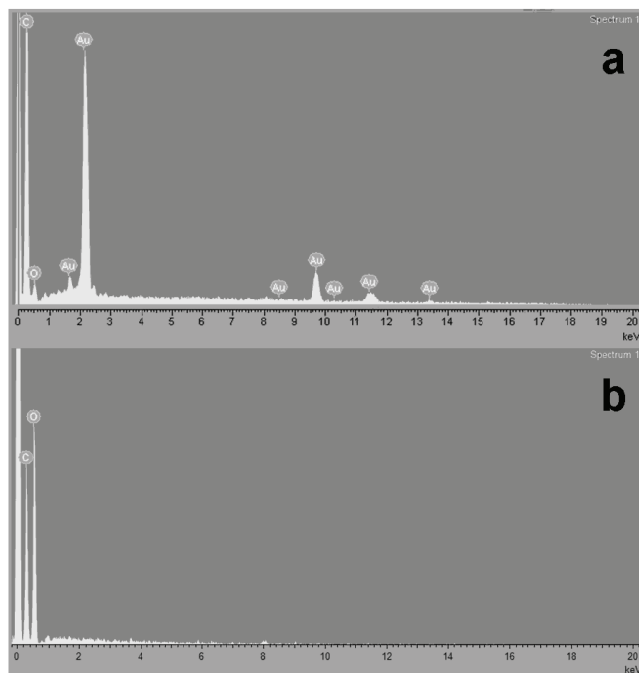


Figure 4.5. EDS analysis of the polymeric nanocapsules before a) and after b) Au core dissolution.

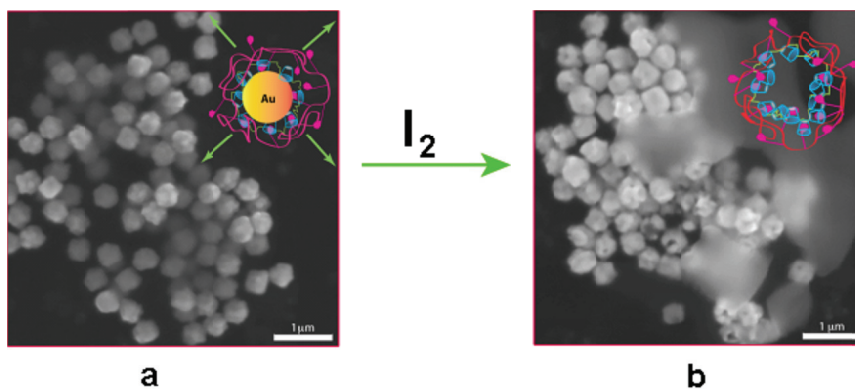


Figure 4.6. SEM images of the polymeric nanocapsules before a) and after b) Au core dissolution.

Confocal images of the nanocontainers also show the absence of the core. In this case, the red fluorescence arising from the first layer cannot be easily differentiated from the green background as in the case of the precursor nanoparticles due to a partial interlocking of the layers originated from the higher mobility of the polymers in the absence of the core although in the filtered images the arrangement of both fluorophores individually is clearly visible.

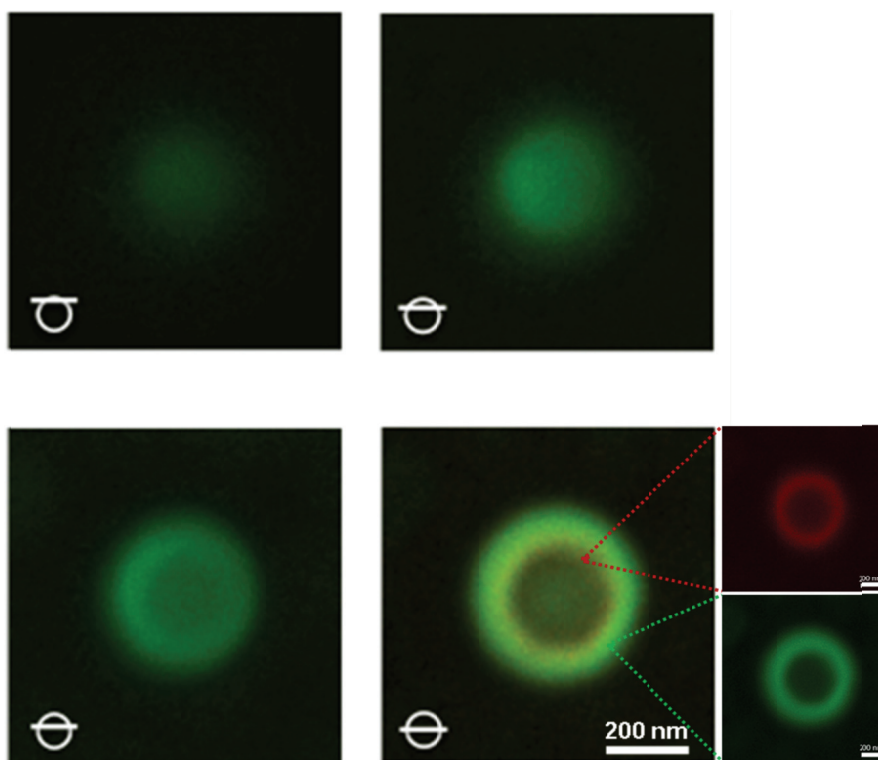


Figure 4.7. Z-stack volume reconstruction of polymeric nanocapsules after Au core dissolution. The filtered images showing the red and green fluorescent layers are shown in bottom right part.

The encapsulation ability of the synthesized polymeric nanocapsules was tested by diffusion of free carboxyfluorescein through the polymer layers of nanocapsules consisting of three polymer layers (CDPSH/**2b/1b**). The encapsulation stage was monitored by confocal imaging and fluorescence measurements (Figure 4.8), where carboxyfluorescein (green) filled in the empty space of the nanocapsules. Some of the dye molecules gradually accumulated in the walls of the capsule.^{21,22} In fact, the inner cyclodextrin polymer surface of the hollow nanospheres has some hydrophobic character owing to the disulfide bonds after gold core removal so that it can accommodate a hydrophobic guests. Moreover, we could speculate that the remaining “empty” β CD hosts may not only play an important role in significantly enhancing solubility of encapsulated molecules but also could protect and allow their release in a more controlled manner. Figure 4.9 shows the confocal image of encapsulated nanocapsules after storage in solution at room temperature for one month. As can be seen, the capsules are stable with time with no leakage observed.

Doctoral Thesis

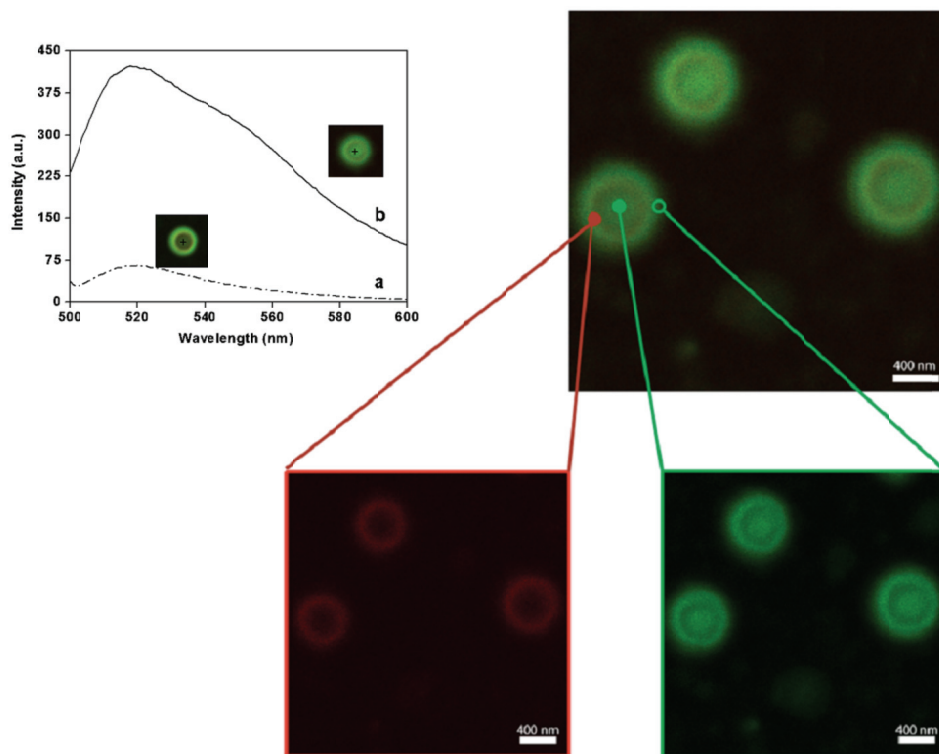


Figure 4.8. Right: Z-stack volume reconstruction of polymeric nanocapsules after exposure to a 1 mM solution of carboxyfluorescein for 48 hours. The filtered images showing the red and green fluorescent layers are placed in bottom part. Left: Fluorescence spectra recorded in the center of free and encapsulated capsules. $\lambda_{\text{exc}} = 494$ nm.

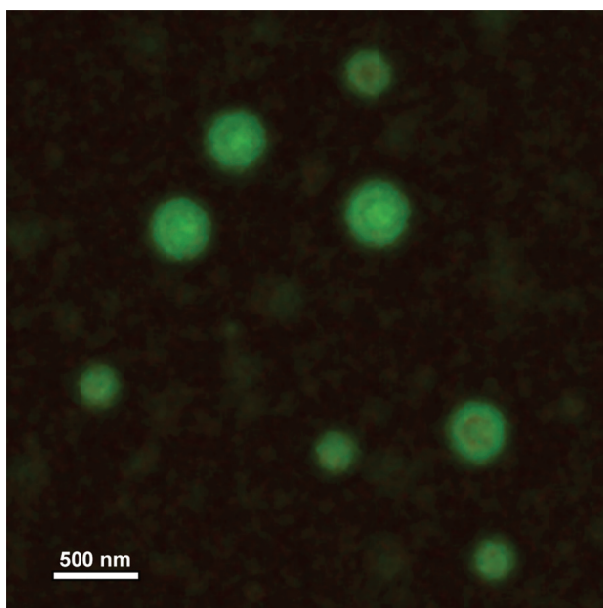


Figure 4.9. Right: Z-stack volume reconstruction of carboxyfluorescein encapsulated nanocapsules after one month of storage at room temperature.

Figure 4.10 shows an overview of the confocal images obtained after each nanocapsule preparation step.

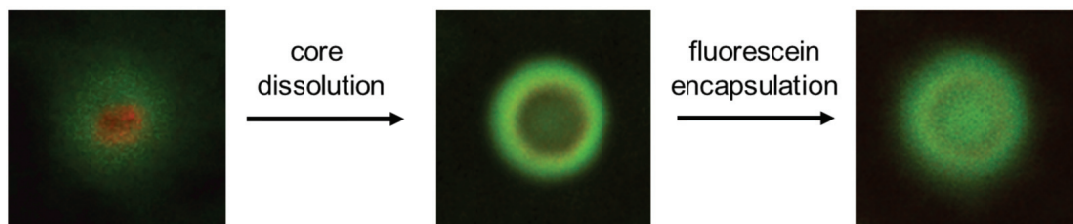


Figure 4.10. Changes in the confocal images (Z-stack volume reconstruction) of prepared nanocapsules after each preparation step.

4.5 CONCLUSIONS

Although the proposed method for nanocapsule formation requires a template and the additional step of core removal, it is simple and can be performed in a simple medium like water where there is no need for the addition of any other solvents or stabilizing agents. In fact, the requirement for use of the templates has its advantage over the size control and uniformity of the created capsules, which could range from nano- to microscale. Additionally, the composition of the capsules also plays a very important role in their programmable properties. Therefore, the proposed model of the bio-friendly polymeric nanocapsules could be used in a broad range of applications, such as encapsulation and release of sensitive macromolecules (enzymes, proteins, DNA), or in the cosmetic industry. The possibility of the modification of the outside polymeric layer (β CD-dextran) with, for example, biomolecular receptors could also be used for targeted drug delivery or in biosensing applications. It is also evident that this approach is not limited only to adamantane polymers. Other types of guest molecules with specific properties such as ferrocene or azo-compounds, which are able to form more sophisticated and stimuli responsive nanocapsules can also be used. This is the subject of Chapter 5.

REFERENCES

1. L. Li, X. Guo, J. Wang, P. Liu, R. K. Prudhomme, B. L. May, S. F. Lincoln, *Macromol.*, 2008, **41**, 8677.
2. F. Manakker, T. Vermonden, C. F. Nostrum, W. E. Hennink, *Biomacromol.*, 2009, **10** 3157.

3. A. Charlot, A. Heyraud, P. Guenot, M. Rinaudo, R. Auzely-Velty, *Biomacromol.*, 2006, **7**, 907.
 4. A. Charlot, R. Auzely-Velty, *Macromol.*, 2007, **40**, 9555.
 5. A. Charlot, R. Auzely-Velty, *Macromol.*, 2007, **40**, 1147.
 6. A. Charlot, R. Auzely-Velty, M. Rinaudo, *J. Phys. Chem.*, 2003, **107**, 8248.
 7. R. Auzely-Velty, M. Rinaudo, *Macromol.*, 2001, **34**, 3574.
 8. R. Auzely-Velty, M. Rinaudo, *Macromol.*, 2002, **35**, 7955.
 9. Z-X. Zhang, X. Liu, F. J. Xu, X. J. Loh, E-T. Kang, K-G. Neoh, J. Li, *Macromol.*, 2008, **41**, 5967.
 10. A. Semenov, A. Charlot, R. Auzely-Velty, M. Rinaudo, *Rheol. Acta*, 2007, **46**, 541.
 11. B. Romberg, W. E. Hennink, G. Storm, *Pharm. Res.*, 2008, **25**, 55.
 12. S. Kim, J-H. Kim, O. Jeon, I. C. Kwon, K. Park, *Eur. J. Pharm. Biopharm.*, 2009, **71**, 420.
 13. H. Maeda, J. Wu, T. Sawa, Y. Matsumura, K. Hori, *J. Controlled Release*, 2000, **65**, 271.
 14. J. Wang, M. Jiang, *J. Am. Chem. Soc.*, 2006, **128**, 3703.
 15. S. Ren, D. Chen, M. Jiang, *J. Polym. Sci., A: Polym. Chem.* 2009, **47**, 4267.
 16. J. Zhang, P. X. Ma, *Angew. Chem., Int. Ed.* 2009, **48**, 964.
 17. S. Y. Cho, H. R. Allcock, *Macromol.*, 2009, **42**, 4484.
 18. C. Li, G-F. Luo, H-Y. Wang, J. Zhang, Y-H. Gong, S-X. Cheng, R-X. Zhuo, X-Z. Zhang, *J. Phys. Chem.*, 2011, **115**, 17651.
 19. L. Sun, R. M. Crooks, V. Chechik, *Chem. Commun.*, 2001, 359.
 20. A. Fragoso, B. Sanromà, M. Ortiz, C. K. O'Sullivan, *Soft Matt.*, 2009, **5**, 400.
 21. G. Ibarz, L. Dähne, E. Donath, H. Möhwald, *Adv. Mater.*, 2001, **13**, 1324.
-

Doctoral Thesis

22. Y. Ma, W. Dong, M. A. Hempenius, H. Möhwald, G. J. Vancso, *Nat. Mater.*,
2006, **5**, 724.

CHAPTER 5

HOST-GUEST ENGINEERED STIMULI-RESPONSIVE NANOCAPSULES

5.1 ABSTRACT

The supramolecular self-assembly of materials through host-guest interactions is a powerful tool to create non-conventional materials. Thus, biodegradable nanocapsules with redox-responsibility were fabricated with non-covalent interactions between β CD and ferrocene (Fc)/or α CD and azobenzene (Azo) units. Different biocompatible polymers, dextran- β CD (β CD-Dex) and dextran-ferrocene (Fc-Dex), dextran- α CD (α CD-Dex) and dextran-azobenzene (Azo-Dex) were assembled in alternating way on gold nanoparticles of two different sizes (100 and 400 nm). The gold nanoparticles were removed by chemical degradation and rhodamine B (RhB) was encapsulated inside the carriers as a model drug. The encapsulation process of the dye molecules was accelerated by oxidation step or by UV-light of the nanocapsules wall, thus enabling easier and faster diffusion through the polymer layers. Confocal laser scanning microscopy (CLSM), scanning electron microscopy (SEM), atomic force microscopy (AFM), RAMAN spectroscopy, UV-spectroscopy and dynamic light scattering (DLS) measurements were employed for the characterization of the nanocapsules.

5.2 INTRODUCTION

Nanoscience and nanotechnology as interdisciplinary fields are among the most dramatically developing areas in science and technology today. They

exhibit an extremely broad range of applications, from electronics to medicine, promising novel, dynamic and radical innovations in different industrial sectors and spheres of human life. Well controlled, self-assembly of block co-polymers may offer new possibilities and broaden the range of applications for biomedical and biotechnological applications such as, drug delivery,¹⁻³ enzyme immobilization,⁴ DNA transfection⁵ or biosensors.^{6,7}

The deposition of well-defined and organized multilayers is crucial for building polymeric carriers, especially for drug delivery applications. In this sense, the layer-by-layer technique (LbL) is a very successful and simple assembling method for template-mediated fabrication of capsules by coating micrometer- and submicrometre-sized particles. The obtained micro- or nano-capsules show precise size and shape, where the thickness and composition of the wall can also be finely tuned. Thus, the core-shell architectures can be formed through self-assembly of copolymers (polymer micelles or vesicles) or by means of surface modification of various particles (inorganic or polymeric) with functional polymers.⁸

As described in Chapter 4, host-guest self-assembly between β -cyclodextrin and “silent” adamantane groups allowed the creation of nanocapsule structures with sufficient permeability to encapsulate small molecules. Selectively tailored molecular assemblies and interfaces can provide a specific chemical function and structure and can change in their environment. For example, responsive polymer materials can adapt to surrounding environments, regulate transport of ions and molecules, change wettability and adhesion of different species on external stimuli, or convert chemical and biological signals into optical, electrical, thermal and mechanical signals, and vice versa. Both types the core-forming polymer (in

micro- and nanogels) and the shell-forming polymer can show stimuli-responsive behavior. Additionally external stimuli can be used to stimulate the self-assembled structures and may induce their reversible or irreversible disintegration, aggregation, swelling and/or adsorption.⁸

Recently, supramolecular materials have attracted a broad range of chemists and material scientists due to their switching and self-healing properties. Invention of switching soft materials such as remotely actuated nanomaterials, artificial molecular muscles, controlled drug delivery and release systems, biosensors, smart and self-healing coatings or shape memory materials was already reported in the literature by several independent research groups. As already explained, various stimuli-responsive nanomaterials can be triggered using different external stimuli such as change in temperature, mechanical force, change in pH, irradiation with light, enzymes and exposure to an electrical or magnetic field.^{8,9}

However, creation of these multi-functional soft materials is sometimes difficult owing to their sophisticated design and synthetic routes. Despite this fact, a number of research groups reported materials that are able to react to external stimulant. Harada and coworkers described stimuli-responsive supramolecular materials built from host and guest polymers. Due to the selective complementary interactions of such materials they can be easily tuned switching efficiencies and functions. They prepared a supramolecular hydrogel with CD or ferrocene grafted polyallylamine polymers that form an inclusion complex that undergo sol-gel transition by applying a redox potential that generates a ferrocenium group that destabilize the inclusion complex.¹⁰ These types of electric stimuli materials have some advantages over other developed materials (e.g. those responsive to ultrasound, light, or

magnetic field), as electric signals are easy to generate and control. In the drug delivery applications there have been constant improvement in the formulation of transporting vesicles that are able to respond to one or even two different external stimulus. Ge and coworkers described a temperature and electric field dual-stimulus responsive nanoparticle system. In their approach they proposed a less invasive and well-controlled drug delivery system in comparison with other similar formulations. The nanoparticles of a conducting polymer (polypyrrole) were loaded with a drug and suspended in a temperature-responsive hydrogel, which is a liquid at low temperature but becomes a gel at body temperature. The drug release from the conductive nanoparticles was controlled by the application of a weak, external electric field.¹¹

Many other examples of various stimuli responsive systems for different applications exist with applications ranging from medicine to cosmetics. They are still being a subject of investigation to improve their efficiency and function. Furthermore, in a case of the biomedical field the biodegradable and non-toxic models are crucial.

In this chapter we report the design and characterization of a new class of stimuli-responsive hollow nanocapsules as an extension of the nanoparticle-templated host-guest strategy described in Chapter 4. The inclusion complex formed between two complementary polymers was regulated either by applying a redox potential or light. For this, two systems were employed using ferrocene or (*E*)-4-((*tert*-butyl)phenyl)diazenyl) grafted dextran polymers (guest) and β CD or α CD grafted dextran polymer (host). All synthesized polymers were water-soluble and the supramolecular LbL self-assembly of the nanocapsules could be performed in aqueous solutions, thus

minimizing the use of organic solvents. Fluorescence labeled β CD-dextran polymers were also synthesized for better visualization of the formation of the nanocapsules. We also report initial results on the encapsulation properties of both types of stimuli-responsive nanocapsules.

5.3 EXPERIMENTAL SECTION

Materials

The polymers used in this work were prepared as described in Chapter 3. Gold nanoparticles (stabilized suspension in citrate buffer) were purchased from Aldrich and used as received. $\text{Ru}(\text{NH}_3)_6\text{Cl}_3$ and rhodamine B (Aldrich) were used as received.

Instrumentation

Zeta-sizer

The mean hydrodynamic diameter and the polydispersity index (PDI) of the nanocapsules were determined by dynamic light scattering (DLS) using a Zetasizer Nano ZS (Model ZEN3500) from Malvern Instrument equipped with a He-Ne laser ($\lambda=633$ nm, scattering angle 173°). Each sample was measured ten times for ten seconds at 25°C and the measurements were made in duplicate; the standard deviation is around 2%. The reported mean value (or Z average size) and the PDI are obtained by cumulant analysis (fit of the logarithm of the correlation function by a third order polynomial) and they are the average of at least three different experiments.

Confocal microscopy

Confocal images were obtained using a NIKON Eclipse, model TE2000-E (Hamamatsu digital camera C8484) confocal microscope, using oil objective 100× with NA = 1.4. Photographs were made using zeta stack (the step size of 0.05 μm) and lambda mode with two channels at 488 nm (Ar laser, blue) and at 543 nm (He-Ne laser, green).

Surface enhanced Raman spectroscopy (SERS)

Raman spectra of nanocapsules were recorded at 20°C by means of a microprobe setup (Raman Spectroscopy, FT-IR. Renishaw). Exciting radiation at 785 nm was focused onto the sample spotted on Klarite® KLA-312 gold coated glass substrates through a 100× objective with NA = 0.9. To avoid unwanted laser-induced transformations, neutral filters of different optical densities were used, whenever necessary.

Spectra were collected in the wavenumber ranges 100–3700 cm⁻¹ with an integration time of 300 s. The resolution was about 0.35 cm⁻¹ per pixel with a typical laser power set at 10 mW. For each sample, 3 series of independent measurements were carried out and for each set, the Raman experiment was repeated 6 times to check the reproducibility of the measurement and to minimize the noise ratio of the signals.

Fluorescence spectroscopy

Fluorescence measurements were performed in a Cary Eclipse spectrofluorimeter (Varian) at 25°C in 1 mm path cells. Excitation and emission slits were set at 10 nm. Rhodamine B was excited at 540 nm.

Atomic Force and SEM Microscopy

ESEM analysis was performed in a scanning electron microscope JEOL model JSM-6400. AFM topographic images were obtained in a Molecular Imaging model Pico SPM II (Pico+) microscope in tapping mode.

Electrochemical Measurements

Electrochemical measurements were conducted on an Autolab PGSTAT12 potentiostat using a three-electrode cell. A glassy carbon rod was used as the working electrode in combination with a Ag/AgCl(sat) reference electrode and a Pt wire which served as the counter electrode. The working electrodes were polished with diamond slurry, sonicated in water and checked for cleanness with 1 mM potassium ferricyanide in 0.1 M KCl.

For the encapsulation studies, solutions of Ru(NH₃)₆Cl₃ (0.1 mM in 0.1M KCl) were prepared immediately before use.

Layer-by-layer self-assembly of Fc-Dex/ β CD-Dex and Azo-Dex/ α CD-Dex multi-layered films on Au nanoparticles

In the initial step, an aqueous suspension of gold nanoparticles (1 mL, at different sizes 40 nm, 100 nm and 400 nm, Aldrich) was added to an aqueous solution of the β - or α CDPSH polymers (1 mM). The reaction mixture was then vortexed immediately and incubated at 4°C overnight, followed by centrifugation at 14000 rpm for 5 min. Next, the supernatant was discarded and the sample was washed two times in water, then re-suspended in water. The resulting solution of gold nanoparticles with β CDPSH or α CDPSH was added dropwise to a Fc-Dex or Azo-Dex polymer solution (40 kDa, 1 mmol) and incubated for another 8 hours. The reaction mixture was then purified by centrifugation and the process was repeated with complementary β CD-Dex

or α CD-Dex polymer (40 kDa, 1 mmol). The whole process was repeated depending on the number of complementary polymer layers (n-layers) to be deposited on the Au templates.

Preparation of hollow nanocapsules by gold core dissolution

For the formation of hollow polymeric nanospheres the Au core was dissolved using I_2 in KI and next, purified using ethyl acetate¹² and dialyzed against water for 48 hours.

Encapsulation/release studies

The encapsulation/release properties of the prepared nanocapsules were measured using either rhodamine B or $Ru(NH_3)_6Cl_3$. The dye or ruthenium solutions (0.1 mM) were mixed with prepared solutions of nanocapsules and stirred for different times to allow the diffusion through the nanocapsule walls (with or without external stimulus) and thus measuring the encapsulation/release efficiency. After the encapsulation step was completed the remaining “free” molecules were purified by dialysis (MWCO 5 kDa) and checked by UV-spectrophotometry. After the release processes the “empty” nanocapsules were also purified by dialysis.

For the Fc-based nanocapsules the “open” and “close” stimuli consisted of applying a potential of +0.2 V or +0.0 V vs. Ag/AgCl, respectively for 1 min in the electrochemical cell.

Meanwhile, for the azo-based nanocapsules the “open” and “close” stimuli consisted of exposing a solution of the nanocapsules to a mercury lamp ($\lambda = 365$ nm) or ambient light for 20 min, respectively, at room temperature.

5.4 RESULTS AND DISCUSSION

Figure 5.1 depicts the chemical structures of the host polymers (β CD-Dex, α CD-Dex) and guest polymers (Fc-Dex, Azo-Dex) used in this work. According to ^1H NMR spectroscopy, the DS of α - and β CD on the dextran polymer were 19 and 23 mol% respectively, while guest grafted dextran polymers Fc-Dex and Azo-Dex were substituted 9 and 6 mol%, respectively. This means that a 2-4 fold excess of the host molecule was used in all cases in order to maximize guest complexation considering the complexity of the polymers used.

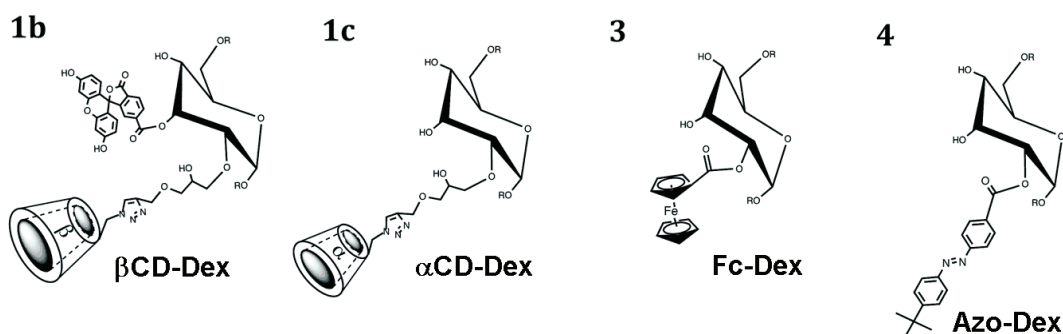


Figure 5.1. Chemical structures of the host polymers β CD-FI-Dex (**1b**) and α CD-Dex (**1c**) and guest polymers Fc-Dex (**3**) and Azo-Dex (**4**).

Figure 5.2 shows the strategy employed for the preparation of hollow nanocapsules. Gold nanoparticles were used as colloid templates for the fabrication of nanocapsules. The deposition of the first support layer for the nanocapsule formation was done by mixing aqueous solutions of either thiolated β CD polymer (β CDPSH) or thiolated α CD polymer (α CDPSH) with 100 or 400 nm gold nanospheres. The interactions between gold and thiol groups are those of covalent bond and surrounding cyclodextrins additionally prevent unwanted aggregations of nanoparticles.¹²

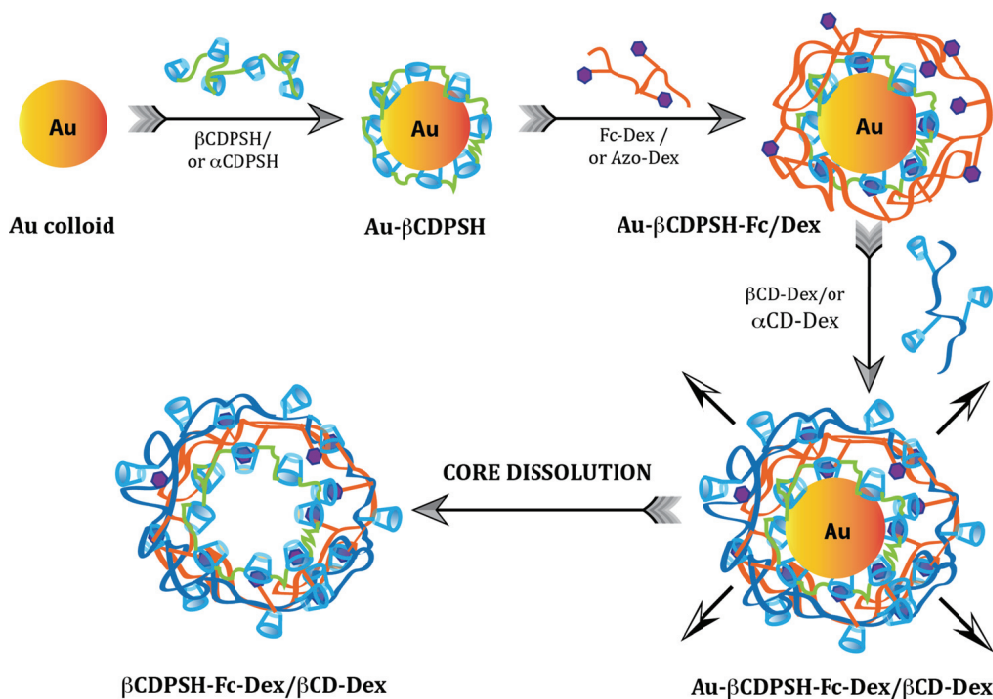


Figure 5.2. Schematic representation of the formation of LbL self-assembled nanocapsules via host-guest interactions between complementary β CD and Fc appended dextran polymers (the same methodology was applied for the α CD/Azo appended dextran polymers).

5.4.1 FERROCENE-BASED REDOX-RESPONSIVE NANOCAPSULES

Deposition of polymer layer on the gold template

The growth of the Au/ β CDPSH/Fc-Dex/ β CD-Dex multilayered films were studied by DLS measurements. Evidently, their size depends on the size of the gold template employed for the next polymer layers deposition. Additionally, DLS measurements also showed a “contraction” of the layers after deposition of Fc-Dex layers on β CD-Dex (Figure 5.3). In this case, substitution of β CD-Dex for an α CD-based polymer provoked only a slight increase in particle size which can be explained considering that the

association constant of Fc for β CD in its reduced state is known to be much larger than that for α CD (Fc/ α CD; $K_a = 0.14 \times 10^3 \text{ M}^{-1}$, Fc/ β CD; $K_a = 17 \times 10^3 \text{ M}^{-1}$).¹⁰

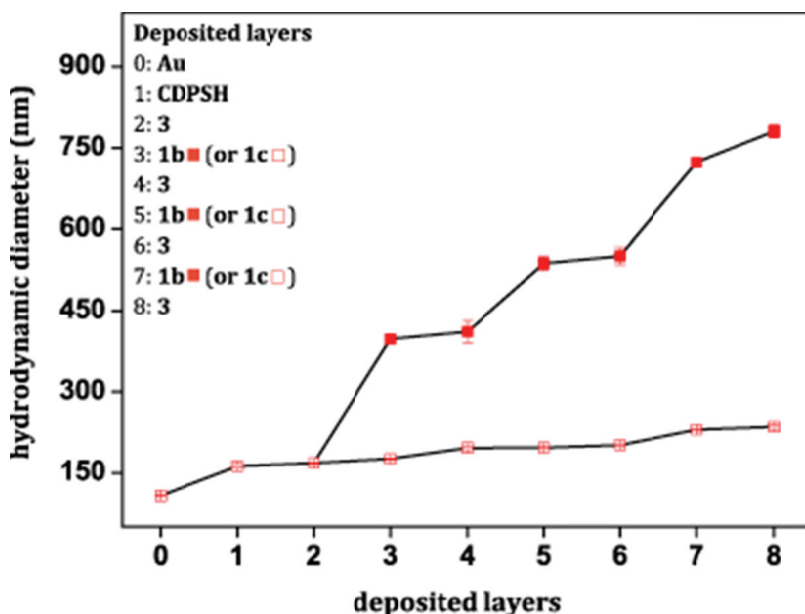


Figure 5.3. Average hydrodynamic particle size as a function of the number of deposited polymer layers onto 100 nm.

ESEM images presented in the Figure 5.4 show the surface of the 400 nm nanoparticles wrapped with three supramolecular polymeric layers. Gold nanoparticles wrapped with polymer layers are better dispersed (less aggregated) as compared with gold nanoparticles without polymers and their surface also differs, displaying more roughness. The particles were also visualized by confocal microscopy, using a fluorescein-labeled β CD-Dex

polymer (Figure 5.5), in which the fluorescent layer is clearly visible around the gold template.

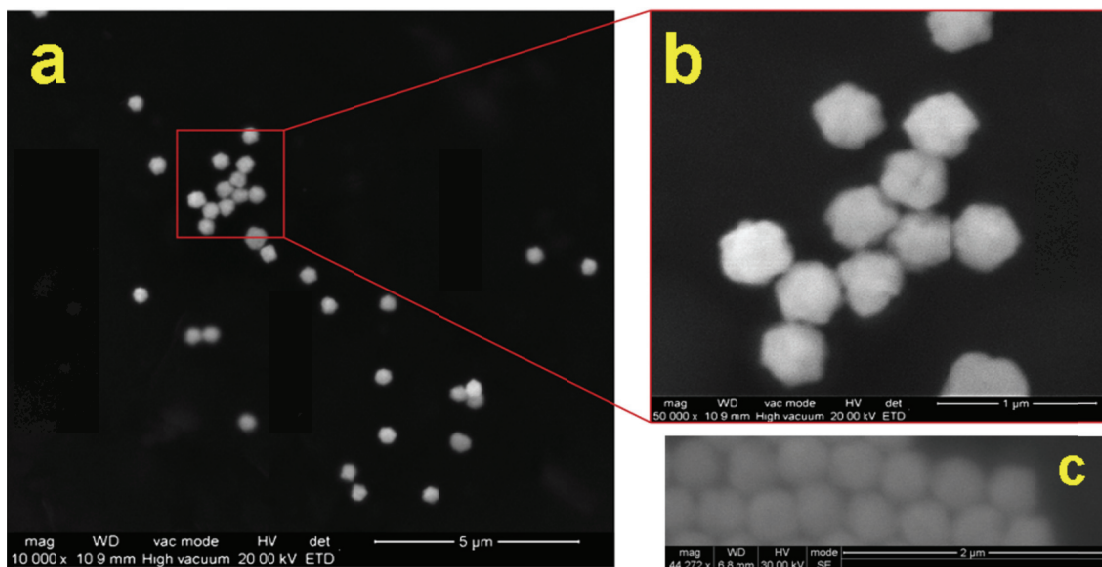


Figure 5.4. a,b) ESEM images of Au nanoparticles (400 nm) wrapped with β CDPSH/Fc-Dex/ β CD-Dex polymers. c) ESEM images of unmodified Au nanoparticles.

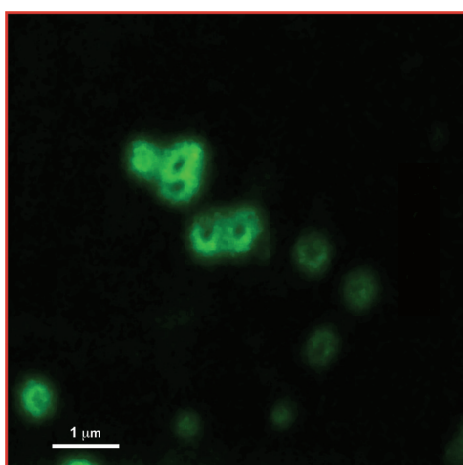


Figure 5.5. Confocal image of Au nanoparticles (400 nm) wrapped with β CDPSH/Fc-Dex/ β CD-Fl-Dex polymers.

The gold core was then removed using iodine to form the hollow nanocapsules that were characterized using different techniques. Figure 5.6 shows ESEM photographs of empty nanocapsules after the gold core dissolution in which a marked change in morphology is evident resulting in a smoother surface, which can be ascribed to a higher mobility of the polymer layers due to the removal of the core. Confocal images (Figure 5.7) shows the cross-section through hollow nanocapsules, starting from the top and cutting slices into the middle of the nanocapsules.

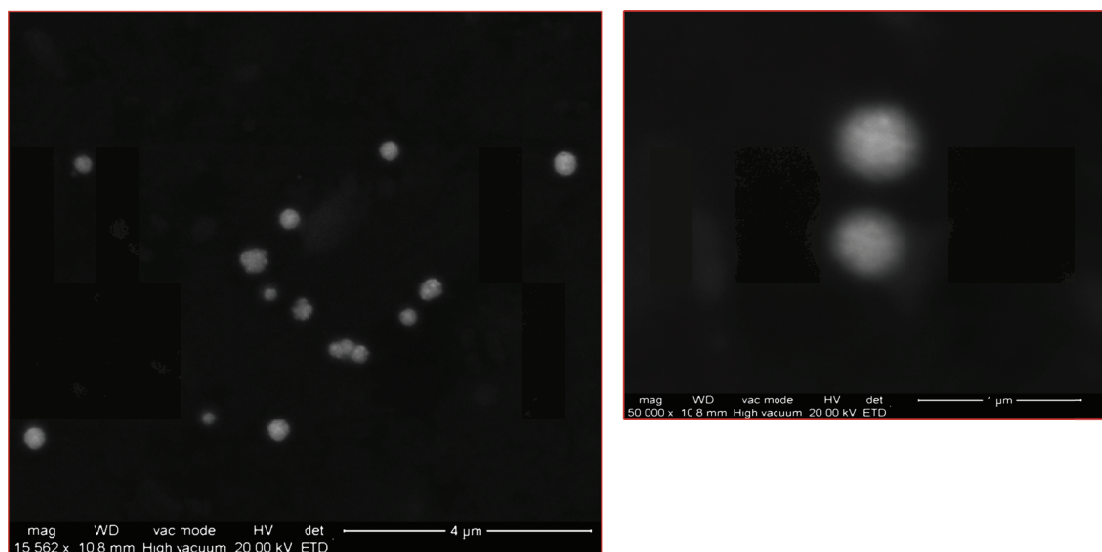


Figure 5.6. ESEM images of empty nanocapsules with β CDPSH/Fc-Dex/ β CD-Dex polymers.

Doctoral Thesis

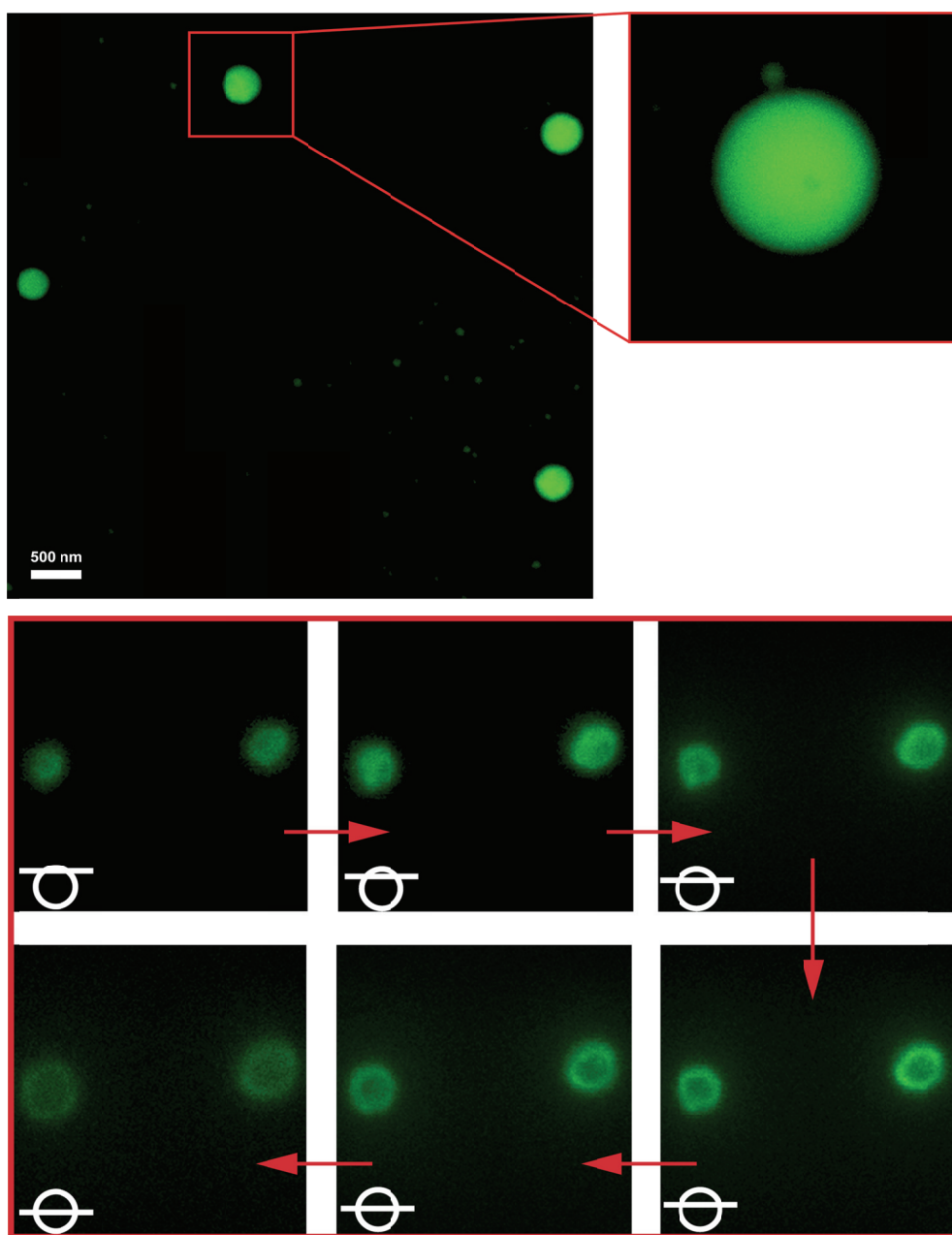


Figure 5.7. Confocal images of Fc-based hollow nanocapsules. Top: distribution of empty nanocapsules. Bottom: cross-section through the β CDPSH/Fc-Dex/ β CD-FI-Dex nanocapsules.

The redox reactions between Fc (reduced state) and Fc⁺ in its oxidized state were followed by UV-spectroscopy using chemical oxidation with NaClO (Figure 5.8). A mixture of β CD-Dex polymer and Fc carboxylic acid at a 1:1 molar ratio of β CD:Fc presents a d-d transition band around 450 nm which disappeared upon oxidation of the Fc molecules. This indicates a breakage of the inclusion complex between Fc and β CD and it is due to the fact that the β CD has a high affinity for the reduced state of the Fc group because of its hydrophobic nature, whereas the oxidized state of the Fc group (Fc⁺) exhibits a low affinity for β CD due to the cationic Fc⁺ group.^{10,13}

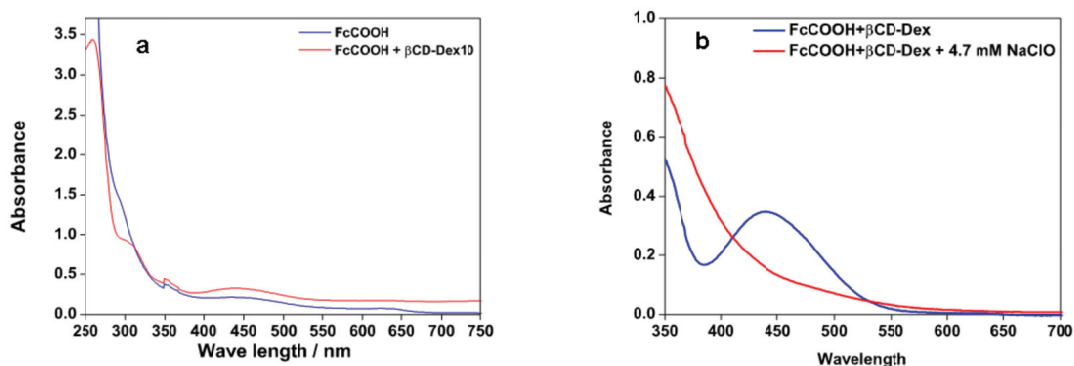


Figure 5.8. UV-spectra of a) Fc and β CD-Dex inclusion complex (reduced state)-visible Cotton band at 450 nm; b) Characteristic Cotton band disappeared after the addition of NaClO indicating that the oxidized ferrocenium group was excluded from the cavity of β CD.¹⁰

Encapsulation properties of the redox responsive nanocapsules.

The encapsulation properties of redox responsive β CDPSH/Fc-Dex/ β CD-Fl-Dex nanocapsules were studied using confocal microscopy. To do that, the capsules were treated with NaClO for 10 min (chemical oxidation) followed by exposure to a solution of rhodamine B with the aim to encapsulate this red-emitting fluorophore by diffusion (Figure 5.9). Noteworthy, applying the

chemical stimulus to the nanocapsules enabled much faster diffusion of dye molecules through the capsules walls and the process was complete in less than 10 minutes. In contrast, non-oxidized nanocapsules showed only partial dye encapsulation after one hour of interaction. Furthermore, rhodamine B gathered mostly in the walls of hollow nanocapsules, which is clearly visible in Figure 5.10.

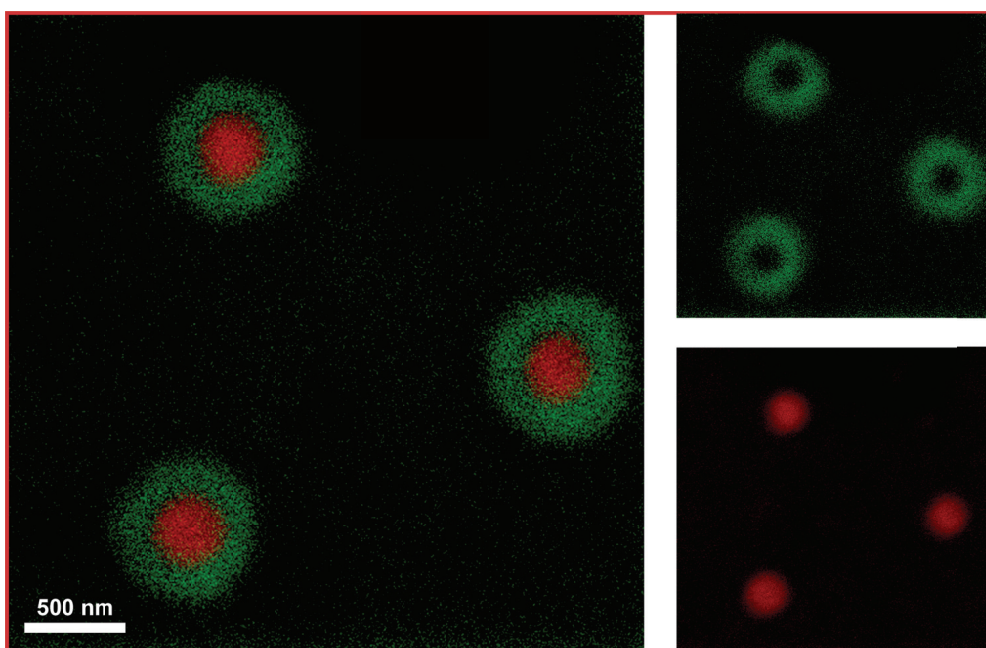


Figure 5.9. Confocal images displaying encapsulated rhodamine B (red) inside the β CDPSH/Fc-Dex/ β CD-FI-Dex nanocapsules (green) *after oxidation* with NaClO.

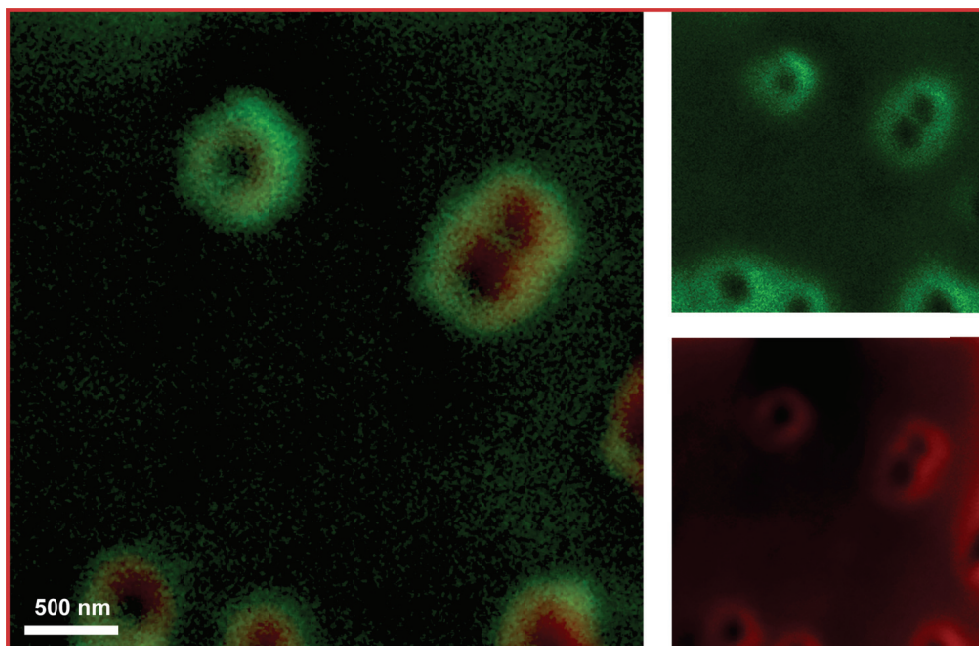


Figure 5.10. Confocal images displaying partially encapsulated rhodamine B (red) and adsorption on the walls of *non-oxidized* β CDPSH/Fc-Dex/ β CD-FI-Dex nanocapsules (green).

The capsules loaded with dye molecules were deposited on mica surfaces and studied by AFM (Figure 5.11). As can be seen, the prepared nanocapsules did not collapsed upon interaction with the solid surface and were able to maintain their original shape. Studies on the effect of tensile loading on the structure of the capsules are currently underway.

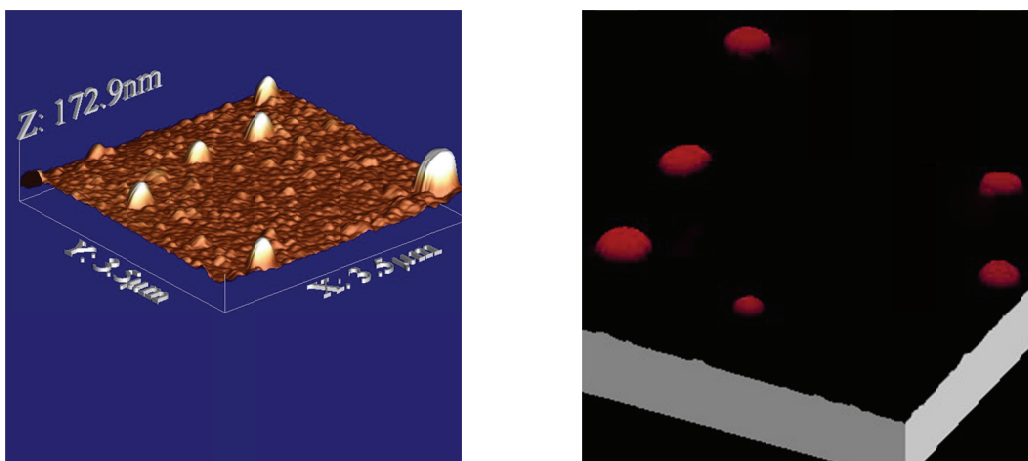


Figure 5.11. AFM images of rhodamine B encapsulated inside the β CDPSH/Fc-Dex/ β CD-Dex nanocapsules (nanocapsules obtained from the gold templates of 400 nm).

Encapsulation/release study of $\text{Ru}(\text{NH}_3)_6^{3+}$ by the redox responsive nanocapsules

Encapsulation and release properties of the redox responsive nanocapsules were then studied using an electroactive marker. For convenience, we selected $\text{Ru}(\text{NH}_3)_6^{3+}$ cations, which undergo a reversible one electron reduction around -0.25 V vs. Ag/AgCl and hence its electrochemical properties do not overlap with those of ferrocene (Figure 5.12).

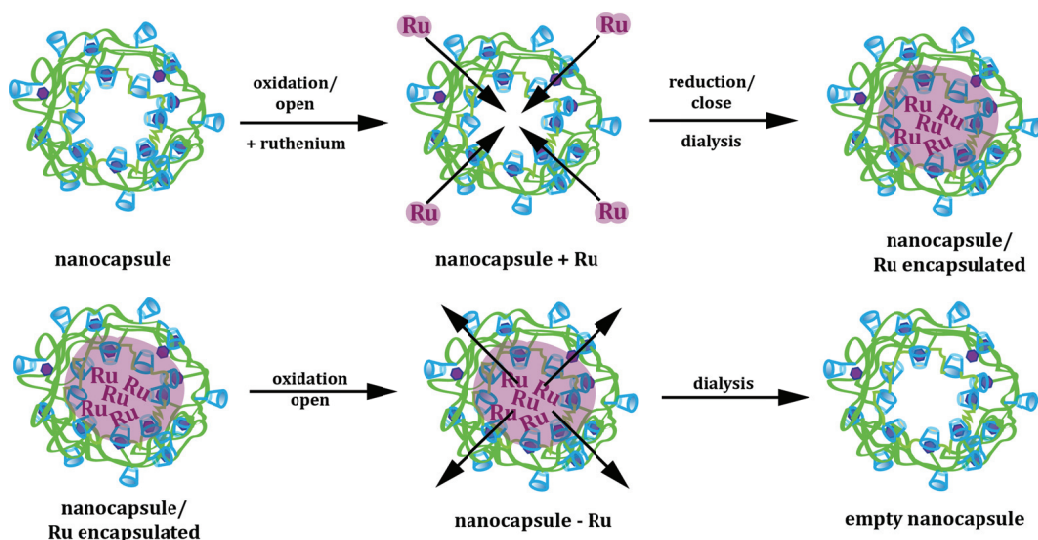


Figure 5.12. Schematic representation of the Ru(NH₃)₆³⁺ encapsulation and release from the Fc-based nanocapsules using a redox stimulus.

The Fc-based nanocapsules were oxidized in solution by applying a potential of +0.2 V for one minute and thus the walls of the nanocapsule “opened” enabling diffusion of the ruthenium marker inside the nanocarrier. After the encapsulation was complete (approx. 10 min) the capsule walls were by closed by applying a potential of 0 V vs. Ag/AgCl for one minute. Ru(NH₃)₆³⁺ encapsulated nanocapsules were subsequently dialyzed against water and studied by differential pulse voltammetry (DPV) (Figure 5.13.). As can be seen, the encapsulated nanocapsules show the signals corresponding to Fc at +0.15 V and Ru(NH₃)₆³⁺ at -0.27 V. Interestingly, the signal of the ruthenium marker is displaced (-0.03 V) to more negative potentials after encapsulation, indicating a slightly hampered electron transfer as a consequence of the encapsulation, although this process does not alter the reversibility of its redox properties.

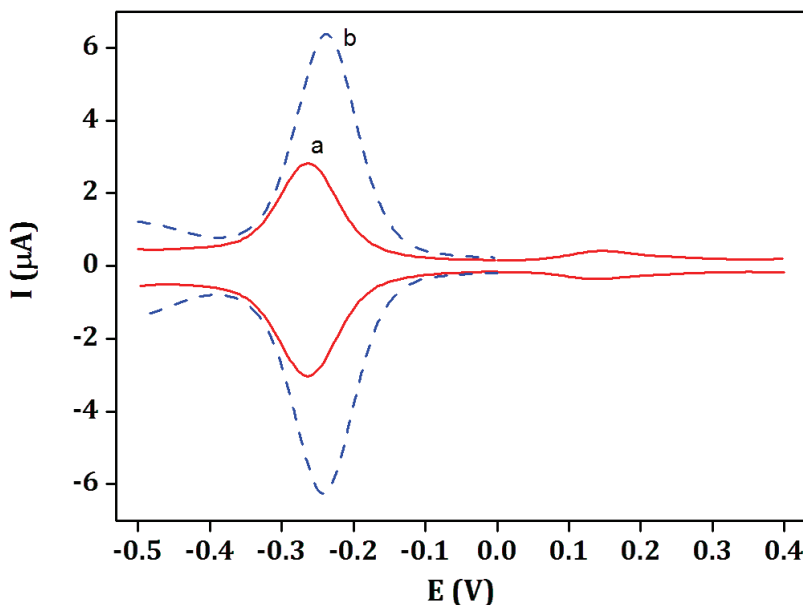


Figure 5.13. DPV voltammograms of $\text{Ru}(\text{NH}_3)_6^{3+}$ encapsulated $\beta\text{CDPSH}/\text{Fc-Dex}/\beta\text{CD-Dex}$ nanocapsules (a) and 0.1 mM $\text{Ru}(\text{NH}_3)_6^{3+}$ in solution. Supporting electrolyte: 0.1 M KCl.

To release the encapsulated ruthenium complex the oxidation/reduction process was repeated in similar conditions as for the encapsulation, the nanocapsules were dialyzed and the content of the ruthenium marker was evaluated by cyclic voltammetry. As it can be seen on the cyclic voltammograms (Figure 5.14) encapsulated ruthenium molecules were released from the ferrocene nanocapsules after oxidation of the walls due to the breakage of the inclusion complex between Fc and βCD molecules. Interestingly, even after extensive dialysis the signal of the ruthenium complex is still visible (about 12% of initial signal), which can be attributed to molecules gathering in the nanocapsule walls or to capsules that were not completely empty. The encapsulation/release process was repeated twice in

the same batch of capsules and they were found to encapsulate and release essentially the same amount of $\text{Ru}(\text{NH}_3)_6^{3+}$ (Figure 5.14, inset).

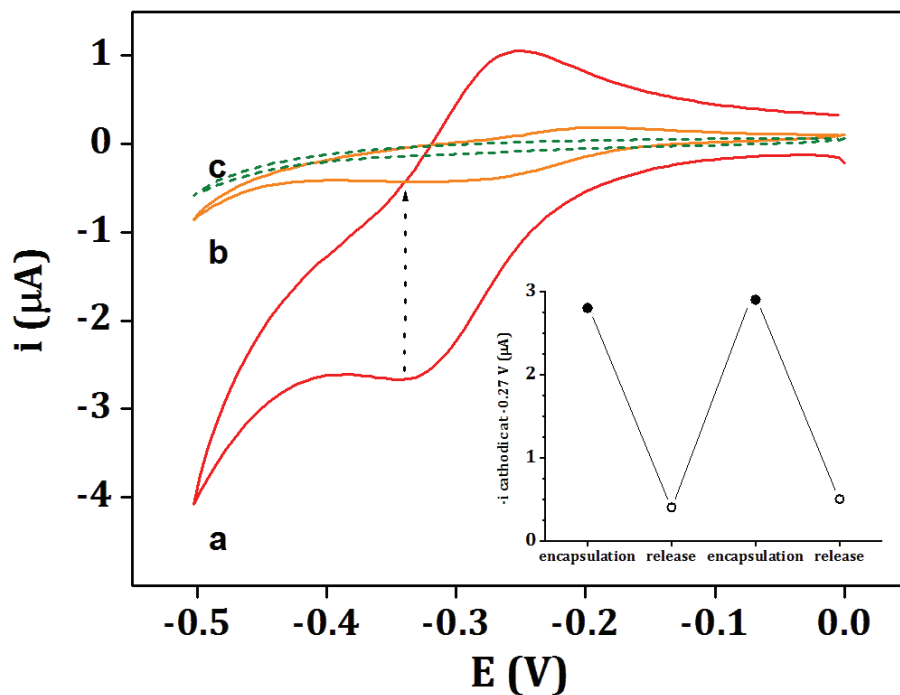


Figure 5.14. Cyclic voltammograms of (a) dialyzed $\text{Ru}(\text{NH}_3)_6^{3+}$ encapsulated Fc-nanocapsules, (b) after electrochemical release and dialysis, (c) supporting electrolyte (0.1 M KCl). Scan rate: 0.1 V/s. Inset: Dependence of cathodic current at -0.27 V for two sequential encapsulation/release processes.

5.4.2 LIGHT RESPONSIVE NANOCAPSULES

Light responsive nanocapsules were based in the well-known *cis/trans* isomerism of azo compounds. For the purposes of this study we synthesized a 4'-derivative of 4-carboxyazobenzene bearing a bulky *tert*-butyl group in order to strengthen the complexation to the cyclodextrin cavities. This azo-compound was then linked to dextran as described in Chapter 3 (Figure 5.15).

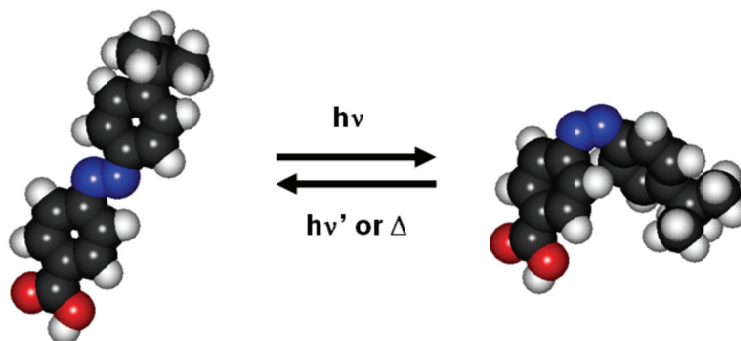


Figure 5.15. Light induced *trans*/*cis* isomerization of azo compounds.

Harada et al. have recently shown that α CD cavities interact much stronger with the *trans*-form of azo compounds ($K_a = 2000 \text{ M}^{-1}$) than with the *cis* isomer ($K_a = 35 \text{ M}^{-1}$). In contrast, the β CD host shows a less selective behavior and also shows a weaker interaction with both forms due its larger cavity, which tolerantly forms an inclusion complex with both *trans*-azo ($K_a = 770 \text{ M}^{-1}$) and *cis*-azo guest molecules ($K_a = 280 \text{ M}^{-1}$).¹⁴ Therefore, to study reversible photoswitching properties of the azobenzene-based nanocapsules we used α CD as a host molecule although both types of capsules were prepared.

Nanocapsule formation with α CD and β CD polymers

The growth of the Au/ α CDPSH/Azo-Dex/ α CD-Dex were studied by DLS measurements and compared with their β CD counterparts (Figure 5.16). In both cases the size profile showed the same tendency of a subsequent layer “contraction” with the addition of the guest-appended polymer.

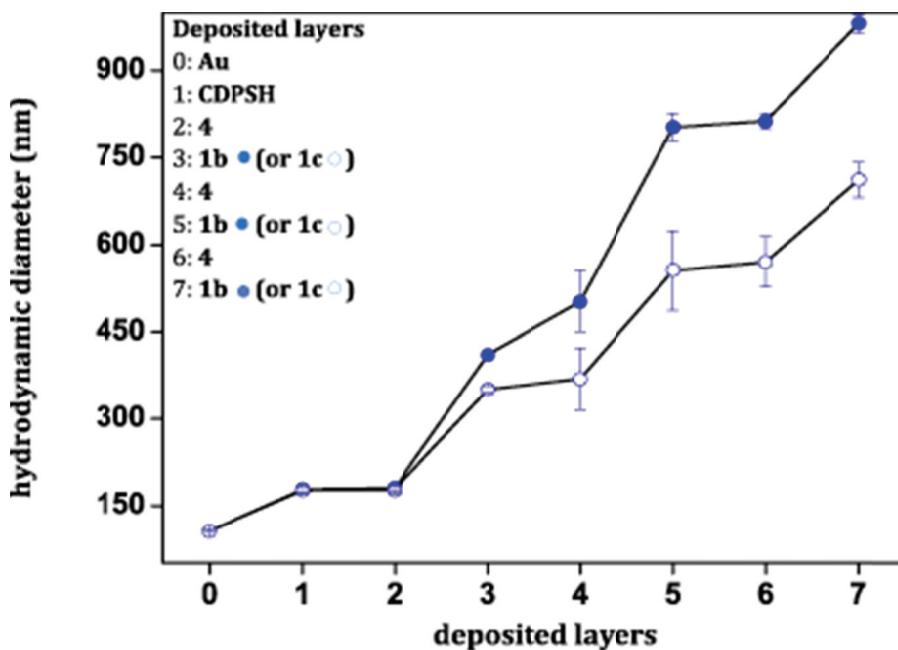


Figure 5.16. Average hydrodynamic particle size as a function of the number of deposited polymer layers onto 100 nm for azo-nanocapsules.

Confocal images of gold nanoparticles subsequently wrapped with thiolated β -cyclodextrin polymer, azo-Dex and β CD-Fl-Dex polymer layers are shown in Figure 5.17, where it can be clearly seen the fluorescent signal of the capsule walls.

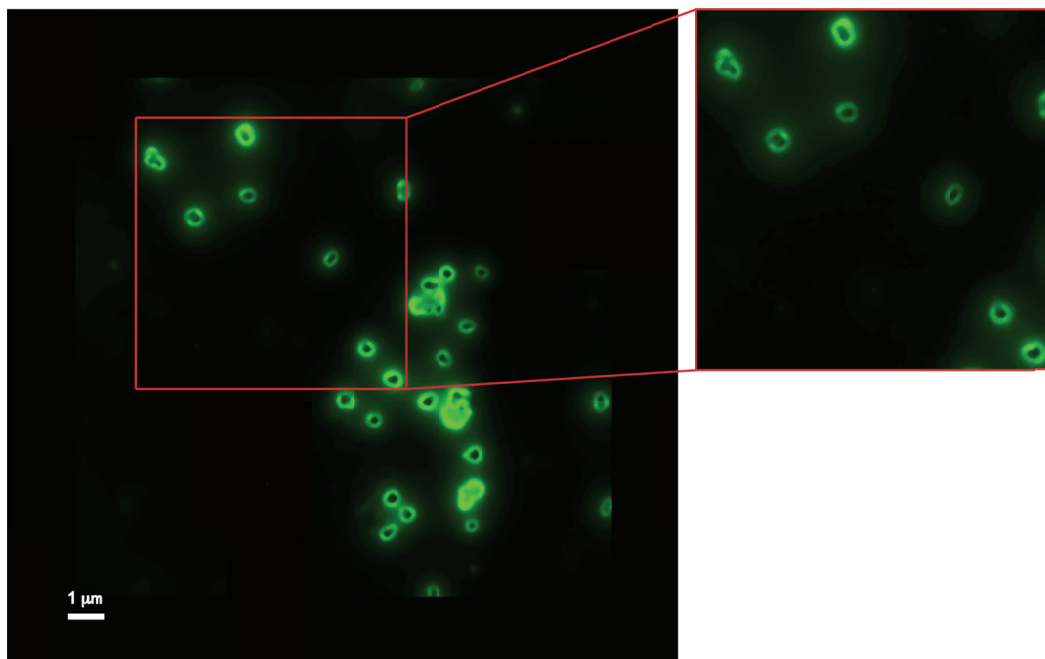


Figure 5.17. Confocal images of the Au nanoparticles (400 nm) wrapped with β CDPSH/Azo-Dex/ β CD-Fl-Dex polymers.

Confocal images exhibit hollow polymeric nanocapsules after the gold core removal (Figure 5.18 shows the cross-section through hollow nanocapsules, starting from the top and cutting slices into the middle of the nanocapsules). As can be seen, the spherical morphology of the particles is essentially similar for the three types of prepared capsules (adamantane, ferrocene and azo) indicating that the templated preparation method employed can be generalized and that the three different guests, even if they do not possess the same affinity for the cyclodextrin cavity, are able to provide structures with enough cohesion to maintain the integrity of the walls, presumably due to the multivalent character of the complementary polymers interaction.

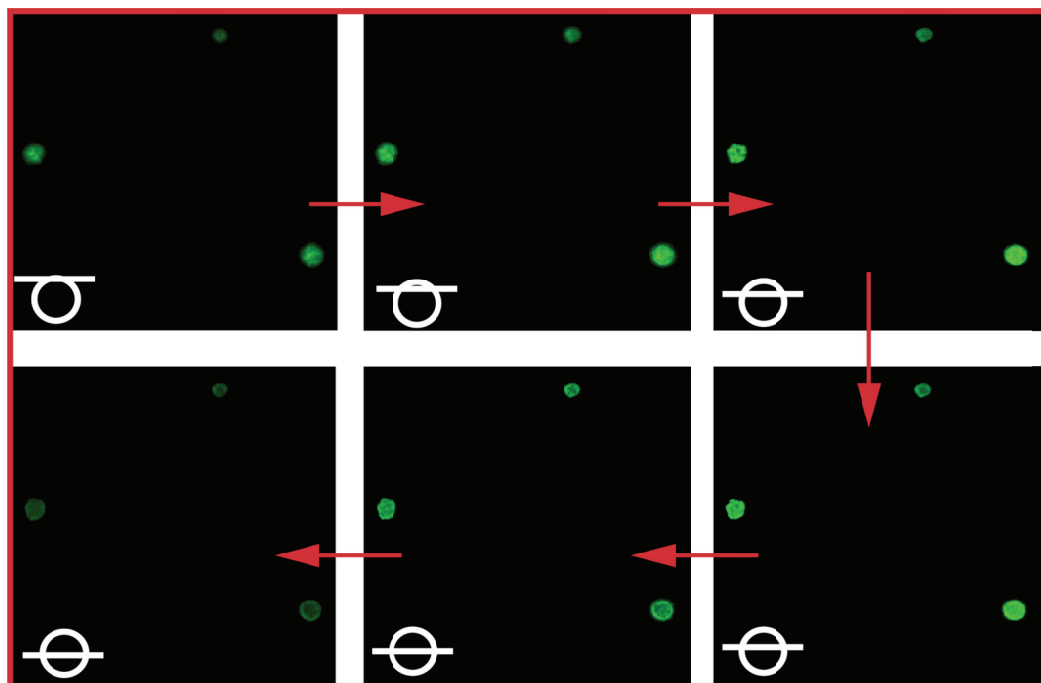


Figure 5.18. Confocal images (cross-section) of hollow Azo-Dex/ β CD-Fl-Dex nanocapsules (prepared from 400 nm template).

Surface-enhanced Raman spectroscopy (SERS) and UV-spectroscopy were employed to study the photoswitchable properties of azobenzene α CD-based nanocapsules (Figure 5.19). Since α CD only forms the inclusion complex with the *trans* form, the two complementary host-guest polymers can disconnect and reconnect after applying the light stimulus. To follow the *trans-cis* photoisomerization we recorded SERS spectra of the azo-Dex/ α CD-Dex nanocapsules before and after irradiation with UV-light at 365 nm. The mechanism of reversible photoswitching of azo molecule relies on transferring from the *trans* form (before UV-light irradiation) to the *cis* form (after UV light irradiation) and back to the *trans* form (after the ambient light irradiation at 450 nm). The intensity drop for the *cis* spectrum is attributed

to loss of conjugation of the *cis* isomer resulting in a reduction in polarizability and Raman intensity.¹⁵

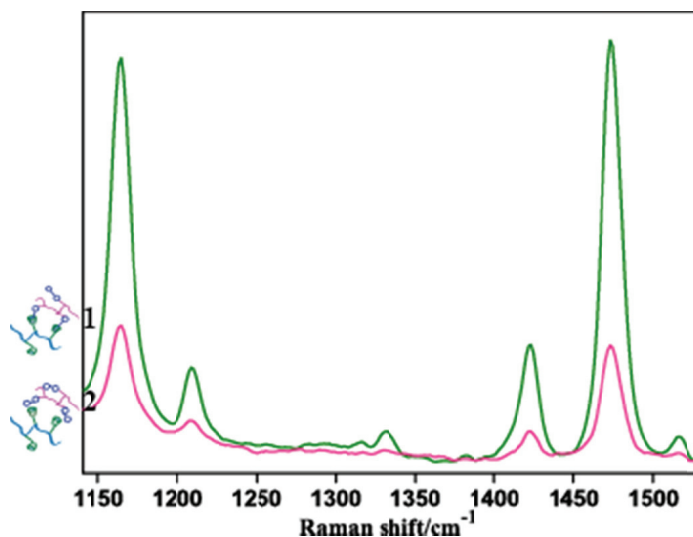


Figure 5.19. Surface enhanced Raman spectra of azo-capsules before (1) and after irradiation at $\lambda=365$ nm (2)

UV-visible spectroscopy also demonstrated the photoswitchable properties of the azo-based nanocapsules (Figure 5.20). The UV spectrum of the *trans* form of the nanocapsules was recorded before UV-light irradiation and two characteristic bands were observed around 230 nm and 340 nm. After irradiating of the Azo-Dex/ α CD-Dex nanocapsules with UV-light at 365 nm for 20 minutes the two bands significantly decreased and a small new band around 260 nm appeared, corresponding to the *cis* form of the azobenzene molecule. After subsequent exposition of the sample to ambient light ($\lambda > 450$ nm) for 20 min the two bands returned to the half of the initial intensity (*trans* form) and the band at 260 nm disappeared. This proves the partly reversible photoswitchable properties of the Azo-Dex/ α CD-Dex nanocapsules in which $\sim 50\%$ of the azo groups are switched. This result

implies that the azo groups in the capsules that are not involved in the *trans-cis* transition can help to maintain the integrity of the capsule wall by host-guest interactions, while the rest of the azi groups are responsible for its permeability. In contrast, the Azo-Dex polymer in solution showed an almost complete photoinduced switch to *cis* form after exposition to UV-light but, surprisingly, no reverse transition to the *trans* form was observed when exposed ambient light, at least in the time frame of the experiment (~ one hour).

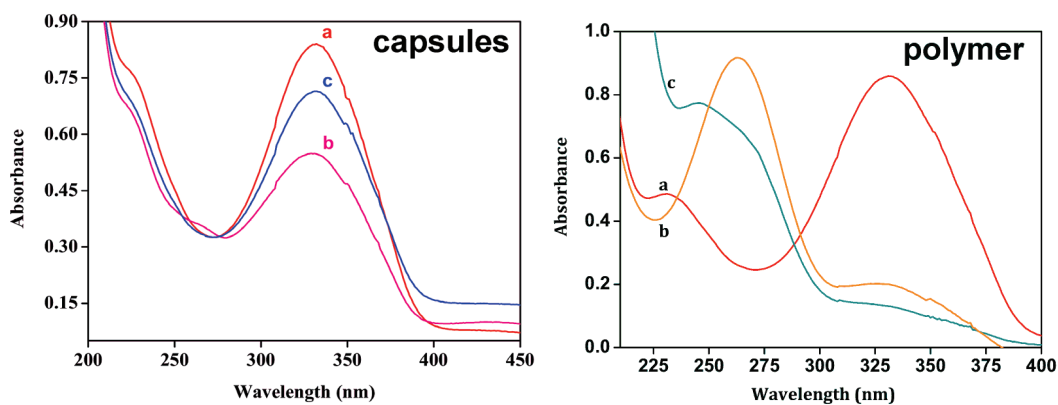


Figure 5.20. UV-spectra of light-responsive α CD nanocapsules (left) and azo-Dex polymer (right) before (a) and after (b) irradiation at $\lambda=365$ nm and after further exposure to ambient light (c).

Encapsulation of rhodamine B on light-responsive Azo-Dex/ α CD-Dex nanocapsules

The encapsulation properties of the light responsive Azo-Dex/ α CD-Dex nanocapsules were also studied using confocal microscopy using rhodamine B as a model. Azo-Dex/ α CD-Dex nanocapsules were irradiated with UV-light

($\lambda=365$ nm) for 60 min. Next, rhodamine B was encapsulated by diffusion for 10 minutes. As can be seen from Figure 5.21, the Azo-Dex/ α CD-Dex nanocapsules showed no dye encapsulation in the absence of the light stimulus and rhodamine B gathered mostly in the walls of hollow nanocapsules what is clearly visible on the Figure 5.21 (left). After irradiation, confocal images clearly showed the dye inside the capsules, indicating that the light stimulus markedly increase the permeability of the nanocapsule walls (Figure 5.21, right).

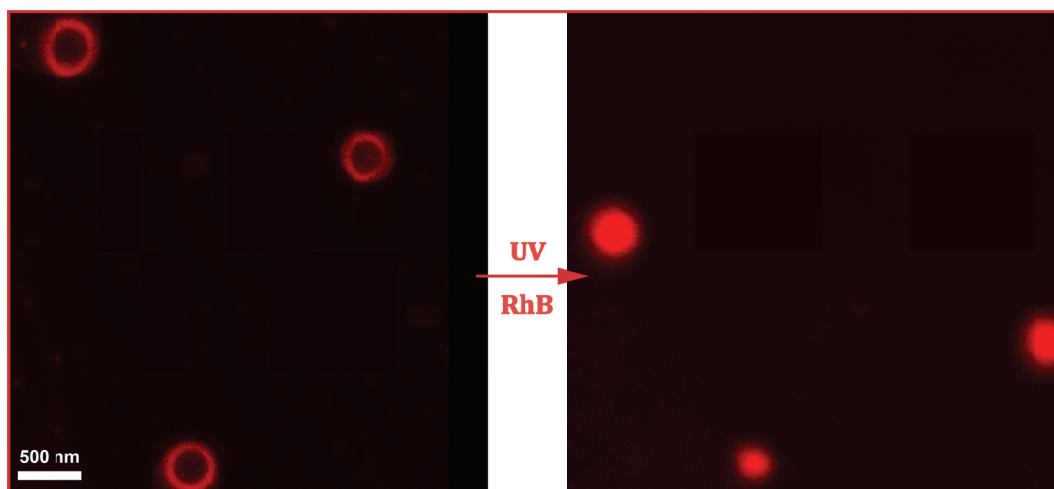


Figure 5.21. Encapsulation of the rhodamine B inside α CDPSH/Azo-Dex/ α CD-Dex nanocapsules without an external stimulus-UV light (left) and after the light stimulus (right).

In contrast, the diffusion through the Azo-Dex/ β CD-Dex nanocapsules was not evident from the confocal images and the dye gathered mostly in the nanocapsule walls, even after applying the light stimulus as shown in Figure 5.22. This indicates that the light stimulus is not able to “open” the walls and that the *cis* form of the azo moiety is still complexed with the β CD cavities

rendering the nanocapsule “closed” due to the similar affinity of both *trans* and *cis* forms for the β CD cavity, as was observed before by Harada in similar host-guest based self-healing polymers.

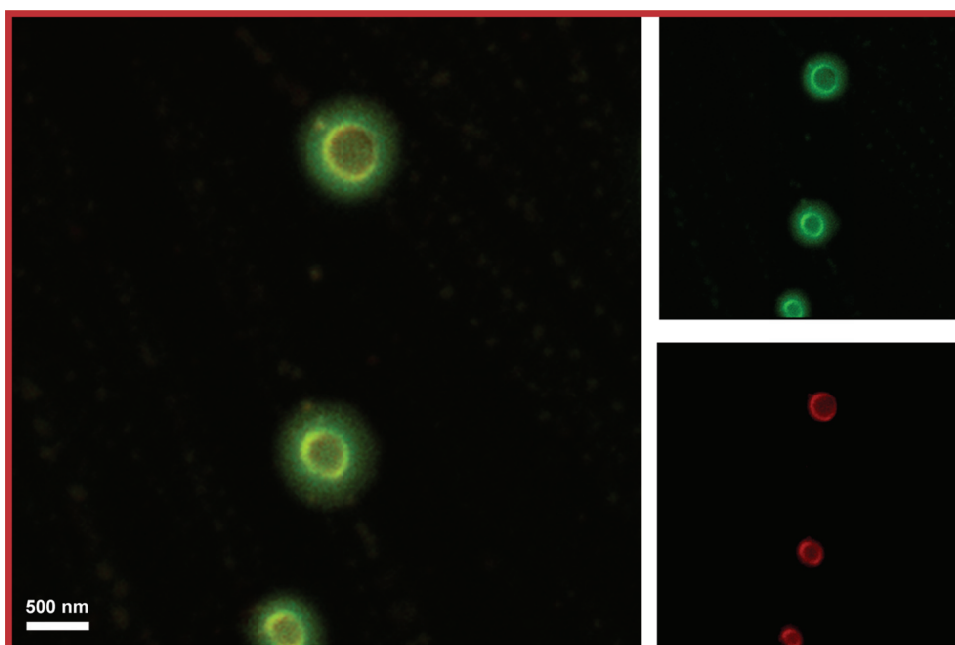


Figure 5.22. Confocal images of β CD-based nanocapsules after incubation with rhodamine B (red) and light stimulus. The green fluorescence is due to a layer of Dex/ β CD-FI-Dex used as the third layer.

The capsules loaded with dye molecules were deposited on mica surfaces and studied by AFM (Figure 5.23). Similarly to Fc nanocapsules, they did not collapsed upon interaction with the solid surface and were able to maintain their original shape. Studies on the effect of tensile loading are currently underway.

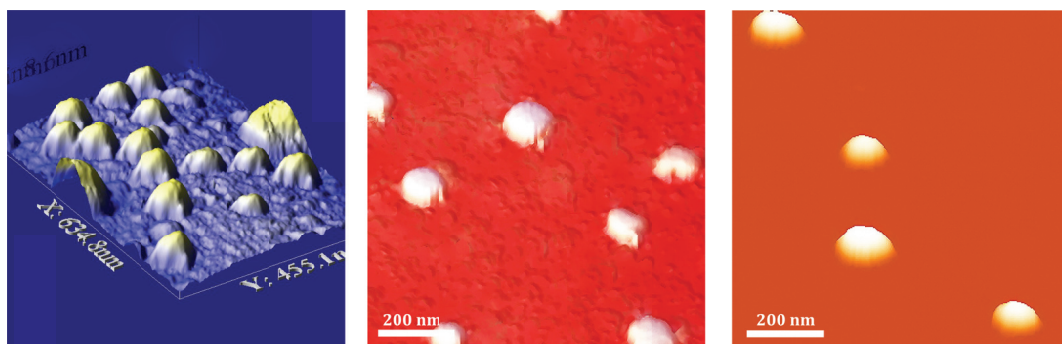


Figure 5.23. AFM images of encapsulated Azo-Dex/ α CD-Dex nanocapsules; (prepared from 100 nm gold template).

Fluorescence study of encapsulation/release of rhodamine B from the light responsive nanocapsules

The encapsulation and release properties of the light responsive α CDPSH/Azo-Dex/ α CD-Dex nanocapsules were also studied using fluorescence spectrophotometry (Figure 5.24).

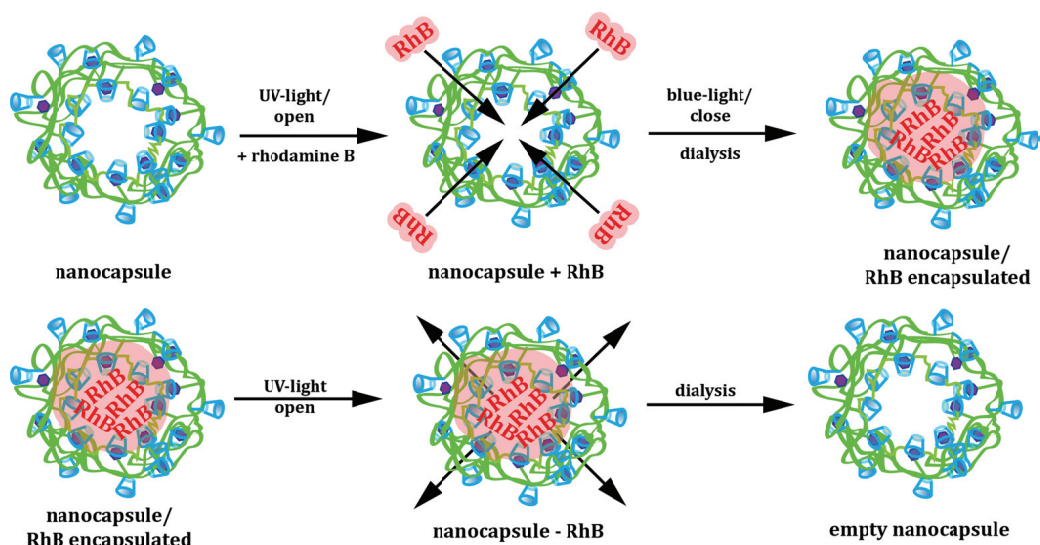


Figure 5.24. Schematic representation of the rhodamine B encapsulation and release from the azo-based nanocapsules using a light stimulus.

Noticeably, the encapsulation process was much faster (approx. 10 min) and efficient with using UV-light to “open” the nanocapsule walls. After the encapsulation of the dye molecules the nanocapsule walls were “closed” by exposing them to the visible light and the fluorescence emission of the rhodamine B retained inside the nanocapsules after dialysis was then measured (Figure 5.25, top). The encapsulation efficiency was also measured without exposition of the nanocapsules to the UV-light and in this case the encapsulation of the dye molecules was much slower (approx. 90 min) and less efficient (Figure 5.25, bottom). The release of the rhodamine B from the azo nanocapsules was done by treating the nanocapsule walls with UV-light and dialyzed. The fluorescence emission of the rhodamine B was measured after approx. 45 min of dialysis and almost all the dye was released.

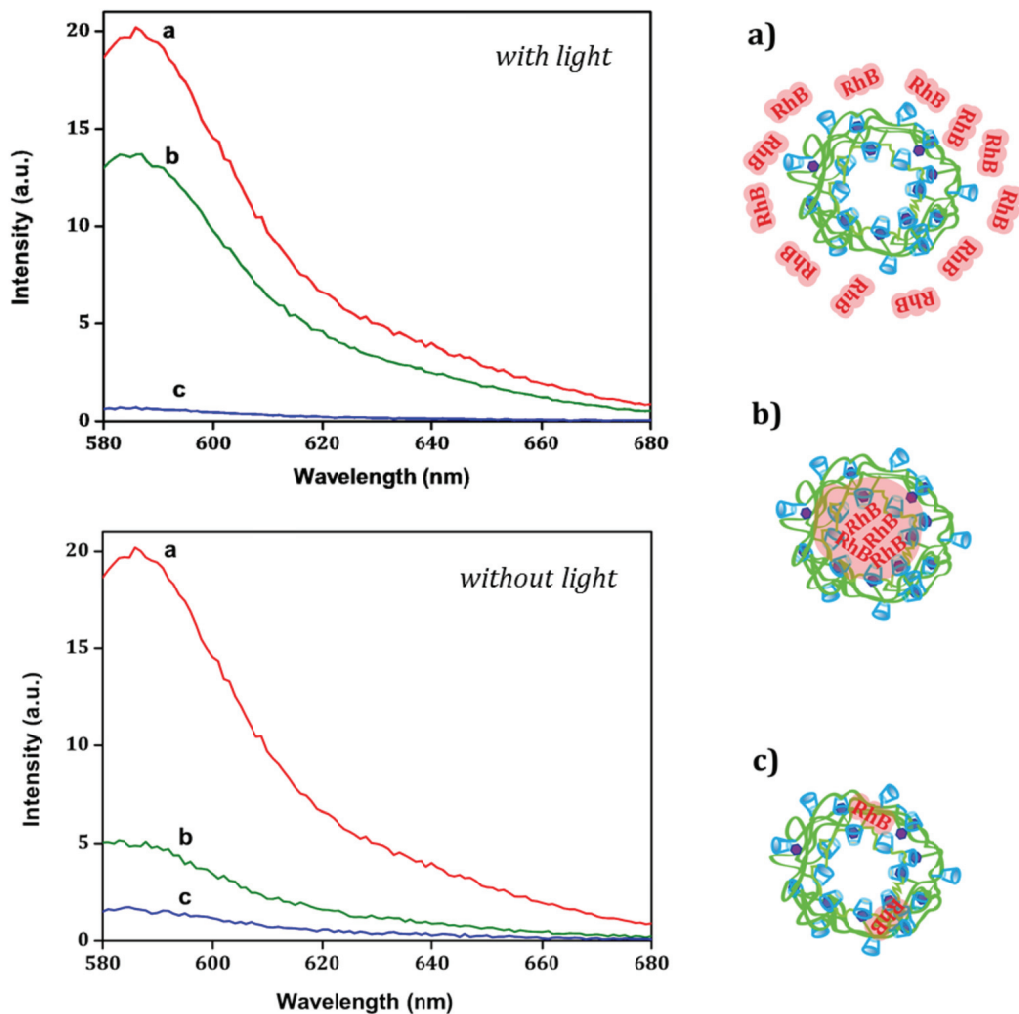


Figure 5.25. Top: Encapsulation *with* light stimulus. Fluorescence emission of rhodamine B (1 μM in water): (a) before the encapsulation, (b) after light stimulus, encapsulation and dialysis, (c) after “opening” the capsule walls using UV-light to release the dye and dialysis. Bottom: Control *without* light stimulus (“a”, “b” and “c” are the same as in the top figure). Conditions: λ_{exc} 540 nm.

5.5 CONCLUSIONS

In this chapter we demonstrate the formation of “intelligent” supramolecular nanocapsules able to modulate their encapsulation properties using external stimuli such as oxidation and light. These systems were formed using dextran polymers bearing specific moieties (ferrocene and azobenzene) that reversibly change their chemical properties or structure upon stimulation such as charge (from neutral to monopositive for Fc) or geometry (*trans* to *cis* for azobenzene). The reversible multipoint crosslinks between Fc-Dex/ β CD-Dex or Azo-Dex/ α CD-Dex are then affected by the stimulus and, in turn, alter the macroscopic properties (wall permeability) of the supramolecular nanocapsules by an *on-off* switching at the microscopic scale of the inclusion complex. The external stimuli ease the encapsulation process making it faster and more efficient than without stimulus. Thus, we believe that these properties may eventually be used in stimuli-responsive drug-delivery carriers, cosmetics or other biomedical applications.

REFERENCES

1. A. S. Hoffman, *J. Control. Release*, 2008, **132**, 153.
 2. D. La Van, D. Lynn, R. Langer, *Nat. Rev. Drug Discov.*, 2002, **1**, 77.
 3. C. L. Bayer, N. A. Peppas, *J. Control. Release*, 2008, **132**, 216.
 4. E. Taqieddin, M. Amiji, C. Lee, *Pharm. Eng.*, 2002, **22**, 1.
 5. H. Pollard, J.-S. Remy, G. Loussouarn, S. Demolombe, J.-P. Behr, D. Escande, *J. Biol. Chem.*, 1998, **273**, 7507.
 6. F. A. Armstrong, G. S. Wilson, *Electrochim. Acta*, 2000, **45**, 2623.
 7. A. Fragoso, J. Caballero, E. Almirall, R. Villalonga, R. Cao, *Langmuir*, 2002, **18**, 5051.
-

8. M. A. C. Stuart, W. T. S. Huck, J. Genzer, M. Müller, C. Ober, M. Stamm, G. B. Sukhorukov, J. Szleifer, V. V. Tsukruk, M. Urban, F. Winnik, S. Zauscher, I. Luzinow, S. Minko, *Nat. Mat. Rev Art.*, 2010, **9**, 101.
9. C. Li, G.-F. Luo, H.-Y. Wang, J. Zhang, Y.-H. Gong, S.-X. Cheng, R.-X. Zhuo, X.-Z. Zhang, *J. Phys. Chem. C*, 2011, **115**, 17651.
10. M. Nakahata, Y. Takashima, H. Yamaguchi, A. Harada, *Nat. Comm.*, 2011, **511**, 1521.
11. J. Ge, E. Neofyton, T. J. Cahill, III, R. E. Beygui, R. N. Zare, *ACS Nano*, 2012, **6**, 1, 227.
12. L. Sun, R. M. Crooks, V. Chechik, *Chem. Commun.*, 2001, 359.
13. J. Bodenheimer, E. Loewenthal, W. Low, *Chem. Phys. Lett.*, 1969, **3** (9), 715.
14. H. Yamaguchi, Y. Kobayashi, R. Kobayashi, Y. Takashma, A. Hashidzume, A. Harada, *Nat. Comm.*, 2012, **3:603**, 1617.
15. Y. B. Zheng, J. L. Payton, Ch.-H. Chung, R. Liu, S. Cheunkar, B. K. Pathem, Y. Yang, L. Jensen, P. S. Weiss, *Nano Lett.*, 2011, **11**, 3447.

CHAPTER 6

PREPARATION OF SOLUBLE CARBON NANO-ONIONS BY FUNCTIONALIZATION WITH DEXTRAN BASED SUPRAMOLECULAR POLYMERS

6.1 ABSTRACT

Small carbon nano-onions (CNOs, 6–12 shells) were prepared in high yields and functionalized with carboxylic groups by chemical oxidation and reacted with β CD-NH₂. A biocompatible dextran polymer was employed for the layer-by-layer supramolecular self-assembly on the β CD-CNOs surfaces. β CD acts as a host molecule and ferrocene as a guest grafted into dextran backbone (Fc-Dex) – for the formation of an inclusion complex. After their functionalization these nanostructures were soluble in aqueous solutions. The resulting product was characterized by transmission electron microscopy (TEM), thermogravimetric analysis (TGA), FT-IR and RAMAN spectroscopies. Moreover, the deposition of the subsequent layers on the surface of the particles was monitored using DLS measurement and Zeta Potential. Through-space interactions between the Fc moieties and the CNOs core and the influence of an additional dextran- β CD outer layer were measured electrochemically.

6.2 INTRODUCTION

Since the revolutionary discovery of fullerenes as new carbon allotropes, the field of carbon nanoscience has expanded considerably and gained large

interest by a number of research groups.¹ The unique all-carbon structure of closed-cage molecules or fullerenes can exhibit many potential uses in areas ranging from material science to medicinal chemistry because of their electronic properties and nanometer dimensions.² During the initial stages of fullerene research two very important discoveries were made, the formation of carbon nanotubes (CNTs) and carbon nano-onions (CNOs).³ CNOs also known as multilayer fullerenes are built from concentric graphitic shells forming quasi-spherical structures. Structurally CNOs can be considered as spherical analogues of multiwalled carbon nanotubes.⁴ However, CNOs were discovered almost at the same time as CNTs, they have received much less attention to date.

In 1992 Ugarte observed CNOs for the first time upon strong electron beam irradiation of CNTs. The manufacture of CNOs has not been carried out for many years since their observation and no more than 13 years ago the effective production of CNOs was executed. Since that time, research on CNOs slowly begun to attract more attention among different scientific groups as they could be prepared more efficiently in higher yields.

Some preparation methods developed for CNOs include high temperature annealing of nanodiamond particles,⁵ implantation of carbon atoms on silver particles⁶ or laser vaporization of composite carbon-metal targets under low helium pressures and in the presence of C₆₀ as a nucleating center.⁷ The last technique is claimed to be very efficient in production of high yields of small CNOs such as the double-shelled C₆₀@C₂₄₀ and the triple-shelled C₆₀@C₂₄₀@C₅₄₀.^{8,9} Producing CNOs with few layers is desirable to maximize the chance to modify them by chemical reaction, since a smaller-radius particle has a greater surface curvature, and thus, higher chemical reactivity.³

Chemical functionalization of CNOs plays crucial role in their potential applications as they exhibit very low solubility or dispersity in most of organic and/or inorganic solvents. Thus, surface modification of CNOs allows their segregation, and improves their solubility or dispersity.¹⁰ Several methods have been reported for covalent functionalization of CNOs, for instance, esterification, amidation,^{3,4} oxidation reactions of defects with nitric acid or mixture of sulfuric and nitric acids,¹⁰ 1,3-dipolar cycloaddition of azomethine ylides,^{12, 13} [2+1] Bingel–Hirsch cyclopropanation,¹⁴ polymerization,¹⁵ treatment with diazonium-based compounds,¹⁶ or fluorination.^{14, 17}

Non-covalent functionalization of carbon nanomaterials also has been described in the literature. Harada et al. reported the modification of single walled carbon nanotubes (SWNTs) by physical absorption of cyclodextrins with guest molecules and the formation host-guest inclusion complexes significantly improved water solubility of SWNTs.¹⁸ Although, the majority of studies for the non-covalent or polymeric modifications have been focused on CNTs, CNOs are considered to be better candidates for these types of functionalization not only because of their higher surface area but also because of their good biocompatibility and very low toxicity, thus being very good candidates for many biomedical applications.¹⁹

The number of articles involving CNOs with polymer functionalization is still very limited.^{20,21} Poly-(4-vinylpyridine-co-styrene)^{22,23} (PVPS) and poly (ethyleneglycol)²⁴⁻²⁷ (PEG) have been frequently used for solubilization of carbon nanostructures in non-polar or polar media. Echegoyen et al. recently reported modification of CNOs with biocompatible polymers for flavonoid incorporation, what can be very promising for biosensing and drug targeting

applications. They attached hydrophilic or hydrophobic chains to synthesize soluble derivatives of CNOs.¹⁹ Earlier reports also demonstrate an impressive amount of research done towards different polymer functionalization of CNOs mainly for their solubilization by constructing CNO-based supramolecular systems, for example, by using complexation with metal ligands. Moreover, such structures may have potential applications in the field of catalysis and hydrogen storage.^{3,4}

In this work, we present the functionalization of the CNOs with β -cyclodextrin (β CDs) and ferrocene grafted dextran polymers (Fc-Dex) through host-guest interactions for the formation of a newly soluble CNO-based supramolecular nanoarchitectures.

6.3 EXPERIMENTAL SECTION

Materials

All chemicals and solvents used were commercially available and used without further purification. Water was purified by a Milli-Q water purification system (Millipore) to a resistivity of 18.2 M Ω cm. Commercially available nanodiamond was purchased from Carbodeon with a crystal size between 4-7 nm. The copper grids for TEM were bought from TED PELLA, Inc. (Prod. No. 01830, 200 mesh, Silicon Monoxide/formvar). Ferrocene dextran polymer (5 kDa Mw) used in this work was synthesized previously as described in Chapter 3.

HR-TEM microscopy

For HR-TEM measurements, samples were deposited on Cu grid holey carbon supports and the solvent was evaporated. Transmission Electron Microscope

images were recorded using an FEI Tecnai™ transmission electron microscope. The accelerating voltage of the electron beam was 200 keV.

Raman, FT-IR and absorption spectroscopy

Raman measurements were performed using a SmartRaman spectrometer equipped with a 180 degree sampling holder from Thermo Scientific using an excitation wavelength of 532 nm. FT-IR spectra were recorded using a Perkin Elmer 100 spectrometer with neat samples. Absorption studies were performed using a Cary 5000 UV-NIR 15 spectrometer from Varian using fused Quartz glass cuvettes with a 1 cm optical path.

Thermogravimetric analysis

For TGA analysis a TGA/DSC analyzer from Mettler Toledo was used. A heating rate of 10 °C/min was employed until 1000 °C. All samples were measured in Alumina crucibles with a volume of 0.7 µl.

Synthesis of CNO

Small CNOs were obtained by annealing nanodiamond powder (Molto, 5 nm average particle size) under a positive pressure of helium at 1650°C for 1 h.⁵ After separation and purification, CNOs were heated at 200°C under CO₂ conditions to remove the amorphous carbon residue from the CNO surface. High-resolution transmission electron microscopy images of the CNOs have been reported elsewhere.¹⁴

Oxidation of CNOs (ox-CNOs)

20 mg of crude 6–12 shell CNOs were dispersed by ultrasonication for 30 min and then treated with a sulfuric acid/nitric acid solvent mixture (3:1, v/v) for 3 h. During this process the defective sites on their surface were

transformed into carboxyl groups by oxidation. The mixture was then centrifuged for 20 min, and the black powder collected at the bottom of the test tube and washed several times with 0.1 M NaOH and Mili-Q water until neutral pH was reached. After that, the product was dried overnight in a vacuum oven ($T= 100^{\circ}\text{C}$).

Functionalization of ox-CNOs with aminated β CDs

5 mg of the ox-CNOs were sonicated in aqueous solution for 30 min. Next, 0.2 mmol of EDC, 0.1 mmol NHS, 1 μmol of $\beta\text{CD-NH}_2$ and 0.2 mmol of DMAP were added to the reaction mixture and stirred for 24 hours at 4°C . The unreacted cyclodextrins were removed by centrifugation at 4000 rpm for 45 min and washed 3 times with Mili-Q water. The purified product was dried overnight in the vacuum oven ($T= 45^{\circ}\text{C}$).

4 mL of aqueous solution of CNOs- βCD was added dropwise to 1 mL solution of 0.45 mmol aqueous solution of ferrocene dextran polymer (Fc-Dex) and stirred overnight at room temperature. The unreacted substrates were removed by centrifugation at 4000 rpm for 45 min and washed 3 times with Mili-Q water.

Electrochemical Measurements

Electrochemical measurements were conducted on a CHI-660 electrochemical workstation by using a three-electrode cell. A glassy carbon rod was used as the working electrode in combination with a Ag/Ag⁺ pseudoreference electrode and a Pt wire which served as the counter electrode. The working electrodes were polished with a diamond slurry, sonicated in water and checked for cleanness with 1 mM potassium ferricyanide in 0.1 M KCl.

6.4 RESULTS AND DISCUSSION

Figure 6.1 shows the mechanism for the preparation of supramolecularly engineered soluble CNOs. The initial step involved an oxidation reaction to create carboxyl groups on the graphitic shell of CNOs. The amidation reaction between ox-CNOs and aminated β -cyclodextrins (β CD-NH₂) resulted in water-soluble carbon nanostructures (CNOs- β CD). Next, Fc-Dex polymer layer was self-assembled through supramolecular interactions by wrapping around the CNO nanoparticles and the formation of inclusion complex between Fc and β CD molecules greatly increased the solubility of the modified CNOs even more, possibly due to well-known solubilizing properties of cyclodextrins and their complexes.³⁴

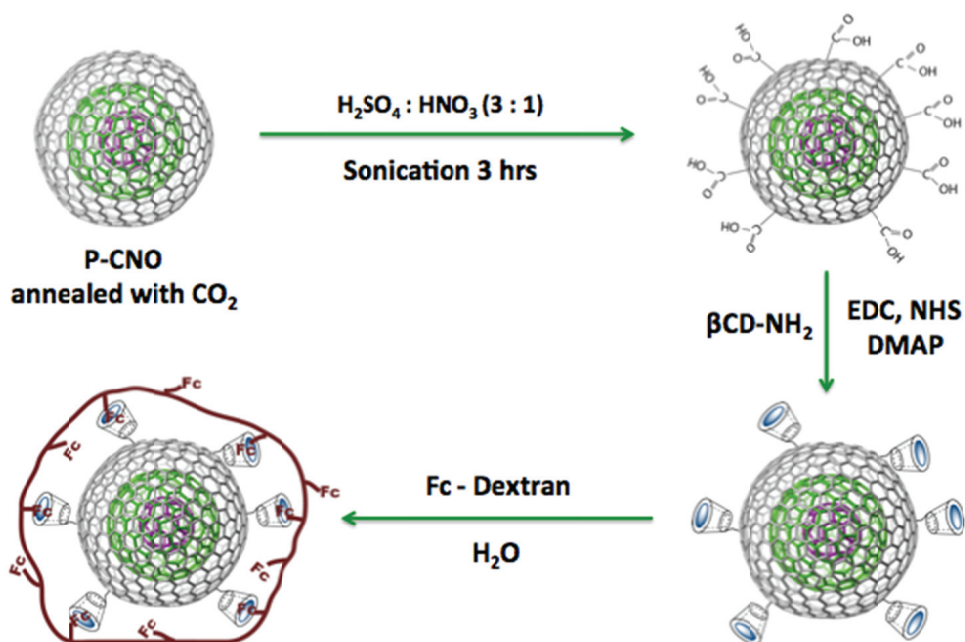


Figure 6.1. Schematic representation of the synthesis of ox-CNOs modified with host (β CD) and guest Fc-Dex polymer via supramolecular interactions.

The first evidence for the functionalization of CNOs was provided by thermogravimetric analysis measurements (TGA). In order to determine the degree of functionalization of the functionalized CNOs- β CD/Fc-Dex, TGA studies were conducted under an inert atmosphere from 30 °C until 1000 °C using a heating rate of 10 °C min⁻¹. Pristine CNOs were used as reference under the same conditions (Fig. 6.2).

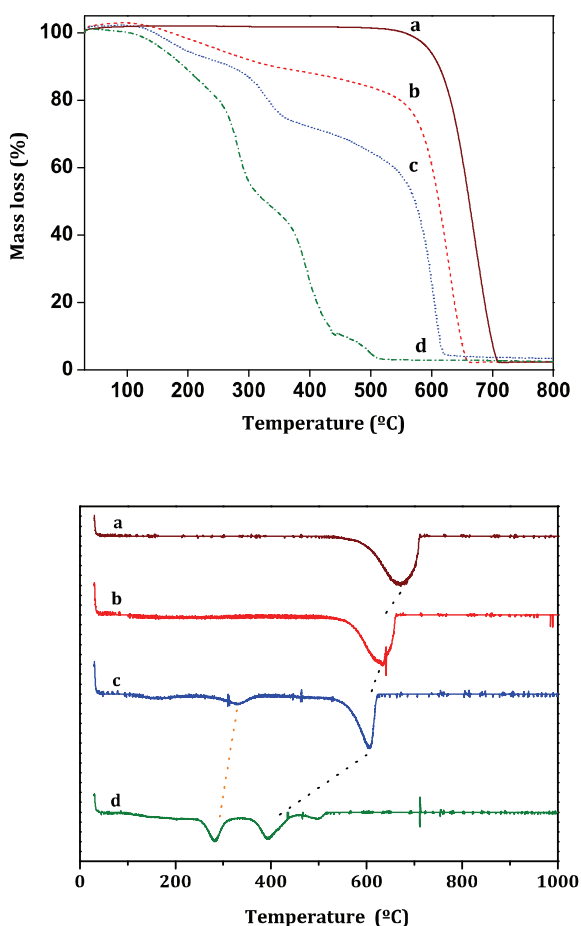


Figure 6.2. Top: TGA analysis of a) pristine CNO, b) oxidized CNOs, c) CNOs- β CD, d) CNOs- β CD/Fc-Dex. Bottom: first derivative plots showing minima at the inflexion points.

The TGA curves can be explained as follow:

- Oxidized CNOs (ox-CNOs) exhibit two different thermal stages for a total mass of loss 15%, at 175 °C, corresponding to the loss of organic material (carboxylic groups) from the surface of the CNOs and final decomposition of the CNOs at 575 °C.
- β CD modified CNOs (CNOs- β CD) show three different thermal stages for a total mass loss 40%, (-25%) at 245 °C corresponding to the removal of the β CDs, (-15%), at 150 °C -COOH groups and final decomposition of the CNOs at 545 °C.
- Fully modified CNOs (CNOs- β CD-Fc-Dex) demonstrate four different thermal stages for a total mass loss 60%, where all organic material started to burn at 100 °C and final decomposition of the CNOs at 385 °C.
- Pristine CNOs remain stable at high temperatures (up until 600 °C), so the lower thermal stability of the functionalized CNOs is probably due to the insertion of “structural defects” upon functionalization, as observed for carbon nanotubes.²⁸

Raman spectroscopy is one of the most powerful methods for the characterization of CNOs, providing unambiguous information about the size and the degree of functionalization of the CNOs by comparison of the relative intensities of the defective bands. The D-band is related to defects in the CNOs lattice (sp^3 -hybridized carbon) and the G-band is due to the vibrations of the sp^2 -hybridized framework. The Raman spectrum of the pristine CNOs exhibits a varying ratio of I_D/I_G , depending on the size of the CNOs. For CNOs prepared by arc discharge of graphite under water (20–30 shells) the $I_D/I_G = 0.8$, but CNOs obtained by annealing of nanodiamond particles (1650 °C)

under an inert atmosphere lead to the formation of small CNOs (6–12 shells) with an I_D/I_G ratio of 1.4, depending on the crystal size of the carbon nanodiamond.¹⁰ Aqueous solutions of pristine CNOs and modified CNOs at each step of their functionalization were deposited onto silicon wafers.

The Raman spectrum of the small pristine CNOs after excitation at 532 nm (Fig. 6.3) shows the typical peaks, namely, the D-band at 1335 cm^{-1} and the G-band at 1577 cm^{-1} . In contrast, the D and G bands for the oxidized and modified CNOs are shifted and noticeably broadened. The D-band is related to the disorder of the graphite lattice^{29,30} and the broad G-band assigned to the E_{2g} species of the infinite crystal. In addition to the G band, another at about 1618 cm^{-1} is observed.¹⁹ This band has been described as a shoulder of the G band.³¹ It is assigned as a D' peak and is also a disorder induced peak³² and thus not observed in highly orientated pyrolytical graphite (HOPG), but often observed in highly defective graphite.³ Furthermore, the I_D/I_G ratio for the oxidized CNOs increased, indicating an increase in the number of defects (sp^3 -hybridized).¹⁰ After the deposition of the supramolecular polymer layer (Fc-Dex) the I_D/I_G ratio gradually decreased which could be attributed to the addition of next layers around small CNOs, thus increasing their size.

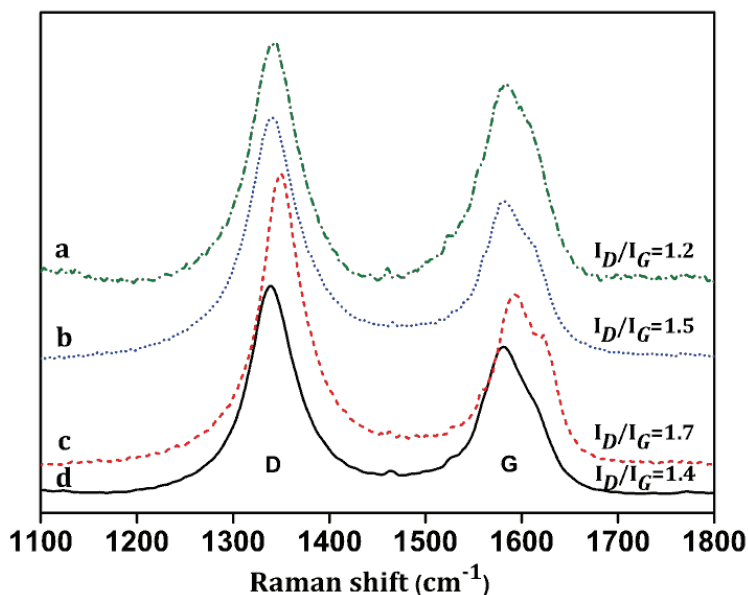
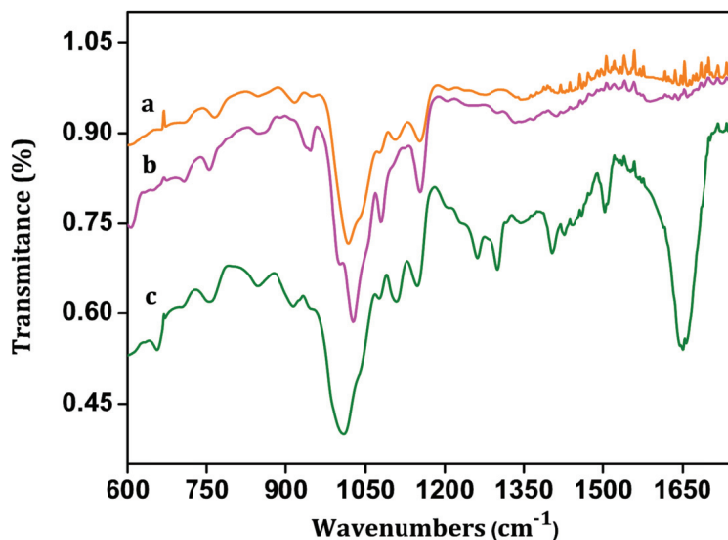


Figure 6.3. RAMAN spectrum ($\lambda=532$ nm) of CNOs- β CD/Fc-Dex (a), CNOs- β CD (b), ox-CNOs (c) and pristine CNOs (d).

Further FTIR studies were conducted to corroborate the covalent attachment of the β CDs on the outer sphere of the CNOs and additional deposition of the Fc-Dex polymer. Peaks in the range from 950 cm⁻¹ to 1150 cm⁻¹ can be assigned to the ν_{C-O} stretching (Figure 6.4 A). Bands at 1650 cm⁻¹ and 1510 cm⁻¹ are assigned to the $\nu_{C=O}$ mode and defined as the “amide I” band and to the N-H bending vibration δ_{N-H} defined as the “amide II” band, respectively. The intensity of the N-H bending absorption is considerably weaker than the carbonyl absorption. It can be concluded that β CD is covalently linked to ox-CNOs through amide bonds. FTIR studies also reveal the appearance of three bands at 2919 and 2876 cm⁻¹ corresponding to the C-H stretching and 3322 cm⁻¹ corresponding to O-H stretching (Figure 6.4 B).^{11, 33}

A.



B.

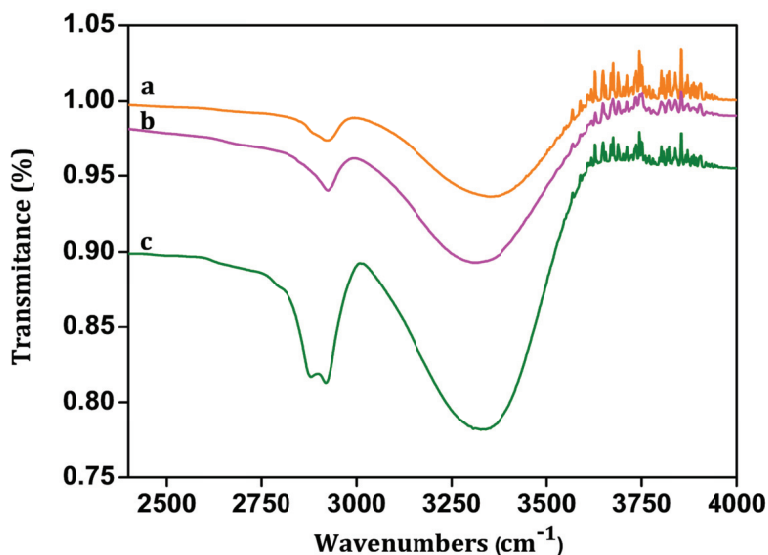


Figure 6.4 FTIR spectra of a) Fc-Dex polymer, b) β CD-NH₂, c) CNOs- β CD/Fc-Dex.

Solubility was determined by filtering CNOs solutions, following the

procedure reported in the literature in aqueous solutions.¹⁰ The functionalized CNOs were dissolved in water (no sonication was needed for the CNOs- β CD/Fc-Dex) and filtered through PVDF filters of 0.2 μ m porosity. This resulted in a more homogenous distribution of CNOs with smaller average size domains (Figure 6.5).

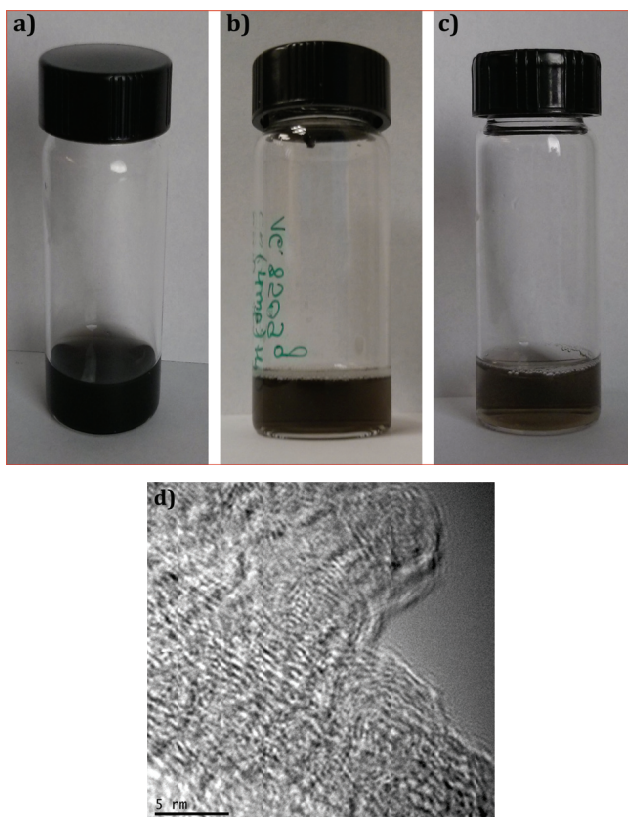


Figure 6.5 Solubility of modified CNOs; CNOs- β CD/Fc-Dex before filtration (a), CNOs- β CD/Fc-Dex after filtration through PVDF 0.45 μ m filter (b), CNOs- β CD/Fc-Dex after filtration through PVDF 0.22 μ m filter (c); HRTEM image of filtered CNOs- β CD/Fc-Dex through PVDF 0.22 μ m filter (d).

The average size of the modified CNOs before and after filtration through PVDF filters of 0.45 and 0.22 μm porosity was studied by dynamic light scattering (DLS) (Figure 6.6). The filtered solutions appear to contain more homogeneously sized CNOs possessing smaller sizes than the pristine CNOs.

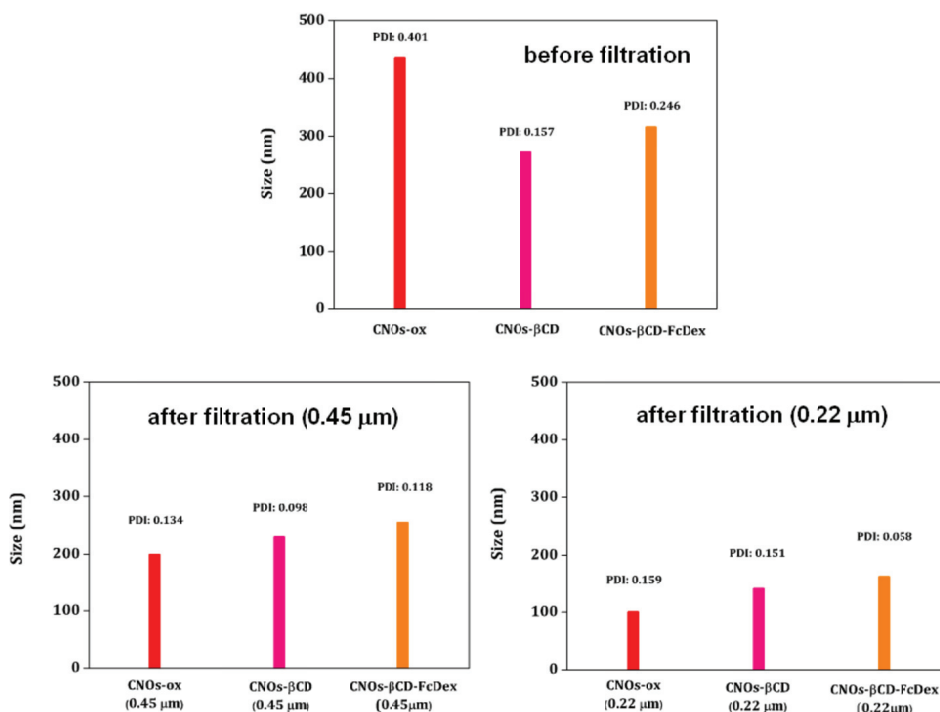


Figure 6.6 DLS measurements of ox-CNOs (red bars), CNOs-βCD (pink bars) and CNOs-βCD/Fc-Dex (orange bars); A) before filtration, B) after filtration through 0.45 μm PVDF filter and C) after filtration through 0.22 μm PVDF filter.

UV spectroscopy also shows a red shift in the characteristic peaks for CNOs¹⁰ gradually growing with the size increase of the particles after βCD functionalization and deposition of the Fc-Dex polymer, filtered through 0.45

and 0.22 μm PVDF filters (Figure 6.7).

Moreover, zeta potential measurements revealed changes in potentials before and after functionalization of CNOs, from -40 mV for the ox-CNOs, -30 mV for CNOs- β CD and -25 mV for the CNOs- β CD/Fc-Dex. This increase toward positive potential can be explained by covering the negative particle surfaces (due to carboxyl groups) with β CD and Fc-Dex polymer (Figure 6.8).

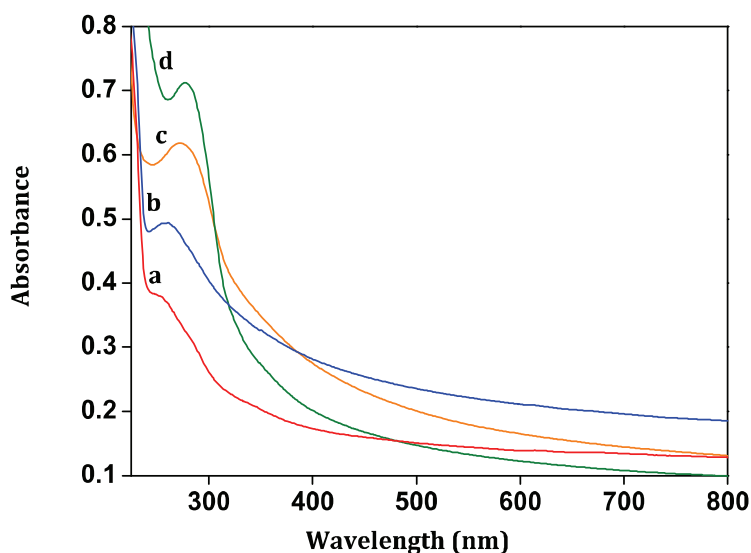


Figure 6.7 UV-spectra of CNOs- β CD (0.22 μm filter) (a), CNOs- β CD (0.45 μm filter) (b), CNOs- β CD/Fc-Dex (0.22 μm filter) (c), CNOs- β CD/Fc-Dex (0.45 μm filter) (d).

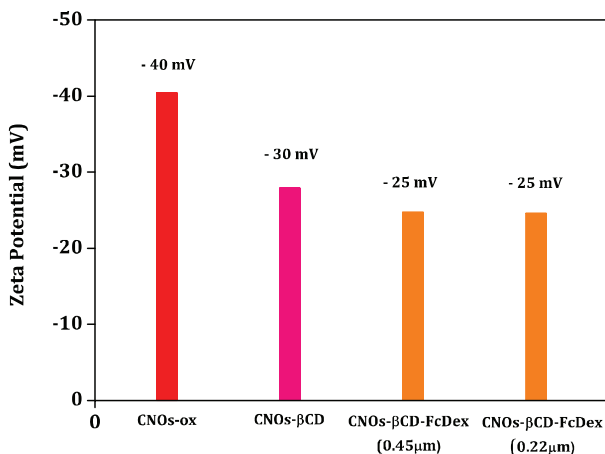


Figure 6.8 Zeta potential changes for ox-CNOs (red bar), CNOs-βCD (pink bar), CNOs-βCD/Fc-Dex (orange bars).

The soluble CNOs-βCD/Fc-Dex particles were further characterized by electrochemical techniques. In most voltammetric techniques such as cyclic voltammetry and square wave voltammetry the intensity of the current signal depends on the diffusion coefficients (D) of the diffusing species, among other factors such as concentration and electrode area. Since ferrocene is electrochemically active and is known to form inclusion complexes with βCD, it is possible to study the interaction of the outer ferrocene units with a βCD polymer. This interaction will increase the molecular weight of the adduct and thus reduces its diffusion coefficient and the current responses (Figure 6.9).

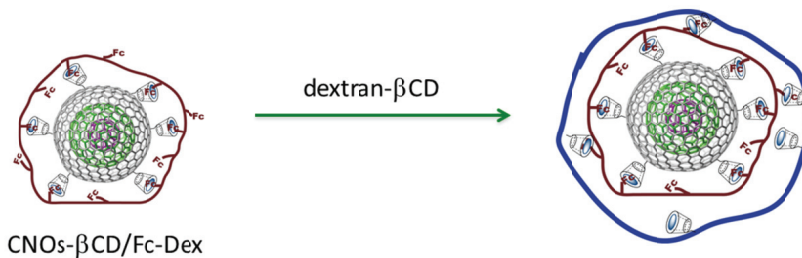


Figure 6.9. Interaction of CNOs-βCD/Fc-Dex particles with a dextran-βCD polymer.

Figure 6.10 A shows the cyclic voltammogram of CNOs-βCD/Fc-Dex particles before and after interaction with a dextran-βCD polymer (10 kDa). The peak-to-peak separation for CNOs-βCD/Fc-Dex is 80 mV, indicating that the attached ferrocene units maintain their reversible electron transfer properties. After interaction of the βCD polymer the signal intensity dramatically decreases, indicating the occurrence of Fc-βCD that fix the polymer on the surface of the modified CNO particles. This signal decrease was also evident by square wave voltammetry (Figure 6.10 B), in which a gradual signal drop is observed after interaction with increasing concentrations of the βCD polymer.

In the Stokes-Einstein model for the diffusion of large spherical particles, the values of D depend inversely on the radius R according to the equation:

$$D = \frac{kT}{6\pi\eta R}$$

where k is the Boltzmann's constant, T is the absolute temperature and η is the solution viscosity. Assuming a radius of ~ 4 nm for the CNOs-βCD/Fc-Dex particles, the estimated value of D is 6×10^{-11} m²/s at 298 K in water ($\eta = 8.9 \times 10^{-4}$ Pa·s), which is in the same order of magnitude of high molecular weight macromolecules.³⁵

On the other hand, the Randles-Sevcik equation for cyclic voltammetry relates the peak current with D at 298 K according to:

$$i_p = 268600 n^{3/2} A c v^{1/2} D^{1/2}$$

where A is the area of the electrode, c is the concentration and v is the scan rate. Using the calculated value of D the estimated peak current is $0.07 \mu\text{A}$ for a $100 \mu\text{M}$ solution at 200 mV/s , which is close to the experimental value observed from the cyclic voltammogram. This justifies the low currents observed by cyclic voltammetry.

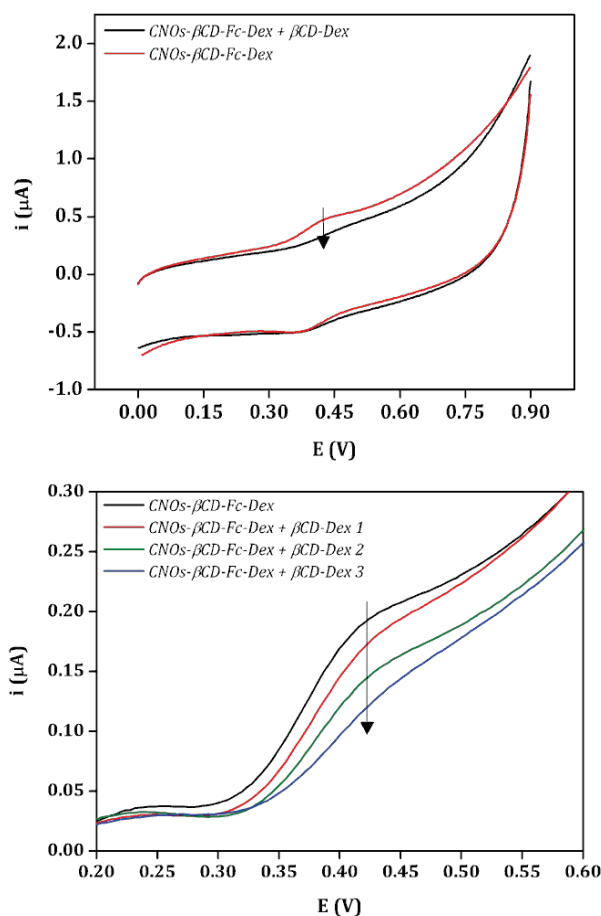


Figure 6.10 Cyclic (top) and square wave voltammograms (bottom) for the interaction of CNOs- β CD/Fc-Dex particles with a dextran- β CD polymer.

Furthermore, after addition of adamantanecarboxylate (which is known to have higher affinity for the β CD cavity), precipitation of the CNOs was observed (Figure 6.11), indicating the displacement of ferrocene molecules from the β CD cavities for the adamantane molecules and confirming the supramolecular nature of the interaction between CNOs- β CD and Fc-Dex.

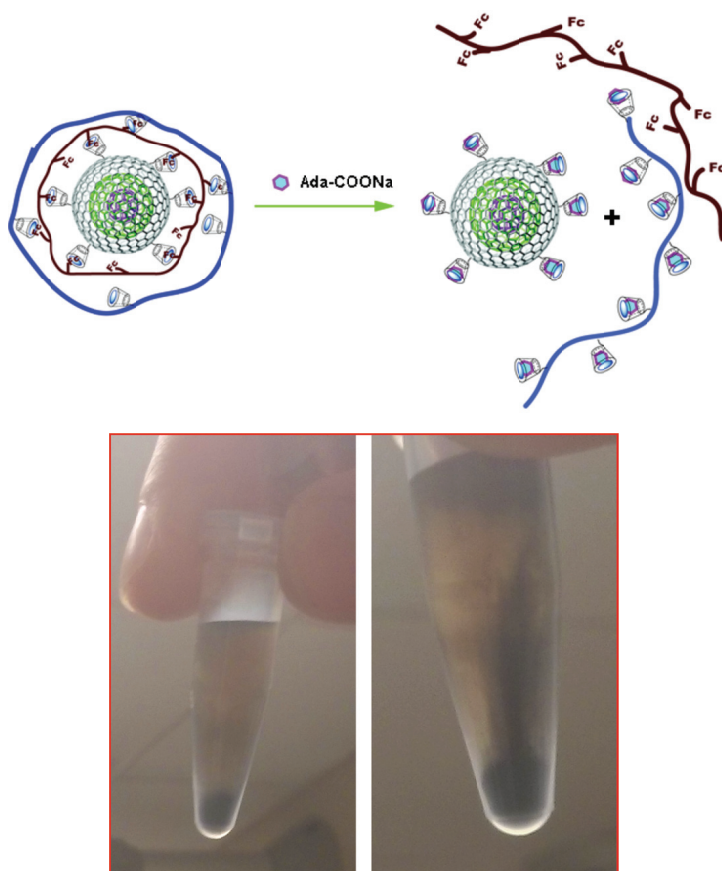


Figure 6.11. *Top:* Schematic representation of the interaction of CNOs- β CD/Fc-Dex particles with a dextran- β CD polymer and displacement of ferrocene by adamantane molecules. *Bottom:* Photograph of precipitated CNOs after addition of adamantanecarboxylate.

6.5 CONCLUSIONS

In summary, the oxidation and modification of CNOs with β CDs resulted in solublizing CNOs and further constructing CNO-based supramolecular nano systems by complexation with Fc-Dex polymer significantly increased their solubility even more. This solubility increase was possibly due to the formation of the inclusion complexes between Fc and β CD moieties appended in a highly hydrophilic dextran polymer. Additionally, after filtration of CNOs through 0.45 or 0.22 μm PVDF filters resulted in smaller and more homogenous nanoparticles. Thus, the supramolecular strategy presented in this Chapter for CNOs solubilization opens the possibility for a wide range of potential applications, such as photovoltaics, molecular electronics or biosensors.

REFERENCES

1. H. W. Kroto, J. R. Heath, S. C. O'Brien, R. F. Curl, R. E. Smalley, *Nature* 1985, **318**, 162.
2. N. Martin, *Chem. Commun.* 2006, 2093.
3. A. S. Rettenbacher, B. Elliott, J. S. Hudson, A. Amirkhanian, L. Echegoyen, *Chem. Eur. J.*, 2006, **12**, 376.
4. A. Palkar, A. Kumbhar, A. J. Athans, L. Echegoyen, *Chem. Mater.*, 2008, **20**, 1685.
5. V. L. Kunetsov, A. L. Chuvilin, Y. V. Butenko, I. Y. Malkov, V. M. Titov, *Chem. Phys. Lett.*, 1994, **222**, 343.
6. T. Cabioch, J. P. Riviere, J. Delafond, *J. Mater. Sci.*, 1995, **30**, 4787.
7. V. Z. Mordkovich, Y. Takeuchi, *Chem. Phys. Lett.*, 2002, **355**, 133.

8. V. Z. Mordkovich, A. G. Umnov, T. Inoshita, M. Endo, *Carbon*, 1999, **37**, 1855.
 9. V. Z. Mordkovich, *Chem. Mater.*, 2000, **12**, 2813.
 10. A. Molina-Ontoria, M. N. Chaur, M. E. Plonska-Brzezinska, L. Echegoyen, *Chem. Commun.*, 2013, **49**, 2406.
 11. J. Luszczyn, M. E. Plonska-Brzezinska, A. Palkar, A. T. Dubis, A. Simionescu, D. T. Simionescu, B. Kalska-Szostko, K. Winkler, L. Echegoyen, *Chem. Eur. J.*, 2010, **16**, 4870.
 12. V. Georgakilas, D. M. Guldi, R. Signorini, R. Bozio and M. Prato, *J. Am. Chem. Soc.*, 2003, **125**, 14268.
 13. C. T. Cioffi, A. Palkar, F. Melin, A. Kumbhar, L. Echegoyen, M. Melle-Franco, F. Zerbetto, G. M. A. Rahman, C. Ehli, V. Sgobba, D. M. Guldi and M. Prato, *Chem.-Eur. J.*, 2009, **15**, 4419.
 14. A. Palkar, F. Melin, C. M. Cardona, B. Elliott, A. K. Naskar, D. D. Edie, A. Kumbhar and L. Echegoyen, *Chem. Asian J.*, 2007, **2**, 625.
 15. L. Zhou, C. Gao, D. Zhu, W. Xu, F. F. Chen, A. Palkar, L. Echegoyen and E. S.-W. Kong, *Chem.-Eur. J.*, 2009, **15**, 1389.
 16. K. Flavin, M. N. Chaur, L. Echegoyen and S. Giordani, *Org. Lett.*, 2010, **12**, 840.
 17. A. S. Rettenbacher, M. W. Perpall, L. Echegoyen, J. Hudson and D. W. J. Smith, *Chem. Mater.*, 2007, **19**, 1411.
 18. T. Ogoshi, M. Ikeya, T. Yamagishi, Y. Nakamoto, A. Harada, *J. Phys. Chem. C*, 2008, **112**, 13079.
 19. M. E. Plonska-Brzezinska, D. M. Brus, J. Breczko, L. Echegoyen, *Chem. Eur. J.* 2013, **19**, 5019.
-

20. M. E. Plonska-Brzezinska, J. Mazurczyk, J. Brezcko, B. Palys, A. Lapinski, L. Echegoyen, *Chem. Eur. J.*, 2012, **18**, 2600.
21. M. E. Plonska-Brzezinska, J. Brezcko, B. Palys, L. Echegoyen, *ChemPhysChem*, 2013, **14**, 116.
22. H. C. Wang, Y. Li, M. J. Yang, *Sens. Act.*, 2007, **124**, 360.
23. S. Qin, D. Qin, W. T. Ford, J. E. Herrera, D. E. Resasco, *Macromolecules*, 2004, **37**, 9963.
24. A. K. Chakraborty, K. S. Coleman, *J. Nanosci. Nanotechnol.*, 2008, **8**, 4013.
25. S. Yesil, G. Bayram, *Polym. Eng. Sci.*, 2011, **51**, 1286.
26. L. Feng, J. Zheng, H. Yang, Y. Guo, W. Li, X. Li, *Solar Energy Mater. Solar Cells*, 2011, **95**, 644.
27. Y. Liu, Ch. Cao, J. Li, *Electrochim. Acta*, 2010, **55**, 3921.
28. S. Campidelli, C. Sooambar, E. Lozano Diz, C. Ehli, D. M. Guldi and M. Prato, *J. Am. Chem. Soc.*, 2006, **128**, 12544.
29. D. S. Knight, W. B. White, *J. Mater. Res.*, 1989, **4**, 385.
30. R. J. Nemanich, S. A. Solin, *Phys. Rev.*, 1979, **20**, 392.
31. D. Roy, M. Chhowalla, H. Wang, N. Sano, I. Alexandrou, T. W. Clyne, G. A. J. Amaratunga, *Chem. Phys. Lett.*, 2003, **373**, 52.
32. A. M. Rao, A. Jorio, M. A. Pimenta, M. S. S. Dantas, R. Saito, G. Dresselhaus, M. S. Dresselhaus, *Phys. Rev. Lett.*, 2000, **84**, 1820.
33. J. Barkauskas, M. Dervinyte, *J. Serb. Chem. Soc.*, 2004, **69**, 363.
34. T. Ogoshi, M. Ikeya, T. Yamagishi, Y. Nakamoto, A. Harada, *J. Phys. Chem. C* **2008**, *112*, 13079.
35. L. He, B. Niemeyer, *Biotechnol. Prog.* 2003, **19**, 544.

CONCLUSIONS AND FUTURE WORK

CONCLUSIONS

The self-assembly of building blocks into nano- or microstructures is an area of intense interest, with host-guest supramolecular interactions being particularly attractive in the formation of capsules. Numerous methods have been reported for the preparation of nano- or microcapsules, many of which, in addition to requiring time-consuming preparative steps and the use of organic solvents, result in heterogeneous capsules populations of uncontrolled size.

In the first part of the presented doctoral thesis, we presented the preparation and characterisation of cyclodextrin nanosponge bioconjugates containing a model antibody and peroxidase. Confocal microscopy indicates that the antibody is located in the outside of the particle while HRP is actually encapsulated in the inner part. CDNS offer the advantage of one step multi-gram preparation and ease of bioconjugation in mild conditions and the signal amplification obtained in the presence of CDNS-Ab-HRP indicates that this type of nanobioconjugates are promising candidates in the development of ultrasensitive biosensors.

In the second part of the thesis we focused on the design and preparation of polymeric nanocapsules that can be performed in a simple medium like water, where there is no need for the addition of any other solvents or stabilizing agents. Moreover, the requirement for use of the templates has its advantage over the size control and uniformity of the created capsules, which

could range from nano- to microscale. Additionally, the proposed model of the bio-friendly polymeric nanocapsules could be used in a broad range of applications, such as encapsulation and release of sensitive macromolecules (enzymes, proteins, DNA), or in the cosmetic industry. The possibility of the modification of the outside polymeric layer (β CD-dextran) with, for example, biomolecular receptors could also be used for targeted drug delivery or in biosensing applications.

Furthermore, other types of guest molecules with specific properties such as ferrocene or azo-compounds were employed for the capsules preparation. They can form more intelligent stimuli-responsive nanocapsules by using dextran polymer as a main chain with a sufficient length and an adequate number of guest molecules to generate reversible multipoint crosslinks between Fc-Dex/ β CD-Dex or Azo-Dex/ α CD-Dex. A redox reaction or UV-light alters the morphology of a supramolecular nanocapsules by controlling the formation of an inclusion complex. The external stimuli ease the encapsulation process making it faster and more efficient than without stimulus.

The last part of the thesis covered the oxidation and modification of CNOs with β CDs resulted in solublizing CNOs and further constructing CNO-based supramolecular nano systems by complexation with Fc-Dex polymer significantly increased their solubility even more. This solubility increase was possibly due to the formation of the inclusion complexes between Fc and β CD and moieties and application of ultrafiltration resulted in smaller and more homogenous nanoparticles.

In summary, with the presented doctoral thesis, newly designed and prepared nanostructures with their use in either biosensor development or as potential drug delivery systems are reported.

FUTURE WORK

- I. Further optimization of the nanosponge cyclodextrin bioconjugates assay performance and applying these novel type of structures in the detection of other targets such as DNA sequences.

- II. Studies of encapsulation/release properties of other molecules using prepared nanocarriers and investigation of different combinations of the synthesized host-guest polymers for the design of novel supramolecular architectures with interesting properties.

- III. Examination of the influence of different polymers with n-deposited layers on the CNOs surface vs their solubility; modification of the outer layer with biomolecules (e.g. antibodies) for the biosensor development.